CHARACTERIZATION OF BISTABILITY AND TRANSITION RATES IN TRANSCRIPTIONAL POSITIVE FEEDBACK LOOPS

Inauguraldissertation

zur

Erlangung der Würde eines Doktors der Philosophie
vorgelegt der
Philosophisch-Naturwissenschaftlichen Fakultät
der Universität Basel

von

VINCENT JAQUET

Von Saint-Imier, Bern

Basel, 2016

Genehmigt von der Philosophisch-Naturwissenschaftlichen Fakultät

auf Antrag von

Prof. Attila Becskei und Mihaela Zavolan

Basel, 18.10.16

<div align="right">

Prof. Dr. Jörg Schibler

Dekan

</div>

Abstract

Positive feedback commonly displays bistability, the ability to maintain overtime in the same conditions two alternative states of activity. The presence and the range of bistability depend on ultrasensitive reactions within the loop. To investigate bistability in genetic network, we constructed synthetic feedback loops in yeast where a transcription factor activates its own expression. By measuring the presence of hysteresis behavior, which is a sign of bistability, in those loops we identified the ultrasensitive reactions supporting bistability: homodimerization and cooperative binding of transcription factor. In the absence of those reactions the feedback loop was strictly monostable and when combined an even wider range of bistability arises than when there was only a single reaction. The detection of those reactions was made possible because we introduced RNA stem-loop upstream of the coding sequence of the transcription factor to reduce its translation rate. Indeed, the initial constructs had strong growth defect due to the overexpression of the transcription factor. Next, we aimed to predict transition rates between the two states of activity. Indeed, Even though the activity converges to either of the two states in the bistable range, due to the noise arising from the low number of some chemical species, transitions between the two states occur. The prediction of those transitions is difficult as the noise is amplified by feedback loop. First, we obtained a deterministic description of the loops by the open-loop approach. By breaking the loops at the mRNA of the transcription factor, we were able to fit the main parameter values of the system and map the steady states and the bistable range. Then, we determined the transient kinetics which is the activation delay which is not inherent to feedback loop, in our case it was the slow diffusion or binding of a ligand of the transcription factor. We determined also the noise of the system by measuring the distribution of mRNA at the steady states of the feedback loops. By building a stochastic model with the information from open-loop approach and expending it and fitting its parameter values to match the transient kinetics and noise observed, we were able to predict the transition rates observed in the feedback loops. With this better understanding, we discovered that the transitions are led by either noise or slow transient kinetics depending whether the system is inside or outside in the vicinity of the bistable range, respectively. Finally, we showed that the transition rates were abruptly changing around the boundaries of the bistable region. Therefore, the bistable region can be estimated in similar feedback loops by simply measuring transition rates.

Contents

Thesis outline

In the first chapter, a brief and general introduction is given for the basic concepts behind the work presented in the forthcoming chapters. The result section is composed of two published papers and the draft of a third manuscript. The three manuscripts used the same feedback loop constructs. In the second chapter, the first manuscript described how we optimized the initial feedback loop to avoid growth defect and how we determined the reactions with an ultrasensitivity response. In the third chapter corresponding to the second manuscript, we applied to open-loop approach on the feedback loop and we predicted the transition rates from the open-loop approach and noise and transient kinetics measurement. In the fourth chapter corresponding to the third manuscript, we estimated the bistable region and modulated it. Finally in fifth chapter we concluded the work.

I. Introduction

Transcription factor

The expression level of proteins in the cell is controlled by many molecular mechanisms from transcriptional initiation to post-translational modification. Transcription factors, which are protein that bind specific DNA sequence, play an important role on this expression modulation as they help to form the transcription initiation complex [1]. Indeed, the transcription factor can promote or inhibit the recruitment of the RNA polymerase for a specific gene by binding to a specific sequence in the vicinity of the regulated gene. These specific sequences are named DNA binding sites. The number and the identity of binding sites in the promoter give to every gene a specific pattern of expression, as different transcription factors will bind [2].

A number of mechanisms can modulate the transcription factor activity including ligand binding and post-translational modification. For instance, nuclear estrogen receptors are transcription factors, which binds DNA once their ligand, estrogen activated them [3]. This permits the cell to communicate or to sense its environment and to adjust the expression level of its protein accordingly.

Cooperative binding of the transcription factors

In order to have a more switch-like response to an increase of the transcription factor concentration, gene often has more than one copy of the binding sites in their regulatory sequence. Indeed, when multiple identical binding sites are present in the regulatory sequence, cooperative binding of the TF is observed. Cooperative binding meant that the binding of transcription factor is enhanced if already another transcription factor is already bound on a near site. The Hill function is generally used in biochemistry to describe cooperative binding. This function describes the fraction of a macromolecule saturated by a ligand as a function of the ligand concentration:

$$f(x) = \frac{x^n}{x^n + K_d{}^n}$$

Where x stands for the ligand concentration, n for the Hill coefficient and K_d is the equilibrium dissociation constant. Here the macromolecule is DNA and the ligand is the transcription factor. This model assumes that the transcription factor has identical affinity to all binding sites, which

6

may vary in-vivo as the DNA sequence of the binding sites varies. A Hill coefficient higher than 1 indicates positive cooperative binding whereas a coefficient lower than 1 indicates negative cooperative binding where the binding of transcription factor is inhibited if another transcription factor binds a near site. A Hill coefficient of 1 indicates that the binding is non-cooperative, independent.
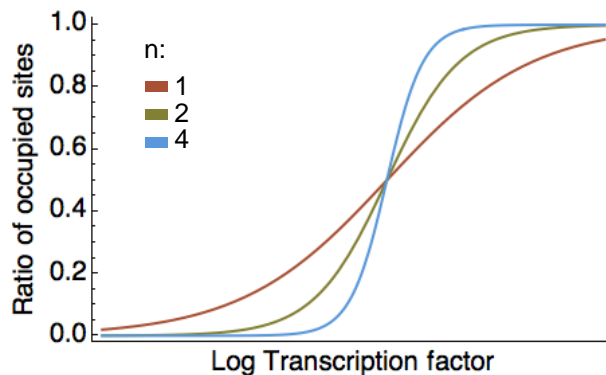

Figure 1: Hill function for different values of the Hill coefficient.

When a single binding site is present in the promoter, the Hill coefficient is 1 and the gene expression as function of the concentration of the transcription factor will be a hyperbolic response (Figure 1). This function saturates at high transcription factor concentration, as the binding site is almost all the time bound and therefore a further increase of transcription factor concentration increases only slightly its occupancy.

When two or more identical binding sites are present in the promoter, the Hill coefficient can be higher than 1 and therefore the response can be sigmoidal (Figure 1). The Hill coefficient is not identical to the number of binding sites as the binding of the transcription factor is not perfectly cooperative. There is some sequential binding so that partially saturated intermediates can exist. This results in a Hill coefficient lower than the number of binding sites (Segel, 1980).

The presence of multiple binding sites is widely used to generate sigmoidal response in gene regulation like in the galactose network where most of genes have more than one binding sites for gal4p in their promoter [4]. A sigmoidal response has the advantage to increases steeply for a narrow range of input.

Positive Feedback loops

More complex mechanisms are often needed to control gene expression patterns like oscillations or cellular memory where the gene expression remains high even when the initial trigger is not anymore present. Those more complex patterns can be only achieved in the presence of feedback loops. Depending on net effect of the interactions, the feedback loop can be either characterize as negative or positive. Transcription factor can generate feedback loop when they activate or inhibit their own gene expression in a direct or indirect way. Here we will introduce only the positive feedback loop.

Monostable positive feedback

Let analyses first a simple positive feedback where a transcription factor activates its own promoter. Here a single differential equation is needed to characterize the system:

$$\frac{dx}{dt} = V_{max} \frac{x^n}{x^n + K_d^{\ n}} + b - \delta_x x$$

Where V_{max} and b correspond to the maximal and basal transcription factor production rate constant, respectively. δ_x stands for the degradation rate constant of the transcription factor. The first term of the equation is a Hill function multiplied by the maximal production rate. This represents the protein production due to binding of transcription factor which initiate the transcription. The second term stands for the basal production rate of the protein and together with the first term they are the total production rate. The third term accounts for the protein degradation as biochemical molecules naturally experience decay. The rate at which it happens depend on how much of the molecule is present.

When the Hill coefficient is 1, the transcription factor concentration will converge to a single steady-state which is at the intersection of the total production and degradation rate curves (Figure 2). This can be understand by looking at the rate curves, when the concentration of transcription factor is higher than the steady-state concentration, the degradation rate is higher than the production rate therefore the concentration will decrease. In opposite, when the transcription factor concentration is lower than its steady-state value, the production rate is higher than the degradation rate and therefore the concentration will increase. The system is classified as monostable as the transcription factor will converge to a single steady-state.
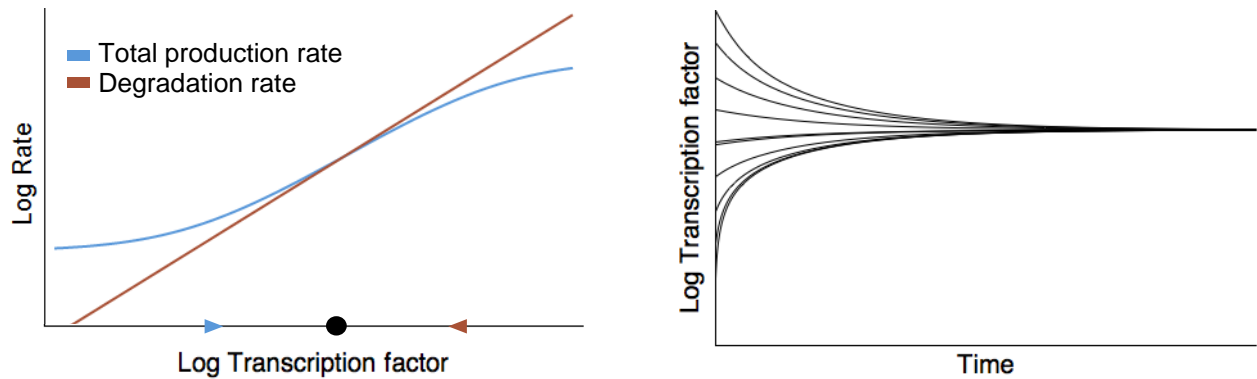
Figure 2: Phase portrait and trajectories for the monostable feedback loop. The stable steady-state concentration of transcription factor is indicated by a full circle. The arrows on the x-axis indicate in which direction the concentration converges by taking the rate difference.

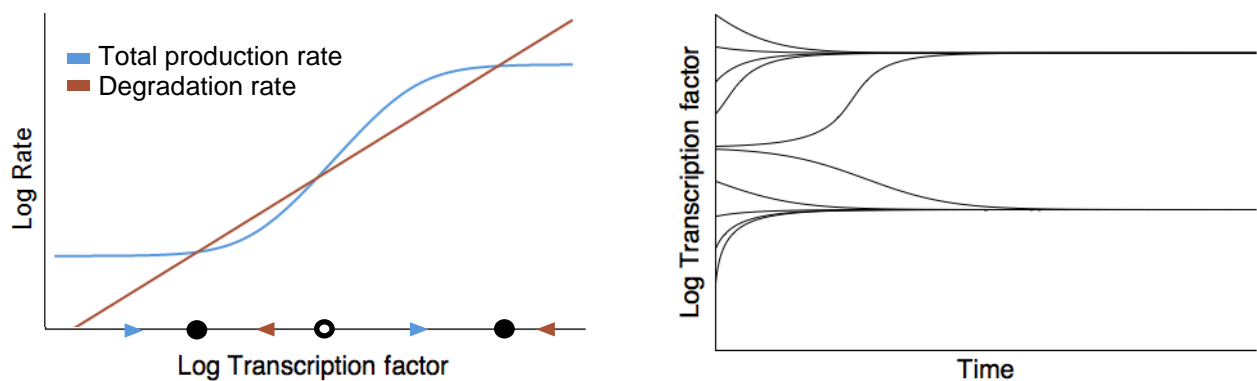**Bistable positive feedback**

Figure 3: Phase portrait and trajectories for the bistable feedback loop. The stable and unstable steady-state concentrations of transcription factor are indicated by full and empty circles, respectively. The arrows on the x-axis indicate in which direction the concentration converges by taking the rate difference.

When the Hill coefficient is higher than 1, the transcription factor concentration can converge to two different stable steady states (Figure 3). In this case, the production rate and the degradation rate have three intersections. The middle intersection is an unstable steady-state, i.e. if the transcription factor concentration is slightly higher or lower it will converge to the highest or lowest steady states, respectively. The lowest and the highest intersections are stable steady states as in the monostable system. This system is classified as bistable as the transcription factor concentration can converge to two different steady states.

Bistability

In the previous section, we presented a bistable system. Here we will go further in the analysis of the bistability as it is the main topic of this work. First, we will discuss the condition for a system to be bistable, then the bistable range as function of the system parameter and finally hysteresis behavior.

Condition for bistability

The presence of a positive feedback is a necessary condition for bistability [5]. However it is not a sufficient condition as we saw earlier with the monostable positive feedback loop. In order to have a bistable system, a reaction within the positive feedback loop should have an ultrasensitive response [6-8].

Goldbeter and Koshland defined input–output relationships to be ultrasensitive if it took less than an 81-fold change in input stimulus to drive the output from 10% to 90% of maximum[9, 10]. We used in this work an alternative definition: An response is ultrasensitive if its logarithm sensitivity is higher than 1 for at least one value of the input [11]. The logarithm sensitivity is defined as $S(\mathrm{x}) = \dfrac{\partial \ln f(\mathrm{x})}{\partial \ln(\mathrm{x})}$. For a Hill function, when the logarithm sensitivity is strictly below or equal to 1, the function has hyperbolic shape. When the logarithm sensitivity is higher than 1, the Hill function has a sigmoidal shape.

For instance cooperative binding of the promoter by transcription factors is a reaction with an ultrasensitive response and also sequestration by inhibitor molecules, dimerization and multiple phosphorylation of a protein [9].

Bistable range

In a system where bistability exists, the bistable range is restricted to a specific parameter space. Indeed, if we take the same model as before for bistable positive feedback example and we now reduce considerably the value of K_d, which corresponds to shift horizontally on the left the total production rate in figure 3, the production and degradation rates will intersect only once. The system will be then monostable. This is also true if K_d is increased sufficiently, the system will be also monostable. Therefore the system is bistable for a specific range of K_d. This can be easily visualized with the help of bifurcation diagram where the steady-state levels are plotted as function of a system parameter in this case K_d (Figure 4). The points at the end of the bistable

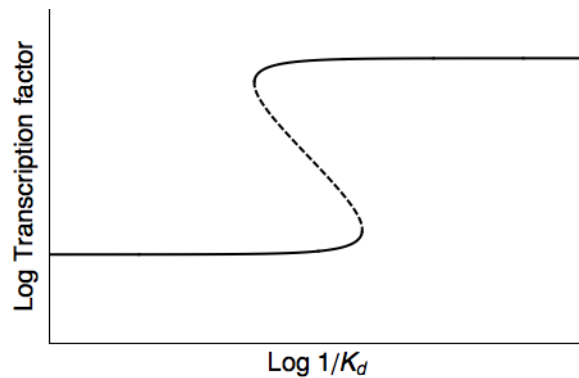range, where the system changes from one to three steady states, are called saddle-node bifurcation points.

Figure 4: Bifurcation diagram of the bistable feedback loop as function of inverse of K_d. The concentrations of transcription factor at stable and unstable steady states are indicated by a full and dashed lines, respectively.

Hysteresis

An interesting feature of this system is that it exhibits hysteresis as the parameter K_d passes back and forth through the bistable range (Figure 5). That is, for low K_d, the system is at the lower stable steady state. As K_d increases, the system remains at the lower steady state, even after entering the bistable range as the lower steady state is stable. Finally, when K_d passes the bistable range the system abruptly jump to the high steady state. Now, if we decrease K_d, the system would remain to the high steady-state until the end of the bistable range where it will switch back to the low steady state. This non-reversibility is called hysteresis [6, 12].

Open-loop approach

As mentioned earlier, the presence of an ultrasensitive response is a necessary condition for bistability. Experimentally, it is not always easy to measure certain parameter values like dimerization affinity constant and therefore to assess if the dimerization in this case is ultrasensitive or not. There is an approach, loop opening, which permits to determine if the system has a bistable range and to map this range [7]. For that, a component in the loop is broken into an input and output. This creates a reaction chain starting by the input passing through all the components of the broken loop and ending at the output. The open-loop function indicates the output as function of the input. This function represents the total response of all reactions within the loop, without the need to resolve any of them separately. If the open-loop function is

ultrasensitive, the feedback loop has a bistable range. The steady states of the system can also be determined by identifying the intersection of the open-loop function with the identity line.
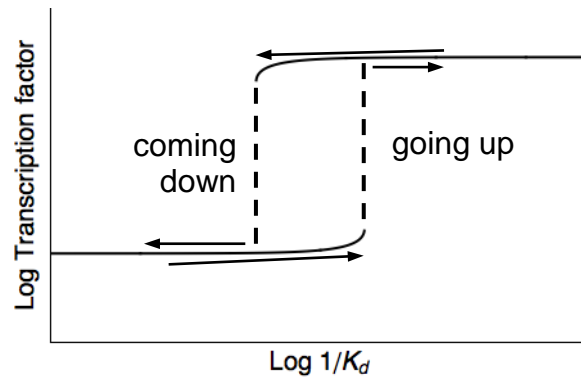

Figure 5: Hysteresis. Bistable circuit exhibits hysteresis, meaning different response curves are obtained depending upon whether the system began at the low or high steady-state concentrations.

Open-loop approach

As mentioned earlier, the presence of an ultrasensitive response is a necessary condition for bistability. Experimentally, it is not always easy to measure certain parameter values like dimerization affinity constant and therefore to assess if the dimerization in this case is ultrasensitive or not. There is an approach, loop opening, which permits to determine if the system has a bistable range and to map this range [7]. For that, a component in the loop is broken into an input and output. This creates a reaction chain starting by the input passing through all the components of the broken loop and ending at the output. The open-loop function indicates the output as function of the input. This function represents the total response of all reactions within the loop, without the need to resolve any of them separately. If the open-loop function is ultrasensitive, the feedback loop has a bistable range. The steady states of the system can also be determined by identifying the intersection of the open-loop function with the identity line.

Stochastic nature of gene expression

Chemical reactions in living cells are driven by random collisions between molecules. If a sufficient number of same events occur per time lapse, this randomness could be averaged out and the process can be considered as behaving deterministically in cells. However, many reactions occur so rarely that substantial relative fluctuations arise spontaneously [13-16]. These

fluctuations can propagate through the network as the rates of the other reactions are affected [17]. The gene expression is particularly sensitive as substantial phenotypical variation can be observed [18, 19].

Stochastic state transition

In the bistable system, the fact that the concentration of the component of the system fluctuate make it possible that the system switches to the other steady state in the bistable range [20]. The transition rates are fitted from the measurement of the proportion of cell at the low expression state overtime from a population initially where all cells were at the high expression state for the high initial condition or at the low expression state for the low initial condition. Those transitions are also simulated by using the Gillespie algorithm [21]. This algorithm generates a statistically possible trajectory of a stochastic equation. By performing several trajectories, statistics can be obtained similarly as single-cell measurements in a population.

Aim of the study

Bistable systems, where the expression switches between two distinct states of activity are widely present in cellular network in processes like cell-fate determination, microbial adaptation by bet-hedging strategy or cancer onset [22-25]. Despite, this large presence, it is only less than 20 years that the first artificial feedback loops were built and therefore permit a better understanding of bistability. The first artificial loop was a double negative feedback loop using prokaryotic transcriptional repressors [26]. A bistable system can however arises from a simple positive feedback loop and this was demonstrated later on in eukaryote [20]. In this artificial positive feedback they observed as expected that the cells clustered in either of the two states but they also observed that time to time the cells switch between the two states. Those transitions arise from the small number of components in the transcription regulation which can relatively substantially fluctuate in a short period of time. This was the beginning of the quantification of the cellular memory. The cellular memory is the capacity of a system to maintain an established phenotype despite the presence of significant fluctuations which tend to switch it to another phenotype. The first attempt to quantify and modulate cellular memory was done with the galactose network in yeast [27]. In addition to map the different stability, monostability and bistability of the system like it was done in the lac operon [28], they also measured the transition rates to characterize further the bistable region between destabilized and persistent memory area.

Bistability is not present in a positive feedback in absence of an ultrasensitive response [6-8]. Different reactions have been found to exhibit ultrasensitivity like cooperative binding, sequestration by inhibitor molecules, dimerization and multiple phosphorylations of a protein [9]. When the feedback system contain many components or when not all reaction rates are known, a powerful method, the open-loop approach can be used to detect the presence of reaction having an ultrasensitive response and map the steady states and therefore the bistable range [7]. The open-loop approach was already applied on transcriptional feedback loop by fusing the transcription factor with a fluorescent protein [29, 30].

Our work built on these findings. They were two main goals in this project. The first was to develop an improved version of the open-loop approach where we opened at mRNA and not by using florescent protein fusion. This was in order to obtain precise value of the main parameters
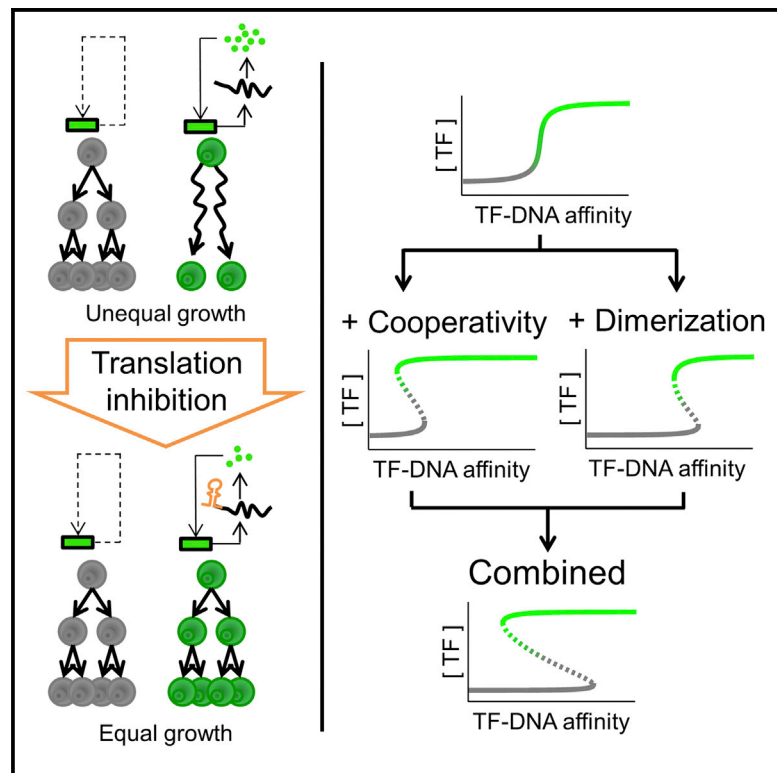
of the feedback loop and with it, the steady states can be predicted with precision as well as the bistable range and of course the presence of ultrasensitive reactions. The second aim was to predict the transition rates between the two states. For that, we used the information from the open-loop and in addition we measured and extended the model to fit the noise and the transient kinetics. The transient kinetics is the activation delay which is not inherent to feedback loop, in our case it was the slow diffusion or binding of a ligand of the transcription factor. The good match between the predicted and the observed transition rates were in good agreement validating both the open-loop approach and the framework used to predict the transition rates.

The work was divided in three manuscripts. The first manuscript described how we optimized the initial feedback loop to avoid growth defect and how we determined the reactions with an ultrasensitive response. In the second manuscript, we applied the open-loop approach on the feedback loop and we predicted the transition rates. In the third manuscript, we estimated the bistable region and modulated it.

II. Protein Dimerization generates bistability in positive feedback loops

Cell Reports

Protein Dimerization Generates Bistability in Positive Feedback Loops

Graphical Abstract

Highlights

- RNA stem loops tune translation rates over two orders of magnitude

- Positive feedback loops with reduced translation generate bistable cell fates

- Dimerizing transcription factors generate bistability without cooperative binding

Authors

Chieh Hsu, Vincent Jaquet,
Mumun Gencoglu, Attila Becskei

Correspondence

attila.becskei@unibas.ch

In Brief

Using RNA stem loops to attenuate translation rates, Hsu et al. designed synthetic feedback loops in yeast to study the sources of bistability. They show that cooperative binding of a transcription factor to its promoter or its dimerization generates bistability. Bistability is particularly robust when the dimerizing transcription factor binds to the promoter cooperatively.

CrossMark

CellPress

Protein Dimerization Generates Bistability in Positive Feedback Loops

Chieh Hsu,[1,2,3] Vincent Jaquet,[1,3] Mumun Gencoglu,[1] and Attila Becskei[1,*]
[1]Biozentrum, University of Basel, Klingelbergstrasse 50/70, 4056 Basel, Switzerland
[2]School of Biosciences, University of Kent, Canterbury, Kent CT2 7NJ, UK
[3]Co-first author
*Correspondence: attila.becskei@unibas.ch
http://dx.doi.org/10.1016/j.celrep.2016.06.072

SUMMARY

Bistability plays an important role in cellular memory and cell-fate determination. A positive feedback loop can generate bistability if it contains ultrasensitive molecular reactions. It is often difficult to detect bistability based on such molecular mechanisms due to its intricate interaction with cellular growth. We constructed transcriptional feedback loops in yeast. To eliminate growth alterations, we reduced the protein levels of the transcription factors by tuning the translation rates over two orders of magnitude with designed RNA stem loops. We modulated two ultrasensitive reactions, homodimerization and the cooperative binding of the transcription factor to the promoter. Either of them is sufficient to generate bistability on its own, and when acting together, a particularly robust bistability emerges. This bistability persists even in the presence of a negative feedback loop. Given that protein homodimerization is ubiquitous, it is likely to play a major role in the behavior of regulatory networks.

INTRODUCTION

Bistability, the persistence of two alternative stable-activity states under identical conditions, can uphold alternative cell fates and differentiation states, store cellular memory of past stimuli, and enhance adaptation in organisms ranging from bacteria to mammals (Angel et al., 2011; Arnoldini et al., 2014; Bouchoucha et al., 2013; Chickarmane et al., 2009; Park et al., 2012).

Positive feedback is a necessary, but not sufficient, condition for bistability in a gene regulatory network. The second requirement is that the feedback loop contains reactions such as cooperative binding, sequestration by inhibitor molecules, and multiple phosphorylation of a protein by a kinase (Chen and Arkin, 2012; Ferrell and Ha, 2014; Májer et al., 2015; Shopera et al., 2015; Thomson and Gunawardena, 2009). These reactions display a sigmoidal, switch-like nonlinear response, also termed ultrasensitive response. Without ultrasensitive responses, a

feedback loop can have only a single steady-state expression level, i.e., the system is monostable.

In transcriptional regulation, dimerization and cooperative binding of a transcription factor are expected to be common sources of ultrasensitivity (Buchler and Louis, 2008). Most transcription factors bind to DNA as dimers, and binding can be cooperative when more than one binding site is present in a promoter (Becskei et al., 2005). Despite the ubiquity of protein homodimerization, its ability to generate bistability remained elusive.

The difficulty to identify the sources of bistability may be explained by the effect of the feedback loop on cell growth. In positive feedback loops, the transcription factors are often expressed at high levels; therefore, they can sequester mediators of transcription (Becskei et al., 2001; Kelleher et al., 1990). This results in squelching of global gene expression, which reduces cellular growth and alters the behavior of networks. Even more, growth alterations rather than ultrasensitivity in the feedback can generate bistability (Brophy and Voigt, 2014; Tan et al., 2009).

In this work, we illustrated a design principle to tackle this difficulty with synthetic feedback loops. We show that alteration of the cell growth caused by overexpression of the transcription factor can be circumvented by using RNA stem loops to adjust translation rates. After translation rate adjustment, we show that either of the two ultrasensitive reactions, cooperative binding to the promoter or homodimerization, can support bistability. When they were both present, a particularly robust bistability emerged.

RESULTS

Design of Synthetic Loop and Control Elements

Synthetic positive feedback loops were created by placing the gene encoding the transcription factor rtTA (reverse tetracycline transactivator) under the control of a promoter containing *tet* operators and inserted into the chromosome of the yeast *S. cerevisiae* (Table S1). rtTA is composed of the bacterial rTetR DNA-binding domain and the VP16 activation domain; rtTA binds to the *tet* operators only in dimeric form (Kamionka et al., 2006). The ligand doxycycline enables rtTA to bind to *tet* operators; thus, the affinity of rtTA binding to DNA was adjusted by the ligand concentration (Figure 1A).
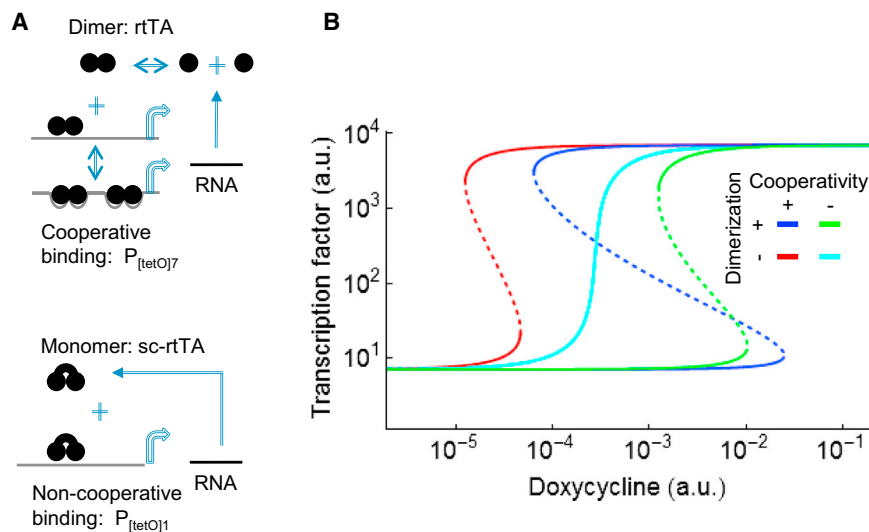
Figure 1. Design and Models of Feedback Loops with Cooperative Binding and Homo-dimerization

(A) Feedback loop design. Two examples are shown for the feedback loops: the loop with two ultrasensitive reactions: cooperative binding and dimerization (upper panel) and the loop without ultrasensitive reaction (lower panel).

(B) The effect of cooperative binding and protein dimerization on the steady-state levels in the feedback loop as a function of the binding strength of transcription factor to DNA, as indicated by the doxycycline concentration. When three (one unstable and two stable) steady-state expression levels are found in a certain range of doxycycline concentration, the system is bistable. The Hill coefficient of the cooperative binding was 1.45, and the equilibrium dissociation constant (K_D) for dimerization was 1,000 (in concentration units identical to that of the transcription factor). See also Supplemental Information.

To study the effect of dimerization, we compared the original dimeric rtTA with a monomeric form. To create this monomeric form, two rTetR DNA-binding domains were fused. The resulting single-chain monomer (sc-rtTA) alone is capable of binding to the palindromic operators, eliminating the ultrasensitive dimerization reaction (Zhou et al., 2007). To study the effect of cooperativity, we changed the number of *tet* operators in the promoter. The binding of rtTA to a single *tet* operator is non-cooperative, while binding to seven operators in a promoter is cooperative (Becskei et al., 2005) (Figure 1A).

If a transcriptional positive feedback loop incorporates cooperative binding or dimerization, bistability is expected in a certain doxycycline concentration range. This range is expected to be broader when both reactions are present (Figure 1B). To test the individual and joint effect of these mechanisms, we constructed all four variants of the feedback loop. We measured the activity of a feedback loop with a GFP reporter controlled by a promoter with *tet* operators (Figure 2A).

Growth Alteration by Overexpression of the Transcription Factor Caused Atypical Hysteresis

We evaluated bistability with hysteresis experiments that test whether the system activity depends on the initial condition, i.e., on its history. Pre-cultures with either low or high expression states of rtTA were prepared, which defines the initial conditions, and the cells were further cultured at different doxycycline concentrations. The range of doxycycline concentrations at which the expression in each culture remains close to the respective initial condition—and, therefore, different from each other—defines the range of hysteresis. To adjust the initial condition, we integrated an inducible rtTA construct into the chromosome. Its expression was controlled by the P_{GAL} promoter. By a transient exposure of cells to galactose, the rtTA is expressed at a high level to establish the high initial condition (Figure 2A).

When hysteresis experiments were performed for the cooperative-dimeric feedback loop, the cell expression deviated markedly from the initial state. Even more, the high expression level was observed only in cells with the low initial condition, while

cells with the high initial condition failed to maintain high expression (Figure 2B). This is the exact opposite of the conventional hysteresis behavior. Similarly unusual was the behavior of the non-cooperative-dimeric feedback loop (Figure S1A).

We suspected that the high expression of the rtTA affects the cell growth and alters the system's behavior. Indeed, a reduced growth rate was observed at a high doxycycline concentration at which the system should have been fully activated (Figure 2C).

Translation Rate Tuning with RNA Stem Loop and Feedback Loop Optimization

To eliminate the growth rate alteration, we lowered the protein expression level by decreasing the translation rate with RNA stem loop. A stem loop upstream of the start codon is expected to reduce the translation rate by preventing ribosome from initiating the translation. When a stem loop with a stem containing six G-C base pairs (or $SL_{6[AT]0}$) (Beelman and Parker, 1994) was incorporated into the cooperative-dimeric feedback loop, no growth defect was detected anymore, and the growth rates in all conditions were identical (Figure 2C). However, the reporter gene expression was very weak, indicating that the rtTA protein concentration was too low to activate the system (Figure 2B).

To reach a sufficient protein expression level without causing growth defect, we synthesized stem loops and measured their respective translation rates. The strength of translation inhibition of the stem loop depends on its structure. We weakened the stem structure of the initial $SL_{6[AT]0}$ by shortening the stem length to five base pairs and by increasing the proportion of A-T base pairs. The absolute translation rate was calculated from the steady-state expression levels of RNA and protein and the protein decay rate. The molecule numbers of RNAs and proteins were measured with single-molecule fluorescence in situ hybridization (smFISH) and mass spectrometry, respectively (Experimental Procedures; Supplemental Experimental Procedures). We obtained a variety of stem loops that can tune the translation rate over two orders of magnitude (Figure 3A). We also checked how robust the stem loops behave in different sequence context. For this purpose, we inserted these stem loops upstream of the
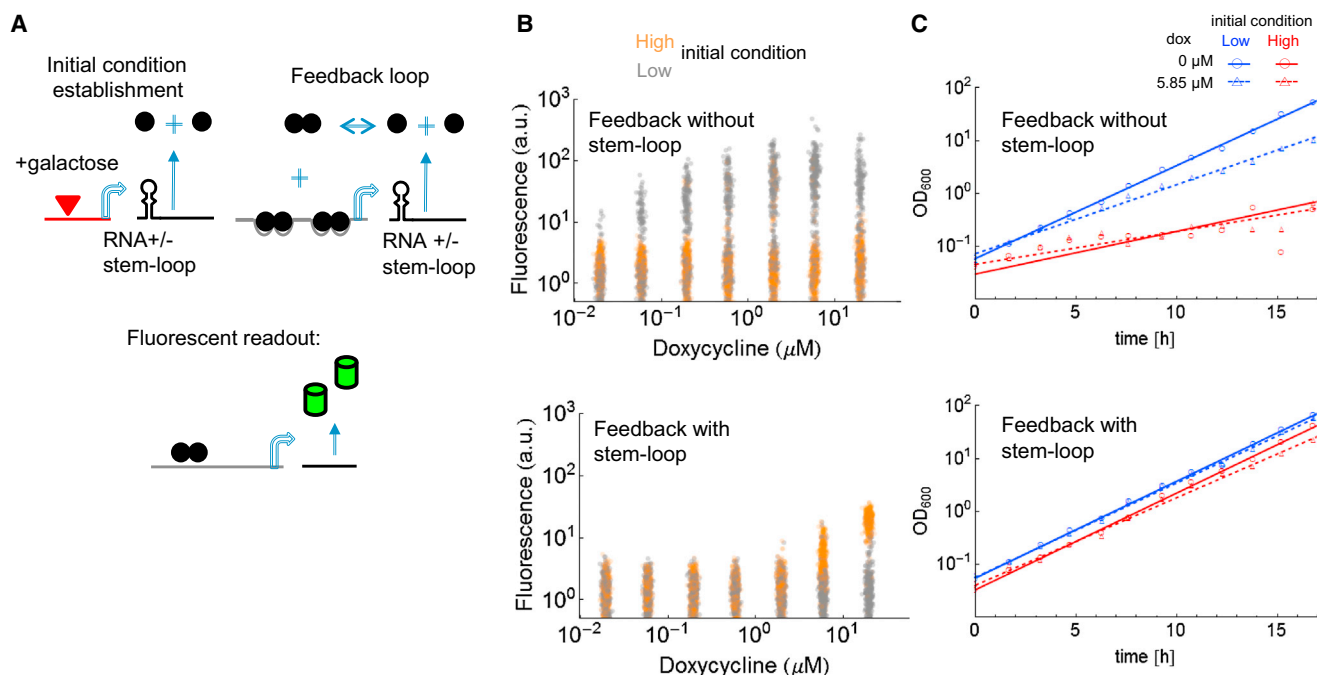
Figure 2. Hysteresis Experiments with Altered Growth Rates

(A) Circuit design. The activity of the cooperative-dimeric loop is reported with a GFP reporter (green) under $P_{[tetO]2}$ and measured with flow cytometry. High and low initial conditions (transcription factor expression levels) were established with the P_{GAL} promoter (red), which can be induced transiently by galactose. Expression of P_{GAL} is independent of the doxycycline-inducible promoters. To reduce the expression level of the transcription factor, a stem loop was incorporated in the RNA upstream of the start codon.

(B) The hysteresis experiment of the dimeric-cooperative loop without (upper panel) or with (lower panel) incorporated non-optimized RNA stem loop ($SL_{6[AT]0}$) to modulate translation. Cells with the low (gray dots) or the high (orange dots) initial condition were grown at the indicated doxycycline concentration for 24 hr.

(C) Growth curves of cells containing the cooperative-dimeric loop without (upper panel) or with (lower panel) incorporated RNA stem loop under indicated initial conditions and doxycycline concentrations during the hysteresis experiments.

See also Figure S1.

start codon of a fluorescent reporter gene, YFP (yellow fluorescent protein). The decrease of fluorescence with increasing stem-loop strength was very similar to that observed for the absolute translation rates of the rtTA mRNA (Figure 3A).

A specific stem loop was selected for each feedback construct in order to eliminate growth alterations without reducing protein concentration to below the level required to activate the feedback loops (Figures 3B and S1).

The decay rates of the rtTA and the sc-rtTA proteins were similar, with half-lives of 79 and 83 min, respectively (Figure 3C). The similar decay rates of the two proteins permit their consistent comparison of the feedback loops in the hysteresis experiments.

Homodimerization and Cooperativity Generate Bistability

With the optimized feedback loops, we observed classical hysteresis behavior: cells with the high initial condition had higher or equal expression than cells with the low initial condition (Figure 4A). The non-cooperative-monomeric loop displayed no hysteresis, the expressions of cells were very similar, independent of the initial condition. When one of the ultrasensitive reactions— either cooperative binding or dimerization—was included in the feedback loop, bistability emerged. The non-cooperative-

dimeric loop displayed hysteresis over one order of magnitude of doxycycline concentration, which is broader than that for the cooperative-monomeric circuit. Combining the two mechanisms, a particularly broad range of hysteresis emerged. The cells with a high initial condition remained in the high expression state; and cells with the low initial condition remained in the low expression state over at least two orders of magnitude of doxycycline concentrations. This represents a robust form of cellular memory. These results confirm the expectations from the theoretical model (Figure 1B).

Negative Feedback Reduces the Robustness of Bistability

Positive feedback loops are often combined with negative ones. This combination is expected to reduce the bistable range (Tian et al., 2009). To extend the cooperative-dimeric positive feedback loop with a negative loop, additional *tet* operators were integrated downstream of the TATA box in the promoter (Figure 4B). The binding of rtTA to these two *tet* operators was shown to repress transcription. At low doxycycline concentration, the binding to the seven upstream *tet* operators activates gene expression, while at higher doxycycline concentration, repression predominates. Consequently, the promoter displays a bell-shaped response (Figure S2A) (Buetti-Dinh et al., 2009).
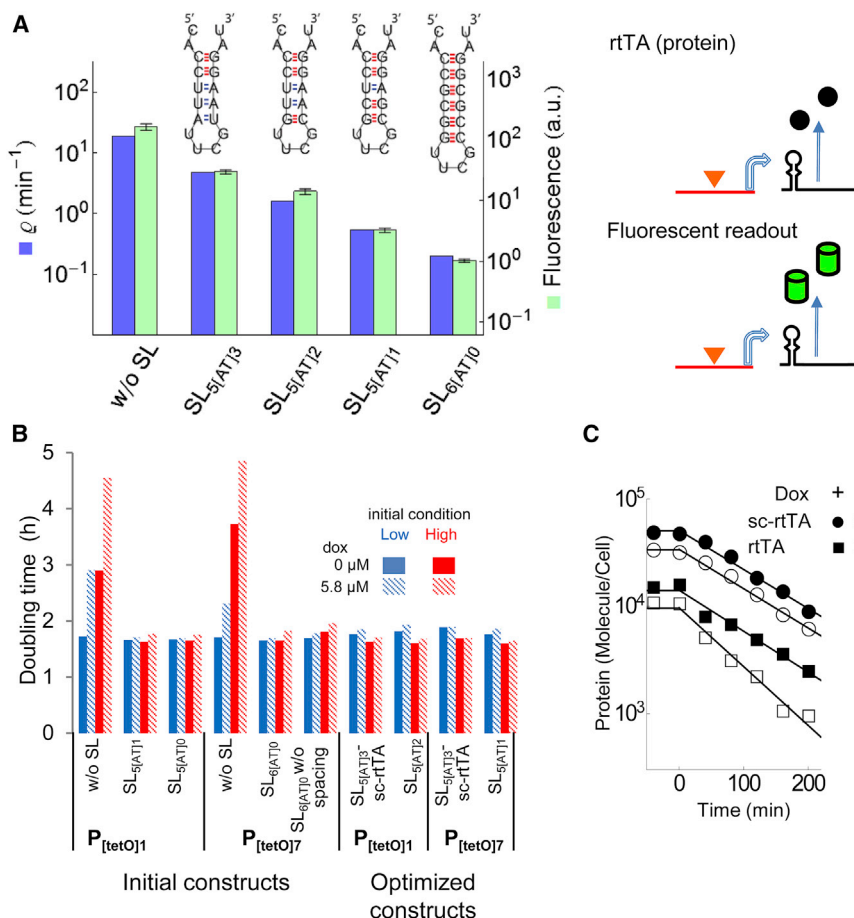
Figure 3. Optimization of Protein Expression Levels with Various RNA Stem Loops

(A) Translation rates of mRNAs with different stem loops. Stem loops with different lengths and AT/GC contents were incorporated upstream of the start codon of the transcription factor rtTA or a fluorescence reporter under control of the P*GAL* promoter as indicated. The absolute translation rates and the relative fluorescence signals were measured. The following values were obtained for the translation rates (left to right): 18.6, 4.8, 1.6, 0.54, and 0.2 min^{-1}.

(B) The effect of stem loop optimization on growth in different feedback constructs. The growth rates of cells containing the indicated feedback loops with various RNA stem loops were determined by linear regression under different initial conditions (init.) and doxycycline (dox) concentrations during the hysteresis experiments.

(C) The decay rates of proteins were measured by shut-off assay (Supplemental Experimental Procedures). The fitted decay rate constants of rtTA protein are 0.0126 ± 0.0009 and 0.0088 ± 0.0006 min^{-1} (estimate ± SE) with and without 20 μM dox, respectively. Both values are 0.0084 ± 0.0004 min^{-1} for sc-rtTA.

See also Supplemental Experimental Procedures and Figure S1.

distinct cell lineages often have disparate growth rates (Cheeseman et al., 2014). In our system, the reduction of cell growth was due to the squelching of gene expression of a highly expressed activator. Interestingly, endogenous transcriptional activators are also known that can repress gene expression by squelching (Guertin et al., 2014; Schmidt et al., 2015).

To eliminate growth alterations, we reduced protein concentration by translational inhibition. Interestingly, the range of inhibition was quite narrow that permitted the activation of the feedback loops without affecting growth rate. This requirement was met by the stem-loops we created because it was possible to modulate the translation rate over a broad dynamic range, which makes them an ideal tool in systems and synthetic biology (Chappell et al., 2015; McKeague et al., 2016). Furthermore, the stem loops reduce the translation of different proteins similarly (Figure 3A). The absolute translation rate without stem-loop was around 20 min^{-1}, while it was around 0.2 min^{-1} with the stem loop having the highest GC content. This means that, on average, 20 protein molecules are translated from an RNA molecule per minute without the stem loop. To our knowledge, no absolute translation rate has been measured in yeast, but a comparison of genome-wide studies on yeast mRNA, protein abundances, and protein half-lives yields similar estimates for the average translation rate (23 min^{-1}) (Belle et al., 2006; To and Maheshri, 2010).

The loop with the monomeric transcriptional activator and a single site in the promoter lacks any ultrasensitive reaction, and bistability was absent. By adding either dimerization or

In theory, a feedback loop with this promoter has a narrower range of bistability compared to the cooperative-dimeric feedback loop (Figure S2B). Furthermore, the higher expression state is predicted to be lower. This may explain why no growth alteration was observed and no stem loop was needed for this feedback loop. The range of hysteresis of this dual positive-negative feedback system was narrower than that of the corresponding positive feedback (cooperative-dimeric). However, it was still wider than the hysteresis range of loops with a single ultrasensitive reaction step (Figure 4C), which indicates again the robustness of the bistability when cooperative binding and homodimerization act together.

DISCUSSION

We observed bistability due to ultrasensitive molecular mechanisms only when cell growth alterations due to the feedback loops were eliminated. This behavior stands in contrast to those systems where bistability arises due to the interaction of the feedback loop and cellular growth. For example, regulators have been identified that slow down cell growth, which then establishes a positive feedback loop to control cell differentiation (Chiodini et al., 2013; Kueh et al., 2013; Tan et al., 2009). Coupling of feedback loops with growth rate is likely to represent an important phenomenon, since differentiating cells that enter
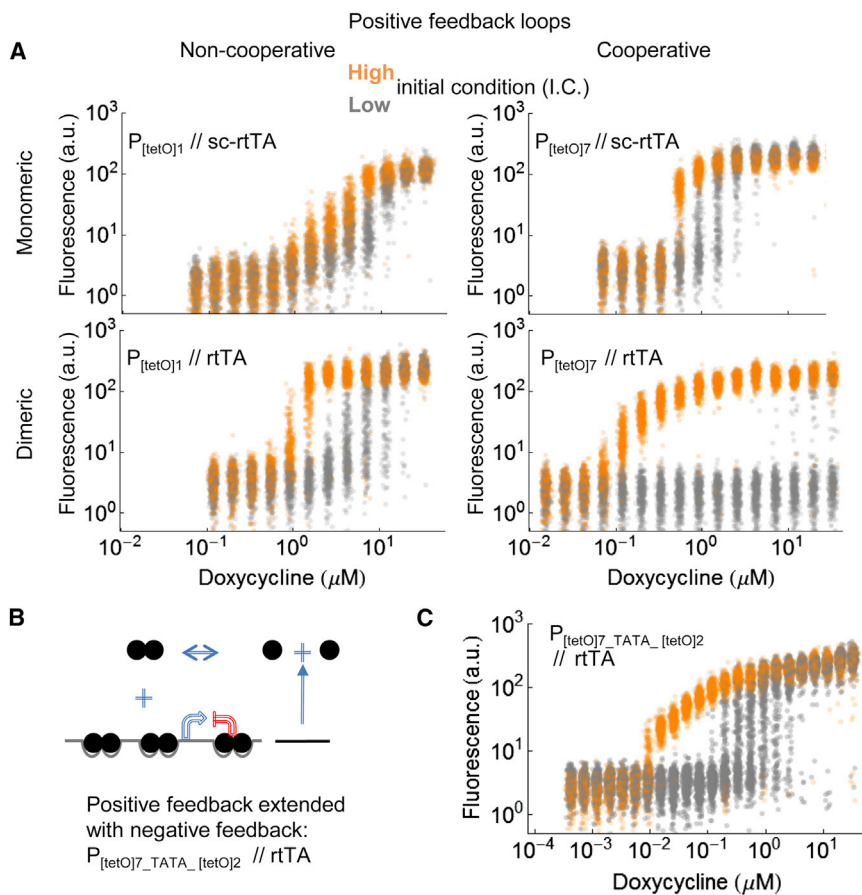
Figure 4. Hysteresis in Feedback Circuits Incorporating Protein Homodimerization or Cooperative Binding to the Promoter

(A) Hysteresis experiments with circuits with optimized stem loops as indicated in Figure 3. Cells with the low (gray dots) or the high (orange dots) initial condition were grown at the indicated doxycycline concentration for 24 hr.

(B and C) Hysteresis in dual positive-negative feedback based on the cooperative-dimeric circuit. The negative feedback was established by inserting transcription factor binding sites downstream of the TATA box site in the promoter, which inhibits transcription (red) (B). Hysteresis experiments were performed with the cells containing this feedback construct without RNA stem loop for 24 hr.

See also Figure S2.

Louis, 2008; Májer et al., 2015). The reduced concentration of the dimerizing protein in our circuits is likely to have facilitated the emergence of bistability.

Positive feedback loops have been uncovered in a broad range of regulatory processes (Chiodini et al., 2013; Kueh et al., 2013; Park et al., 2012). Our study provides clues on how to detect the bistability due to homodimerization in feedback loops. It has the potential to contribute to other dynamical behaviors, such as oscillation and pattern formation (Ferrell and Ha, 2014). Given the ubiquity of homodimerization, it is likely that it plays an important role in these processes as well.

EXPERIMENTAL PROCEDURES

Design of Synthetic Circuits and Yeast Strains

Each feedback strain contained a feedback circuit, a fluorescent reporter construct ($P_{[tetO]2}$- yEGFP), and a P_{GAL}-rtTA/sc-rtTA expression cassette. The P_{GAL}-rtTA/sc-rtTA expression cassette was utilized to generate the high initial condition by adding 0.5% galactose for the hysteresis experiments. Galactose activates expression driven by the P_{GAL} promoter through the endogenous Gal4p. The P_{GAL} is a modified version of P_{GAL1} (denoted as P_GAL1UAS-CYC1c in Table S1).

All yeast strains are derivatives of *S. cerevisiae* W303 (Table S1). All genetic constructs were integrated into the chromosome with a single copy, with the exception of the $P_{[tetO]2}$-GFP construct, which has three copies. To minimize the position effect, genes with promoters containing *tet* operators were integrated to the *ura3* locus, and those with P_{GAL} were integrated to the *ade2* locus.

The synthetic genetic components share a common core promoter and transcriptional terminator of *CYC1*, unless otherwise specified. The *CYC1* core promoter, *CYC1*c, is a 137-bp sequence upstream of the start codon of *CYC1*, which contains the TATA box. The upstream activation sequences (UASs), including tetO and *GAL1*, were attached to this core promoter sequence. The Mig1p-binding site in the UAS from *GAL1* was inactivated. A BamHI site was introduced between *CYC1*c and the start codon.

cooperative binding to the circuit, we can assess their contribution to bistability separately. In principle, the following two feedback loops can generate identical bistable ranges: (1) the dimeric transcription factor that binds to a single site in the DNA, provided the concentration of the protein is less than its dimerization equilibrium dissociation constant; and (2) a monomeric factor that binds cooperatively to multiple sites in a promoter with a Hill coefficient of 2 (Májer et al., 2015). However, the binding of rtTA to the cooperative promoter has a Hill coefficient of 1.45 (Becskei et al., 2005). Thus, the larger potential ultrasensitivity of dimerization may explain why bistability had a broader range in the presence of homodimerization than in the presence of cooperative binding (Figure 4A).

Bistability based on dimerization reactions has eluded detection, although the majority of proteins di- or multimerize across all domains of life (Lynch, 2012; Marianayagam et al., 2004). This apparent paradox may have several reasons. First, it is difficult to separate the specific effect of dimerization exactly, because it is ubiquitous. In typical networks, dimerization is combined with other, more evident, ultrasensitive reactions exemplified by sequestration or cooperative binding. Second, a dimerization reaction becomes ultrasensitive and, thus, can support bistability only if the protein concentration is low enough (Buchler and

The stem loop sequences were derived from the following $SL_{6[AT]0}$ sequence, 5′-<u>CCGCGG</u>TTCG<u>CCGCGG</u>-3′ (Beelman and Parker, 1994): 5′-<u>CCGCG</u> TTCG<u>CGCGG</u>-3′ ($SL_{5[AT]0}$), 5′-<u>CCTCG</u>TTCG<u>CGAGG</u>-3′ ($SL_{5[AT]1}$), 5′-<u>CCTTG</u> TTCG<u>CAAGG</u>-3′ ($SL_{5[AT]2}$) and 5′-<u>CCTTA</u>TTCG<u>TAAGG</u>-3′ ($SL_{5[AT]3}$). The stem loops were inserted into the *CYC1*c region of the promoter with a 13-bp spacing before the start codon. The sequences upstream and downstream of the stem loop were ATTACCGGATCA and ATTCGGGggatccATG; the ATG at the 3′ end is the start codon, and ggatcc is a BamHI recognition site. The design of the stem loop was checked by the free energy calculated from the Vienna RNA Websuite (Gruber et al., 2008).

For the rtTA protein, the S2 version of the reverse tetracycline transactivator was used (Becskei et al., 2005). sc-rtTA is a chain of two connected tetRs followed by a single VP16 activation domain. The F86Y and G138D mutations (FYGD) were introduced in both tetRs to enhance transcription activity (Zhou et al., 2007). To reduce recombination within the sc-rtTA sequence, an extra *Hin*DIII site was introduced to the rtTA sequence (silent mutation, position 102 in ORF [open reading frame]), and the sequence of a codon-humanized FYGD version of tetR (Zhou et al., 2007) containing the linker was inserted into the *Hin*DIII site. The *Stu*I and BamHI sites in the ORF sequence were inactivated.

Hysteresis Experiment

General growth conditions and flow cytometry are described in the Supplemental Experimental Procedures. Low and high expression states were created as initial conditions, termed low and high initial conditions. The high initial condition was generated by culturing cells overnight with 2 μM doxycycline and 0.5% galactose, while no inducers were added for the low initial condition. Subsequently, the cultures were transferred to fresh media starting at an optical density at 600 nm (OD_{600}) of 0.2 and grown for additional 4 hr. These cells were then inoculated into media containing a doxycycline concentration range so that cells with different initial conditions were grown in identical conditions. There was no need to wash the cells prior to inoculation to remove the inducers, since the inoculum was diluted at least 1,000 times. The initial culture density was adjusted so that the OD_{600} reaches values between 0.6 and 1.0 at 24 hr.

Translation Rate Constant Determination

The translation rate was determined in steady-state conditions. The protein concentration $[P]$ is governed by:

$$\frac{\mathrm{d}[P]}{\mathrm{dt}} = \rho[mRNA] - \delta_P[P].$$

δ_P is the protein decay rate constant; ρ is the translation rate constant; and $[P]$ and $[mRNA]$ represent the copy numbers of protein and mRNA in a cell, respectively.

Therefore, ρ is equal to $(\delta_P[P]/[mRNA])$ in steady state.

The decay rate constant of the protein was determined as explained in the Supplemental Information. To determine the effect of stem loops on translation, strains (indicated by "Translation rate determination" in the Function column of Table S1) were constructed that express rtTA with different stem loops under the control of GEV. GEV also binds to and activates the GAL promoters, but only in the presence of estradiol. The RNA expression can be tuned over a broad range by adjusting the estradiol concentration (Bonde et al., 2014). In this way, it was possible to express rtTA without growth alterations. Cells were grown for 24 hr with 10 nM or 100 nM estradiol to reach steady-state expression. The culture was split for the quantification of RNA with qPCR and protein with absolute protein quantification by mass spectrometry. To convert the mRNA data measured by qPCR to absolute counts, we measured the ratio of the RNA levels obtained by qPCR to that by smFISH (Supplemental Experimental Procedures). The reported translation rates are averages calculated from the two steady-state expression levels induced with 10 nM or 100 nM estradiol.

The absolute translation rates were verified by assessing relative translation efficiencies with fluorescent reporters, in which the same stem loops were inserted. These haploid strains, indicated in Table S1 with "translation efficiency

strains," were incubated with 80 nM estradiol for 24 hr to reach steady-state expression levels of the fluorescent reporter.

Mathematical Modeling

Details are provided in the Supplemental Information.

SUPPLEMENTAL INFORMATION

Supplemental Information includes Supplemental Experimental Procedures, two figures, and one table and can be found with this article online at http://dx.doi.org/10.1016/j.celrep.2016.06.072.

REFERENCES

Angel, A., Song, J., Dean, C., and Howard, M. (2011). A Polycomb-based switch underlying quantitative epigenetic memory. Nature *476*, 105–108.

Arnoldini, M., Vizcarra, I.A., Peña-Miller, R., Stocker, N., Diard, M., Vogel, V., Beardmore, R.E., Hardt, W.D., and Ackermann, M. (2014). Bistable expression of virulence genes in salmonella leads to the formation of an antibiotic-tolerant subpopulation. PLoS Biol. *12*, e1001928.

Becskei, A., Séraphin, B., and Serrano, L. (2001). Positive feedback in eukaryotic gene networks: cell differentiation by graded to binary response conversion. EMBO J. *20*, 2528–2535.

Becskei, A., Kaufmann, B.B., and van Oudenaarden, A. (2005). Contributions of low molecule number and chromosomal positioning to stochastic gene expression. Nat. Genet. *37*, 937–944.

Beelman, C.A., and Parker, R. (1994). Differential effects of translational inhibition in cis and in trans on the decay of the unstable yeast MFA2 mRNA. J. Biol. Chem. *269*, 9687–9692.

Belle, A., Tanay, A., Bitincka, L., Shamir, R., and O'Shea, E.K. (2006). Quantification of protein half-lives in the budding yeast proteome. Proc. Natl. Acad. Sci. USA *103*, 13004–13009.

Bonde, M.M., Voegeli, S., Baudrimont, A., Séraphin, B., and Becskei, A. (2014). Quantification of pre-mRNA escape rate and synergy in splicing. Nucleic Acids Res. *42*, 12847–12860.

Bouchoucha, Y.X., Reingruber, J., Labalette, C., Wassef, M.A., Thierion, E., Desmarquet-Trin Dinh, C., Holcman, D., Gilardi-Hebenstreit, P., and Charnay, P. (2013). Dissection of a Krox20 positive feedback loop driving cell fate choices in hindbrain patterning. Mol. Syst. Biol. *9*, 690.

Brophy, J.A., and Voigt, C.A. (2014). Principles of genetic circuit design. Nat. Methods *11*, 508–520.

Buchler, N.E., and Louis, M. (2008). Molecular titration and ultrasensitivity in regulatory networks. J. Mol. Biol. *384*, 1106–1119.

Buetti-Dinh, A., Ungricht, R., Kelemen, J.Z., Shetty, C., Ratna, P., and Becskei, A. (2009). Control and signal processing by transcriptional interference. Mol. Syst. Biol. *5*, 300.

Chappell, J., Watters, K.E., Takahashi, M.K., and Lucks, J.B. (2015). A renaissance in RNA synthetic biology: new mechanisms, applications and tools for the future. Curr. Opin. Chem. Biol. *28*, 47–56.

Cheeseman, B.L., Zhang, D., Binder, B.J., Newgreen, D.F., and Landman, K.A. (2014). Cell lineage tracing in the developing enteric nervous system: superstars revealed by experiment and simulation. J. R. Soc. Interface *11*, 20130815.

Chen, D., and Arkin, A.P. (2012). Sequestration-based bistability enables tuning of the switching boundaries and design of a latch. Mol. Syst. Biol. *8*, 620.

Chickarmane, V., Enver, T., and Peterson, C. (2009). Computational modeling of the hematopoietic erythroid-myeloid switch reveals insights into cooperativity, priming, and irreversibility. PLoS Comput. Biol. *5*, e1000268.

Chiodini, F., Matter-Sadzinski, L., Rodrigues, T., Skowronska-Krawczyk, D., Brodier, L., Schaad, O., Bauer, C., Ballivet, M., and Matter, J.M. (2013). A positive feedback loop between ATOH7 and a Notch effector regulates cell-cycle progression and neurogenesis in the retina. Cell Rep. *3*, 796–807.

Ferrell, J.E., Jr., and Ha, S.H. (2014). Ultrasensitivity part III: cascades, bistable switches, and oscillators. Trends Biochem. Sci. *39*, 612–618.

Gruber, A.R., Lorenz, R., Bernhart, S.H., Neuböck, R., and Hofacker, I.L. (2008). The Vienna RNA websuite. Nucleic Acids Res. *36*, W70–W74.

Guertin, M.J., Zhang, X., Coonrod, S.A., and Hager, G.L. (2014). Transient estrogen receptor binding and p300 redistribution support a squelching mechanism for estradiol-repressed genes. Mol. Endocrinol. *28*, 1522–1533.

Kamionka, A., Majewski, M., Roth, K., Bertram, R., Kraft, C., and Hillen, W. (2006). Induction of single chain tetracycline repressor requires the binding of two inducers. Nucleic Acids Res *34*, 3834–3841.

Kelleher, R.J., 3rd, Flanagan, P.M., and Kornberg, R.D. (1990). A novel mediator between activator proteins and the RNA polymerase II transcription apparatus. Cell *61*, 1209–1215.

Kueh, H.Y., Champhekar, A., Nutt, S.L., Elowitz, M.B., and Rothenberg, E.V. (2013). Positive feedback between PU.1 and the cell cycle controls myeloid differentiation. Science *341*, 670–673.

Lynch, M. (2012). The evolution of multimeric protein assemblages. Mol. Biol. Evol. *29*, 1353–1366.

Májer, I., Hajihosseini, A., and Becskei, A. (2015). Identification of optimal parameter combinations for the emergence of bistability. Phys. Biol. *12*, 066011.

Marianayagam, N.J., Sunde, M., and Matthews, J.M. (2004). The power of two: protein dimerization in biology. Trends Biochem. Sci. *29*, 618–625.

McKeague, M., Wong, R.S., and Smolke, C.D. (2016). Opportunities in the design and application of RNA for gene expression control. Nucleic Acids Res. *44*, 2987–2999.

Park, B.O., Ahrends, R., and Teruel, M.N. (2012). Consecutive positive feedback loops create a bistable switch that controls preadipocyte-to-adipocyte conversion. Cell Rep. *2*, 976–990.

Schmidt, S.F., Larsen, B.D., Loft, A., Nielsen, R., Madsen, J.G., and Mandrup, S. (2015). Acute TNF-induced repression of cell identity genes is mediated by NFκB-directed redistribution of cofactors from super-enhancers. Genome Res. *25*, 1281–1294.

Shopera, T., Henson, W.R., Ng, A., Lee, Y.J., Ng, K., and Moon, T.S. (2015). Robust, tunable genetic memory from protein sequestration combined with positive feedback. Nucleic Acids Res. *43*, 9086–9094.

Tan, C., Marguet, P., and You, L. (2009). Emergent bistability by a growth-modulating positive feedback circuit. Nat. Chem. Biol. *5*, 842–848.

Thomson, M., and Gunawardena, J. (2009). Unlimited multistability in multisite phosphorylation systems. Nature *460*, 274–277.

Tian, X.J., Zhang, X.P., Liu, F., and Wang, W. (2009). Interlinking positive and negative feedback loops creates a tunable motif in gene regulatory networks. Phys. Rev. E Stat. Nonlin. Soft Matter Phys. *80*, 011926.

To, T.L., and Maheshri, N. (2010). Noise can induce bimodality in positive transcriptional feedback loops without bistability. Science *327*, 1142–1145.

Zhou, X., Symons, J., Hoppes, R., Krueger, C., Berens, C., Hillen, W., Berkhout, B., and Das, A.T. (2007). Improved single-chain transactivators of the Tet-On gene expression system. BMC Biotechnol. *7*, 6.

Supplemental Information

Protein Dimerization Generates Bistability

in Positive Feedback Loops

Chieh Hsu, Vincent Jaquet, Mumun Gencoglu, and Attila Becskei

Protein dimerization generates bistability in positive feedback loops

Chieh Hsu, Vincent Jaquet, Mumun Gencoglu & Attila Becskei

Supplemental Figures
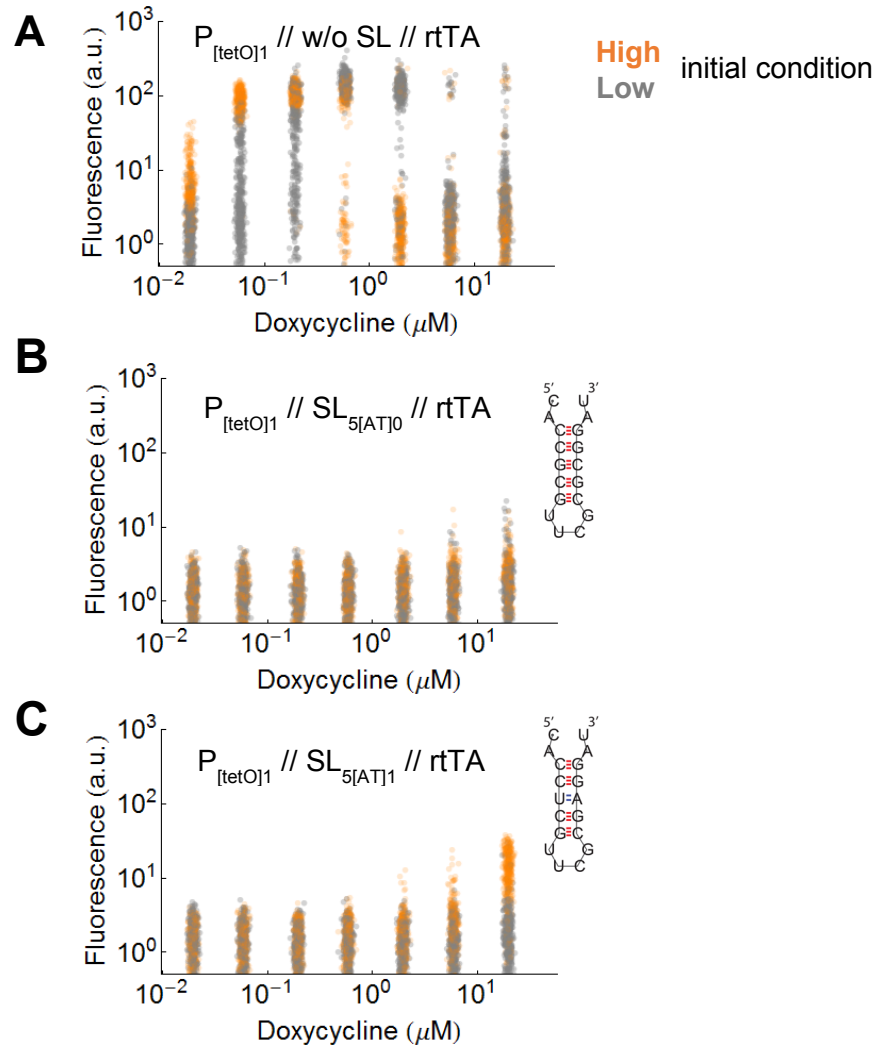
Figure S1. Hysteresis experiments of the non-optimized non-cooperative-dimeric feedback loops.

Related to Figure 2.

Cells with low (gray dots) or high (orange dots) initial condition were grown at the indicated doxycycline concentrations for 24 h. **(A)** Without stem-loop, the non-cooperative-dimeric feedback loop displayed atypical hysteresis; cells with both initial conditions had low expression at high doxycycline concentration. **(B-C)** Too strong stem-loops prevented the system from reaching the high expression state.

Figure S2. Comparison of bistability in positive and dual positive-negative feedback loops.

Related to Figure 4.

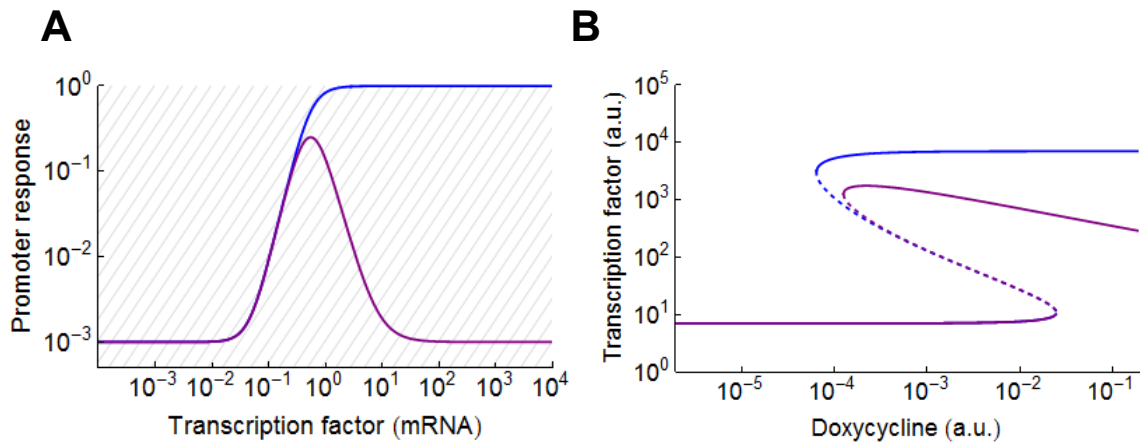**(A)** Response of promoters incorporated into the positive and the dual positive-negative feedback loops. The blue line stands for the response of the cooperative promoter to the dimeric transcription factor, with the same parameters as in Figure 1B. The purple line denotes the corresponding bell-shaped response. The promoter response is the gene expression controlled by the transcription factor (TF). The TF is expressed in units of the mRNA encoding the TF. The ultrasensitivity of the two responses is similar, as indicated by the similar relative slopes (see in comparison gray lines, which mark the minimal steepness for an ultrasensitive response). **(B)** Bistability in the feedback loop incorporating the promoter with cooperative (sigmoidal, blue curve) or bell-shaped response (purple curve). The stable (solid) and unstable (dashed) steady-state expression levels are shown. The blue curve is identical to that in Figure 1B. Details for equations are provided in the Supplemental Experimental Procedures.

Supplemental Table

Table S1. Yeast strains. Related to Experimental Procedures.

Diploid Strain	Haploid parents	ade2:: **ADE2_**	ura3:: **URA3_**	his3:: **HIS3_**	Function
	A				
	alpha				
Yvj87.2	Yvj79.2		P_[tetO]7- *CYC1*c | SL_5[AT]1 | rtTA (pCH068)	P_*MRP7* | GEV (pPR1)	Feedback
	Yvj70.1	P_*GAL1*UAS-*CYC1*c | SL_5[AT]1 |rtTA (pVJ46)	P_[tetO]2- *CYC1*c | *yEGFP* (pABG10)		
Yvj99	Yvj89.1		P_[tetO]1- *CYC1*c | SL_5[AT]2 | rtTA (pVJ42)	P_*MRP7* | GEV (pPR1)	Feedback
	Yvj91.6	P_*GAL1*UAS-*CYC1*c | SL_5[AT]2 |rtTA (pCH094)	P_[tetO]2-*CYC1*c | *yEGFP* (pABG10)		
Ych260.2	Yvj80.1		P_[tetO]7- *CYC1*c | SL_5[AT]3 | sc-rtTA (pCH91)	P_*MRP7* | GEV (pPR1)	Feedback
	Ych250.2	P_*GAL1*UAS-*CYC1*c | SL_5[AT]3 | sc-rtTA (pCH102)	P_[tetO]2- *CYC1*c | *yEGFP* (pABG10)		
Yvj109.5	Yvj107.5		P_[tetO]1- *CYC1*c | SL_5[AT]3 | sc-rtTA (pCH083)	P_*MRP7* | GEV (pPR1)	Feedback
	Ych250.2	P_*GAL1*UAS-*CYC1*c | SL_5[AT]3 | sc-rtTA (pCH102)	P_[tetO]2- *CYC1*c | *yEGFP* (pABG10)		
Yvj151.3	Yvj150.3	P_[tetO]7-TATA-[tetO]2 *CYC1*c | rtTA (pMG01)		P_*MRP7* | GEV (pPR1)	Feedback
	Ych178.2	P_*GAL1*UAS-*CYC1*c | rtTA (pCH099)	P_[tetO]1- *CYC1*c | *yEGFP* (pCH001)		
Ych270	Yvj92.7		P_[tetO]1- *CYC1*c | *yEGFP* (pCH001)	P_*MRP7* | GEV (pPR1)	Translation rate determination
	Ych171.2	P_*GAL1*UAS-*CYC1*c | rtTA (pCH099)			
Ych267	Yvj92.7		P_[tetO]1- *CYC1*c | *yEGFP* (pCH001)	P_*MRP7* | GEV (pPR1)	Translation rate determination
	Ych240.8	P_*GAL1*UAS-*CYC1*c | SL_5[AT]3 |rtTA pCH101			
Ych235.7	Yvj92.7		P_[tetO]1- *CYC1*c | *yEGFP* (pCH001)	P_*MRP7* | GEV (pPR1)	Translation rate determination
	Ych169.7	P_*GAL1*UAS-*CYC1*c | SL_5[AT]2 |rtTA (pCH094)			
Ych268	Yvj92.7		P_[tetO]1- *CYC1*c | *yEGFP* (pCH001)	P_*MRP7* | GEV (pPR1)	Translation rate determination
	Yvj67.4	P_*GAL1*UAS-*CYC1*c | SL_5[AT]1 | rtTA (pVJ46)			

Diploid Strain	Haploid parents	Integration locus (plasmid)			Function
	A	*ade2:: **ADE2_***	*ura3:: **URA3_***	*his3::* **HIS3_**	
	alpha				
Ych271	Yvj92.7		P_[tetO]1- *CYC1*c ǀ *yEGFP* (pCH001)	P_*MRP7* ǀ GEV (pPR1)	Translation rate determination
	Ych084.1	P_*GAL1*UAS-*CYC1*c ǀ SL_6[AT]0 ǀ rtTA (pCH059)			
Yvj10.1	Yvj8.1	P_[tetO]7- *CYC1*c ǀ rtTA (pJK34)			Initial feedback construct
	Yvj1.3		P_[tetO]2- *CYC1*c ǀ *yEGFP* (pABG10)	P_*GAL1*UAS ǀ rtTA (pMG2)	
Yvj47.4	Yvj44.4	P_[tetO]1- *CYC1*c ǀ rtTA (pJK32)			Initial feedback construct
	Yvj1.3		P_[tetO]2- *CYC1*c ǀ *yEGFP* (pABG10)	P_*GAL1*UAS ǀ rtTA (pMG2)	
Yvj130	Yvj29 [*]				Initial feedback construct
	Yvj36.5	P_[tetO]7- *CYC1*c ǀ SL_6[AT]0 ǀ rtTA (pVJ11)	P_[tetO]2- *CYC1*c ǀ *yEGFP* (pABG10)	P_*GAL1*UAS ǀ rtTA (pMG2)	
Yvj131	Yvj29 [*]				Initial feedback construct
	Yvj49.1	P_[tetO]1- *CYC1*c ǀ SL_5[AT]0 ǀ rtTA (pVJ23)	P_[tetO]2- *CYC1*c ǀ *yEGFP* (pABG10)	P_*GAL1*UAS ǀ rtTA (pMG2)	
Yvj132	Yvj29 [*]				Initial feedback construct
	Yvj55.8	P_[tetO]1- *CYC1*c ǀ SL_5[AT]1 ǀ rtTA (pVJ26)	P_[tetO]2- *CYC1*c ǀ *yEGFP* (pABG10)	P_*GAL1*UAS ǀ rtTA (pMG2)	
Ych294	Yvj40.3			P_*MRP7* ǀ GEV (pPR1)	smFISH negative control
	Ych89.2	(pRS402)	P_[tetO]2- *CYC1*c ǀ *yEGFP* (pABG10)		
MAT A	Ych242.6	P_*GAL1*UAS-*CYC1*c ǀ ǀ rtTAΔ(45/45)::YFP (pCH93)		P_*MRP7* ǀ GEV (pPR1)	Translation efficiency
MAT A	Ych248.5	P_*GAL1*UAS-*CYC1*c ǀ SL_5[AT]3 ǀ rtTAΔ(45/45)::YFP (pCH100)		P_*MRP7* ǀ GEV (pPR1)	Translation efficiency
MAT A	Ych247.3	P_*GAL1*UAS-*CYC1*c ǀ SL_5[AT]2 ǀ rtTAΔ(45/45)::YFP (pCH095)		P_*MRP7* ǀ GEV (pPR1)	Translation efficiency
MAT A	Ych211.2	P_*GAL1*UAS-*CYC1*c ǀ SL_5[AT]1 ǀ rtTAΔ(45/45)::YFP (pVJ47)		P_*MRP7* ǀ GEV (pPR1)	Translation efficiency
MAT A	Yvj136.5	P_*GAL1*UAS-*CYC1*c ǀ SL_6[AT]0 ǀ rtTAΔ(45/45)::YFP (pCH60)		P_*MRP7* ǀ GEV (pPR1)	Translation efficiency

[*] Yvj29: *leu2*::*LEU2* (pRS305)

Supplemental Experimental Procedures

Growth conditions

Cells were cultured at 30°C in synthetic medium containing yeast nitrogen base, 2% filter-sterilized raffinose and 0.02% glucose as carbon source and the -Ade/-His/-Ura drop-out supplement, unless otherwise indicated. Overnight and refreshment cultures (5ml) were grown in 50 ml culture flasks. Cultures of 0.6 ml were induced by doxycycline (dox) and were grown in 96-well plates with 1.2 ml capacity. The doxycycline concentration did not exceed 40 μM, above which toxic effects can arise (Ratna and Becskei, 2011). The plates were covered with breathable rayon films and shaken at 600 rpm. Alternative growth conditions are specified in context.

Shutting off gene expression to determine protein decay rate

To determine protein decay rate constants shut-off assays were performed. The cells were cultured overnight with 0.5 % galactose and transferred to a refreshment medium containing 0.05% galactose for further growth for 4 hours. To shut off P_{GAL} expression, the cells were pelleted and cultured further in medium without galactose. 5 ml culture was collected at each indicated time point. The cell density was kept below an OD600 of 1.0 throughout the course of the experiment.

Flow cytometry

The flow cytometry was used to read out the activity of rtTA through reporter genes. GFP fluorescence was measured by FACSCanto™ II (BD bioscience) Flow Cytometer using the 488 nm laser and the 530/30 nm band pass emission filter, coupled to a 502 nm long pass dichroic mirror. Gating based on the forward- and side-scatter signal was performed to omit the cell debris and clusters. At least 5,000 cell events were recorded for a single measurement.

Single mRNA fluorescence *in situ* hybridization (smFISH)

Cell handling, image acquisition and quantification methods for smFISH were performed as previously described (Bonde et al., 2014) with minor modifications**.** The Stellaris probe set for rtTA (fluorescence label: quasar 670, 30 probes) was designed to cover the sequence of the TetR domain of rtTA (S2 version) which detect both rtTA and sc-rtTA RNA species. The probe set did not cover the VP16 sequence to prevent cross-detection of GEV. Probe set for a proteasome gene, *PRE2*, (quasar 570, 39 probes) was used as a positive control for cell integrity.

The following sequences were used to detect rtTA / scrTA: (5'->3'): TAAGCCCCCTAGGTACGGAT, AATCTATTTTCATTTCACTA, GTCGCGTAATCTCGACGAAT, CCCCAGCCTTAGCTTCCAAA, GTTGGGCATTTGAGCGGGTC, CTGCTGTTCCTTTGAGCGAG, TTCGAACCACATCTCGTCGG, GTAACATAACCGTACATTTT, ATTCGCCCGAAACGAGCTGC, AATGGGTAACTCTACAATCT, CCGTGGTATGAGTGAAAACG, AAATCTTCCCCTTTCGACCG, CTAAAAAATGCATTATTGCG, TTTCAATATCTACACGAAAT, TTCAGTAGCGCTACCTCGTT, CATGTAAATCCATGTGCCGG, GTCTTTTTGTCATACTTTGA, GCTTTTAGTTAATCGGAAAA, ACGGTTGTTCCAAAAAGTGA, TCTTACGTAATATACGTGAG, GCGACACCTGGTGAAATGAA, CCAACGCATAACCTTCTTGT, TCGTAGTTCAGCGATTTCTT, TTCCCTTTGTGGATGATGAC, TCATACGGCGGTAATAATGC, TTCGATAGCTTAATAAACTA, GGTTCCACGTCTCGGTCGGA, AATAAGCCGGAACTTAACTA, ATACGCCTAATCTTTTTGTT & ATTTACACTTTCACCCAGGC.

The following sequences were used to detect PRE2: (5'->3'): TACGTTCGATAACGGCTATC, AGTCACATGGTTTGTCTAAC, ATTCCTTGAAGTTATACTGT, CTTGTTTTGAATCTCTCGCT, AGCATTGCCCGCGGAGGGTC,AGTTGCAAACCGTGGTAGCG, TGCCAAGGTGGTTAACGCAG, GTGTCGTCAAAAATTCTCGT, GTGTCTACTAAGTGCTTTGG, CTGACATTTTAGTTCTAGCG, TACCATGATGTTGGAATCGT, ATCTAAAGTTCCGCCATAAT, CACCGTCATCTAAGAGCACG, GACGGCCGTTAACCCAACGA, AGTTTGACACTTCTTTCAAT, CTCTAGTTGGGTAAAAATAA, CATGTTACCGACCACCACGC, TCTAACAGTTAAAACCCTTT, ACCGATCCAAGAGTCACATC, ACGTGCTCGACTCCCTTTTC, TGCATATAGACAGCGTCGGC, AGGTTCTAAAATTCGTTAAA, ATATGGTTATATTTCCCCGG, AAATAGTTACCCATGATACT, ACACCAATGTGATCCTTCCT, CGGGTTGGTAAATAATGCAG, GAGTCTGCCATGTTCTAATT, CCACTGTATAAGACGCAACC, GTCCAGTTTGTAAACGTATA, ACAAGATCTGAGATTGATAT, ACCCTAAATAGGCAACTTCT, ATATAGATCCATTCTCTAGA, AAATCGACGACGGGTATCTC, CGAATGAGACCACCAAGACA, TATAGTACAATGGCTCCTAC, ACCTATATAGTGCCATTAGT, TGCATCCACTTGATAAAACC, CCAGTTCCTTCTCCTTCCTA & AAGTTGTTGCAATAACCGAT.

Images were obtained with Deltavision microscopic system and the exposure settings were fixed within an acquisition batch. RNA spots were detected by FISH-quant toolbox in MATLAB (Mueller et al., 2013). At least 140 cells were quantified for the measurement.

Quantification of RNA by qPCR

The quantification of mRNA was performed by qPCR unless otherwise specified. Cell samples were snap-frozen with liquid nitrogen and the RNA was isolated with the RiboPure Kit (Ambion). oligo(dT) was used to prime reverse transcription (Superscript III, Invitrogen). The qPCR was performed with

KAPA SYBR FAST qPCR Kit (Kapa Biosystems) using the Lightcycler 480 II system (Roche). To quantify the intact full-length rtTA and sc-rtTA RNA, we used primer pairs for qPCR that anneal to the upstream parts of the cDNA. The forward primer sequence covers the start codon and part of the 5'UTR and it is identical for both rtTA / sc-rtTA (F: 5'-CGGGGGATCCATGCCTAGATTA-3', R: 5'-GCGAGTTTACGGGTTGTTAAACCTT-3') primer pairs.

The obtained Cp values were used to calculate RNA levels taking account of the efficiency of reverse transcription and amplification (see below). RNA expression levels were normalized by the geometric mean of UBC6 and TFC1 expression, which were shown to have minimal variations across different growing conditions (Teste et al., 2009).

We measured the overall efficiency of the enzymatic steps in the RNA quantification process, comprising the reverse transcription (RT) and PCR amplification. For this purpose, a series of target RNA concentrations was prepared by mixing RNA isolated from cells having the target genes and that lacking it, in different ratios. Before mixing, the RNA samples were diluted to have equal concentrations. The concentration of RNA was assessed with the help of spectrophotometer at a wavelength of 260 nm. The overall efficiency of the enzymatic steps was determined with linear regression to model the relationship between the cycle numbers (Cp) and mixing ratio of the target RNA. The efficiency for the rtTA/ sc-rtTA primer pair was 1.931.

The specificity of the primer set was checked *in silico* with primer-Blast. In addition, we verified experimentally this specificity and we obtained Cp values of 32.08 for a control strain, lacking the above sequences. In comparison, Cp value of 25.59 was obtained for the cooperative-dimeric feedback strain where the gene is expressed at a basal level. Thus, the nonspecific background signal is around 100 times less than the signal corresponding to the lowest RNA levels encountered in our experiments.

Absolute mRNA quantification with qPCR and smFISH

To convert the RNA quantified in qPCR to the absolute mRNA number in the cell, we performed both qPCR and smFISH at high expression states with the non-cooperative – dimeric feedback strain (Yvj99). The mRNA was measured as 27.03 (relative to the geometric mean of *UBC6* and *TFC1* expression) with qPCR and 77.30±1.72 (mean±*SE*) with smFISH (*n*=143 cells). We obtained a constant ratio of these two measurements:

$$\frac{\left[Number\ of\ mRNA\ per\ cell\ as\ in\ smFISH\right]}{\left[qPCR\ RNA\ quantification\right]} = \frac{77.30}{27.03} = 2.86$$

As the control of smFISH detection, all cells were *PRE2* positive with 10.97±0.32 (mean±*SE*) RNA molecule per cell in the same experiment. The background level of rtTA RNA (false positive) count was ~0.03 spots per cell, in cells without the rtTA construct (Ych294). The spot intensity distribution was unimodal, indicating that a single molecule was detected at each spot (Raj et al., 2008).

Absolute protein quantification by mass spectrometry

Protein quantification was performed by mass spectrometry as previously described, with minor modifications (Picotti et al., 2009). Cell samples were snap-frozen with liquid nitrogen. Cell pellets were resuspended in 100µl lysis buffer (100 mM ammoniumbicarbonate, 8M urea, 0.1% RapiGest™). The cells were disrupted by vortexing for 3 x 30 seconds followed by sonication (100% amplitude, 0.5 cycle, 3×10 s) in a VialTweeter (Hielscher). 10 µl aliquot of the supernatant was taken to determine the protein concentration of each sample using a BCA assay (Thermo Fisher Scientific). Proteins obtained from the different samples were reduced with 5 mM tris(2-carboxyethyl)phosphine (TCEP) for 60min at 37°C and alkylated with 10 mM iodoacetamide for 30min in the dark at 25°C. After quenching the reaction with 12 mM N-acetyl-cysteine, the proteins were proteolyzed for 4 h at 37°C using sequencing-grade Lys-C (Wako Chemicals) at 1/200 w/w. Then, the samples were diluted with 100 mM ammoniumbicarbonate buffer to a final urea concentration of 1.6 M and further digested by incubation with sequencing-grade modified trypsin (1/50, w/w; Promega, Madison, Wisconsin) over night at 37°C. The samples were acidified with 2 M HCl to a final concentration of 50 mM, incubated for 45 min at 37°C and the cleaved detergent removed by centrifugation at 14,000 g for 5min. Subsequently, an aliquot of the heavy reference peptide mix were spiked into each sample at a concentration of 200 fmol of heavy reference peptides per 1µg of total endogenous protein mass. All peptide samples were then desalted by C18 reversed-phase spin columns according to the manufacturer's instructions (Macrospin, Harvard Apparatus), separated in aliquots of 150 µg peptides, dried under vacuum and stored at -80ºC until further use. For LC-MS analysis, samples were solubilized in solvent A (98% water, 2% acetonitrile, 0.15% formic acid) at a concentration of 0.5 µg/µl and 3 µl were injected per LC-MS run.

For absolute quantification of rtTA, heavy reference peptides were selected matching the sequence of the endogenous peptide with the highest precursor ion MS-intensity determined in the label-free quantification experiment. Peptides containing missed cleavages or a glutamine at the N-terminus were excluded. The following endogenous peptides were detected after scan run for the full spectrum: (1) ALLDALPIEMLDR, (2) ETPTTDSMPPLLR, (3) FEGDTLVNR, (4) FSVSGEGEGDATYGK, (5) LGVEQPTLYWHVK, (6) LSFLPAGHTR, (7) VHLGTRPTEK, (8) VINSALELLNGVGIEGLTTR, (9)

CALLSHR, (10) QAIELFDR. To synthesize heavy isotope labelled peptides, five peptide sequences were selected (2, 3, 5, 6, 7) that had the highest peaks.

To generate the selective reaction monitoring (SRM) assays, a mixture containing 500 fmol of each reference peptide was analyzed by shotgun LC-MS/MS using high collision dissociation (HCD) fragmentation, database searched by Mascot applying the same settings as above with two changes; isotopically labeled arginine (+10 Da) and lysine (+8 Da) were added as variable modifications and the mass tolerance for MS2 fragments was set to 0.02 Da. The resulting dat-file was imported to skyline version 1.4 (https://brendanx-uw1.gs.washington.edu/labkey/project/ home/software/Skyline/begin.view) to generate a spectral library and select the best transitions for each peptide. After collision energy optimization, the final transition list were imported to a triple quadrupole mass spectrometer (TSQ Vantage) connected to an electrospray ion source (both ThermoFisher Scientific). Peptide separation was carried out using an Easy-LC systems (ThermoFisher Scientific) equipped with a RP-HPLC column (75 μm x 20 cm) packed in-house with C18 resin (Magic C18 AQ 3 μm; Michrom BioResources) using a linear gradient from 95% solvent A (0.15% formic acid, 2% acetonitrile) and 5% solvent B (98% acetonitrile, 0.15% formic acid) to 35% solvent B over 90 minutes at a flow rate of 0.2 μl/min. Each sample was analyzed in duplicate. All raw-files were imported into Skyline for protein quantification.

Based on the number of cells counted for each sample, absolute abundances for the selected proteins (in copies/cell) were calculated across all samples.

Mathematical modeling of positive feedback loops

The response of the promoter to the transcription factor C is denoted $f(C)$:

$$f(C) = \frac{C^n}{C^n + \dfrac{K}{dox}} + \frac{b}{V_{max}} \tag{1a}$$

V_{max} and b defines the maximum and minimum expression rate; n is the Hill number, which indicates the cooperativity of the transcription factor (TF) binding to the promoter; dox represents concentration of the ligand, doxycycline, which controls the binding strength (K) of the transcription factor to the promoter.

For the promoter with a bell-shaped response, C has both an activating and inhibitory effect:

$$f(C) = \frac{C^n}{C^n + \dfrac{K}{dox}} \cdot \frac{\dfrac{K}{dox}}{C^n + \dfrac{K}{dox}} + \frac{b}{V_{max}} \tag{1b}$$

When the TF dimerizes, the following set of differential equations describe the feedback loop:

$$\frac{dM}{dt} = V_{max}\, f\left(C\right) - \delta_M\, M \tag{2}$$

$$\frac{dA}{dt} = \rho\, M - 2k_a A^2 + 2k_d\, C - A\delta_A \tag{3}$$

$$\frac{dC}{dt} = k_a\, A^2 + k_d\, C - C\delta_C \tag{4}$$

where M stands for mRNA, ρ for translation rate, and A and C for the monomeric and dimeric forms of the transcription factor, respectively; k_a and k_d denote for the association and dissociation constants; all species are subjected to exponential decay with decay rates (δ_M, δ_A & δ_C).

For the cooperative-dimeric loop, the system's parameters were assigned as following: $V_{max} = 238$; $b = V_{max}/1000$; $n=1.45$; $K = 1$; $\delta_M = 2.079$; $\rho = 32.4$; $k_a = 1$; $k_d = 1000$; $\delta_A = \delta_C = 0.528$. The time units are given in hr, so that the translation rate corresponds to 0.54 min^{-1}.

For the monomeric feedback loop, only equations (2) and (5) are used:

$$\frac{dC}{dt} = \rho M - \delta_C C \tag{5}$$

C stands for the monomeric TF in (5). For the feedback loop with non-cooperative promoter binding, $n = 1$.

The total protein concentration of the TF (2C+A for the dimeric TF, and C for the monomeric TF) was solved numerically at steady state and plotted against dox in Figure 1B and S2B. In Figure S2A, the promoter functions (1) were plotted with (3) and (4) at steady state and against mRNA, M. The binding strength of transcription factor to DNA was fixed at $dox = 1$.

Supplemental References

Becskei, A., Kaufmann, B.B., and van Oudenaarden, A. (2005). Contributions of low molecule number and chromosomal positioning to stochastic gene expression. Nat Genet *37*, 937-944.

Bonde, M.M., Voegeli, S., Baudrimont, A., Seraphin, B., and Becskei, A. (2014). Quantification of pre-mRNA escape rate and synergy in splicing. Nucleic Acids Res *42*, 12847-12860.

Mueller, F., Senecal, A., Tantale, K., Marie-Nelly, H., Ly, N., Collin, O., Basyuk, E., Bertrand, E., Darzacq, X., and Zimmer, C. (2013). FISH-quant: automatic counting of transcripts in 3D FISH images. Nat Methods *10*, 277-278.

Picotti, P., Bodenmiller, B., Mueller, L.N., Domon, B., and Aebersold, R. (2009). Full dynamic range proteome analysis of S. cerevisiae by targeted proteomics. Cell *138*, 795-806.

Raj, A., van den Bogaard, P., Rifkin, S.A., van Oudenaarden, A., and Tyagi, S. (2008). Imaging individual mRNA molecules using multiple singly labeled probes. Nat Methods *5*, 877-879.

Ratna, P., and Becskei, A. (2011). Construction of cis-Regulatory Input Functions of Yeast Promoters. Methods Mol Biol *734*, 45-61.

Teste, M.A., Duquenne, M., Francois, J.M., and Parrou, J.L. (2009). Validation of reference genes for quantitative expression analysis by real-time RT-PCR in Saccharomyces cerevisiae. BMC Mol Biol *10*, 99.

III. Contribution of bistability and noise to cell fate transitions determined by feedback opening

jmb
Journal of molecular biology

Special Issue :
Glycosylation in Cellular Processes and Disease

Contribution of Bistability and Noise to Cell Fate Transitions Determined by Feedback Opening

Chieh Hsu[1,2,†], Vincent Jaquet[1,†], Farzaneh Maleki[1] and Attila Becskei[1]

1 - *Biozentrum, University of Basel, Klingelbergstrasse 50/70, 4056 Basel, Switzerland*
2 - *School of Biosciences, University of Kent, Canterbury, Kent CT2 7NJ, UK*

Correspondence to Attila Becskei: attila.becskei@unibas.ch
http://dx.doi.org/10.1016/j.jmb.2016.07.024
Edited by Sarah A. Teichmann

Abstract

Alternative cell fates represent a form of non-genetic diversity, which can promote adaptation and functional specialization. It is difficult to predict the rate of the transition between two cell fates due to the strong effect of noise on feedback loops and missing parameters. We opened synthetic positive feedback loops experimentally to obtain open-loop functions. These functions allowed us to identify a deterministic model of bistability by bypassing noise and the requirement to resolve individual processes in the loop. Combining the open-loop function with kinetic measurements and reintroducing the measured noise, we were able to predict the transition rates for the feedback systems without parameter tuning. Noise in gene expression was the key determinant of the transition rates inside the bistable range. Transitions between two cell fates were also observed outside of the bistable range, evidenced by bimodality and hysteresis. In this case, a slow transient process was the rate-limiting step in the transitions. Thus, feedback opening is an effective approach to identify the determinants of cell fate transitions and to predict their rates.

Introduction

Genetically identical cells with two distinct phenotypes can coexist and persist in an identical environment, provided they were exposed to different conditions in the past and can display bistability. Bistability plays important rules in adaptation and cell differentiation in uni- and multicellular organisms. Typically, bistability arises due to positive feedback loops [1–3].

In a bistable feedback, a feedback component can have either low or high concentration in the steady state. Which state is reached depends only on the initial condition. If, initially, an external factor induces a cell to express a sufficiently high concentration of a component, the high expression will persist even after the factor is removed. Such a purely deterministic view of steady-state bistability needs to be modified in biological systems because transitions occur between two states. Transition rates can span a broad range; it is a rare event, for example, in the lysis–lysogeny cycle of the lambda phage. On the other hand, bacteria can switch to the competent form at high frequency [4,5]. The prediction of these

rates is crucial because they determine the proportion of the two cell types in a cell population and the efficiency of cellular reprogramming [6,7].

Typically, noise is considered a driving force of such transitions in genetic systems [8]. The interaction between a bistable system and noise is often conceptualized by depicting the deterministic bistable system by a potential landscape; the two stable states correspond to the two lowest points in the potential wells, which are separated by a barrier (Fig. 1a) [9]. When the system is exposed to noise, small fluctuations may not be sufficient to switch the cells to the other state, but larger fluctuations would do this (Fig. 1a, lower left panel). On the other hand, if the barrier is lower, even weak noise can switch the cells (Fig. 1a, lower right panel).

Thus, bistability amplifies the effect of noise; a sufficiently strong noise can induce most of the cells to switch to the higher state even though the deterministic description predicts the system to be at the low state. Consequently, the deterministic and stochastic descriptions of bistable systems are completely different [10], which makes the prediction
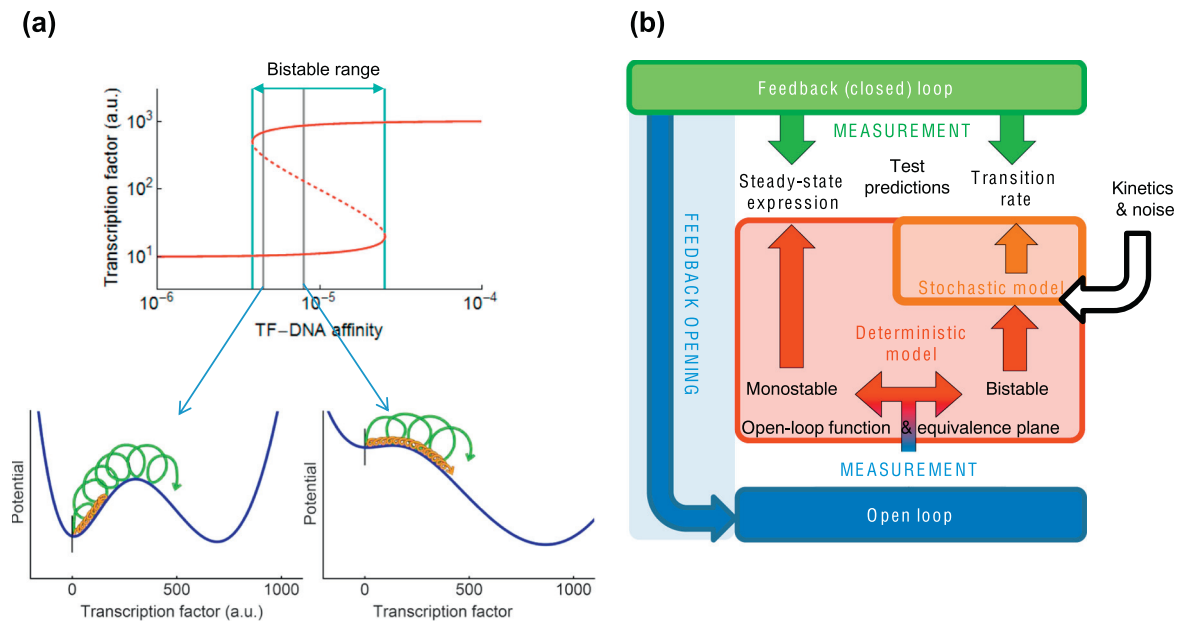
(a)

(b)

Fig. 1. Prediction of transition rates in bistable feedback loops. (a) A positive feedback loop displays bistability in a certain range of TF-DNA affinities. The two stable states correspond to potential wells. At higher TF-DNA affinity, the lower potential well becomes shallower (right panel) and the cells can more easily switch to the high state. The frequency of the transition is also influenced by noise intensity: weak noise (orange) and strong noise (green). (b) Prediction of transition rates and steady-state expression by feedback opening. The feedback loop is opened experimentally. The resulting open-loop function and the equivalence plane constitute a simple deterministic model. If they have a single intersection, the parent feedback is monostable. In this case, the intersection, which we termed open-to-closed loop mapping, can be directly compared to the measured steady-state expression in the feedback loop. If the parent feedback is classified as bistable, the open-loop function must be extended to a model by fitting the parameters to kinetic and noise measurements. The resulting stochastic model predicts the transition rates. The predictions are verified by measuring the feedback loop.

of the rates difficult. A possible way to predict the transitions is to measure individual reactions *in vitro* or *in vivo* and to combine all the reaction parameters into a model. However, many parameters in a circuit are experimentally inaccessible; their reported values can also scatter broadly, which hampers the prediction [11,12].

Here, we opted for a different approach comprising two stages. First, we employed a method termed feedback opening [13]. We opened synthetic feedback loops in the yeast *Saccharomyces cerevisiae*. Synthetic circuits have been playing an important role to characterize the fundamental properties of feedback behavior [14–18]. In the open loop, bistability is eliminated, and noise-induced transitions are bypassed. Therefore, we can obtain an open-loop function (f_{OLM}), which is the total response of all the reaction steps in the loop, without the need to resolve any of them individually. Since the f_{OLM} contains all the information on the deterministic steady-state expression, it can be used to determine if the parent closed (feedback) loop is bistable or monostable (Fig. 1b, deterministic model). In the second stage, we measured noise and the time scale of reactions, and by reintroducing noise into the model, we successfully predicted the transition rates (Fig. 1b, stochastic model).

Results

Design of the input and output constructs for the loop opening

To open a feedback loop, one of its components has to be split into an input and an output [13]. The resulting open loop is thus a reaction chain starting with the independently controllable input that triggers the biochemical reactions; the chain ends with the output, which has no effect on the reaction chain (Fig. 2a).

We opened transcriptional feedback loops at the RNA level in yeast (gray box, Fig. 2a), and thus, both the input and output are RNA molecules. The expressed input RNA is translated, which triggers the subsequent reactions, such as the transcription factor (TF) dimerization, the binding of the TF to the promoter, and lastly, the synthesis of the output RNA. The reactions between the input and output RNA are illustrated as a black box in Fig. 2a.

The input RNA is identical to the original RNA in the feedback loop. On the other hand, the output RNA has to be designed by mutating the original RNA. The mutation has to meet two requirements. First, the protein translated from the output mRNA must not interfere with the reactions in the loop
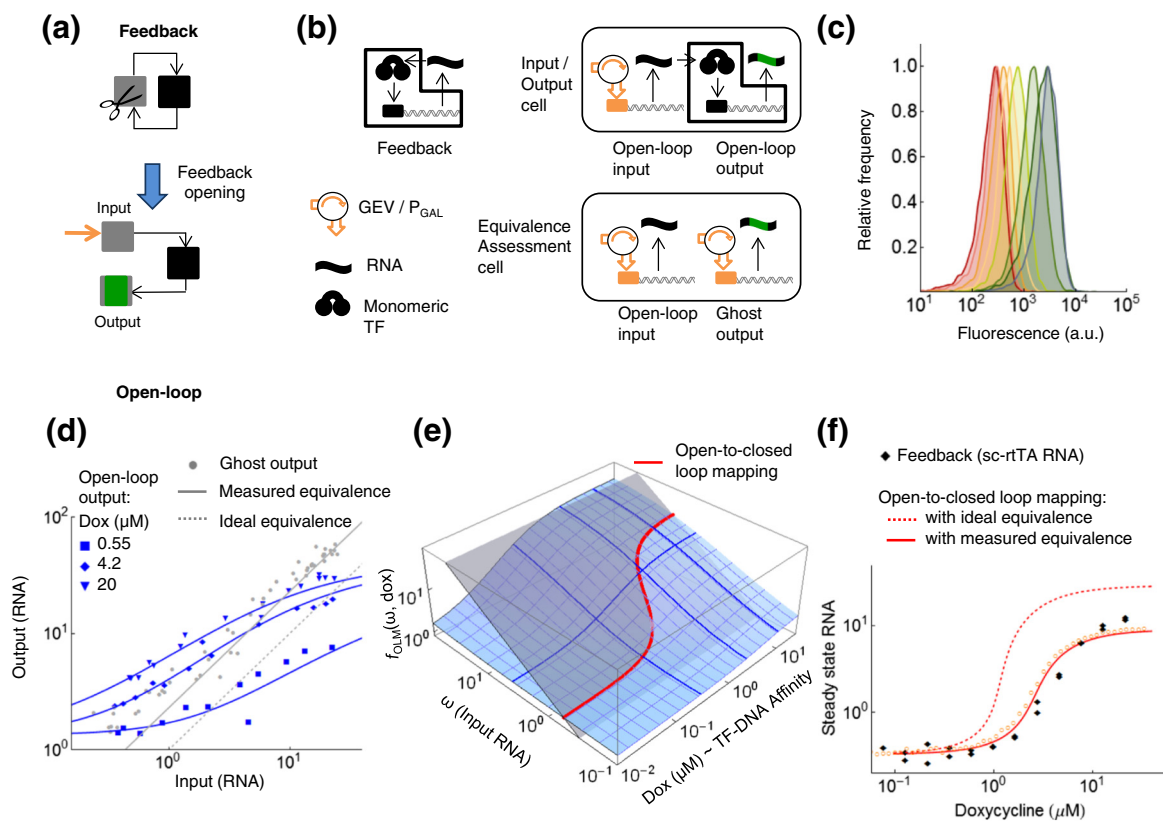
Fig. 2. Opening of the monomeric–noncooperative feedback loop ($P_{[tetO]1}$-sc-rtTA) classifies the parent loop as monostable. (a) To open a feedback loop, a component is chosen to be broken into an input and output. (b) The green segment in the output represents a heterologous sequence inserted for the feedback opening. (c) GFP fluorescence distribution in an open-loop-like construct, which contains a GFP reporter gene downstream of a [tetO]1 promoter controlled by sc-rtTA. Cells were exposed to a gradient of dox concentrations (0.07, 0.12, 0.20, 0.33, 0.55, 0.91, 1.52, and 2.53 μM). (d) Open-loop measurements. The input and output RNA is measured, as the activity of the *GAL* promoter was varied by estradiol (see Materials and Methods) at three different fixed values of dox. (e) The measured equivalence (gray) and open-loop (blue) functions fitted to data shown in (d). The traces of the function denoted by blue thick lines correspond to the dox and estradiol concentrations used in the experiments (see also Fig. S3a). (f) Comparison of the open-to-closed loop mapping (red lines) with the steady-state expression measured for the feedback loop. The predicted mean steady state values from the stochastic simulation using the extended and fitted noise model are shown by orange circles.

(Fig. S1a). Second, the output RNA must preserve the original properties of the RNA, such as the decay rate and dynamic range of expression. We found that retaining only 45-bp long sequences at each end of a gene was sufficient to preserve much of the original expression range (Fig. S1b; Design of the output construct in the Materials and Methods). Therefore, we used this strategy to build the output construct (Fig. 2b). Since we used the TF rtTA (reverse tetracycline transactivator) in the feedback loops, we built an output construct for rtTA and tested for interference. The protein translated from such an output RNA contains only short peptide sequences from rtTA (15 aa at each end) and is unlikely to interfere with the reactions in the loop, which we confirmed experimentally (Fig. S1c–e).

By creating the input and the output constructs with the aforementioned method, the feedback is opened. The cells containing the open-loop input and output constructs were named Input/Output cells (Fig. 2b).

Validation of the loop opening with a monostable feedback loop

We opened three synthetic transcriptional feedback loops, in which a monomeric or dimeric version of the synthetic TF rtTA regulates its own expression. rtTA binds to the DNA when it is complexed with the ligand, doxycycline (dox) [19]. These feedback loops contained one (cooperative binding), two (homodimerization and cooperative binding), or no reactions that can support bistability [20]. First, we opened the

monomeric–noncooperative loop, in which a monomeric TF binds to a single binding site in its own promoter. The monomeric protein is a single-chain fusion of the dimeric rtTA [20].

Upon opening this loop, the input and output RNAs were quantified by qPCR (quantitative PCR; Materials and Methods; Figs. 2, S2, and S3a). Thus, RNA values represent the averages of a cell population. The expression of the input was varied by tuning the P_{GAL} promoter activity with the TF GEV (Gal4-estrogen receptor-Vp16, Fig. 2d). We applied different concentrations of dox to adjust the TF-DNA binding affinity. Subsequently, we fitted an open-loop function, $\eta = f_{OLM}(\omega, dox)$, to these data. η, ω, and f_{OLM} denote the output, the input, and the open-loop function fitted to the measured data, respectively.

Initially, we analyzed the logarithmic sensitivity (S) of the f_{OLM} with respect to the input (ω), $S(\omega) = \partial \ln(f_{OLM}) / \partial \ln(\omega)$. If $S > 1$, the feedback loop can display bistability [21]. It is monostable if $S \leq 1$. $S(\omega)$ of the fitted $f_{OLM}(\omega, dox)$ did not exceed one at any value of ω and dox (Supplementary Information, Fitted open-loop functions). Thus, the monomeric–noncooperative feedback is classified as monostable upon the opening. This is in agreement with the expectations since the feedback does not contain any known reaction that can support bistability.

The intersection points of the f_{OLM} and the equivalence function (f_{EQ}) define the steady-state expression for the feedback loop [13,22]. The ideal f_{EQ} is an identity function, that is, it is the line at which the output and input have equal values, $\eta = \omega$ (Fig. 2d). The ideal equivalence assumes that the output and input RNAs have identical properties (expression range, synthesis, and decay rate). However, the heterologous sequence in the output RNA may cause a departure from the ideal equivalence. To

assess this departure, we expressed the input and output mRNAs under the control of identical promoter, P_{GAL}. The expression of the output RNA in this construct is not controlled by the input; therefore, we termed it ghost output (Fig. 2b). Although their decay rates of the mRNAs were similar (Fig. S2a and b), their expression levels differed (Fig. S2c–e), possibly because of the different RNA synthesis rates. There was a linear relationship between their expression levels with a non-unity slope (Fig. 2d). This slope defines the scaling factor (s) for the measured (nonideal) equivalence line, which runs in parallel to the ideal equivalence line (Fig. 2d): $f_{EQ}(\omega) = s \, \omega$.

The intersection of the measured f_{EQ} and f_{OLM} is a function of one variable (dox), which we termed open-to-closed loop mapping since it determines the steady-state expression in the closed feedback loop based on open-loop measurements (Fig. 2e and f, red full line). Importantly, there was a good agreement between the open-to-closed loop mapping and the steady-state expression measured in the feedback loop. If we had relied on the ideal equivalence plane, with a unity slope, the open-to-closed loop mapping would have deviated markedly from the values measured in the feedback loop (Fig. 2f, red dashed line). This underscores the importance of the equivalence assessment cells.

In summary, we validated the feedback opening in two main steps. First, we analyzed the open-loop constructs. The expression of a fluorescent reporter in open-loop-like constructs displays a unimodal distribution (Fig. 2c). The S of the f_{OLM} is less than one, which implies that the parent feedback loop is monostable. Since there are no noise-induced transitions between two stable states in a monostable feedback loop, the deterministic and stochastic descriptions of the steady-state expression levels
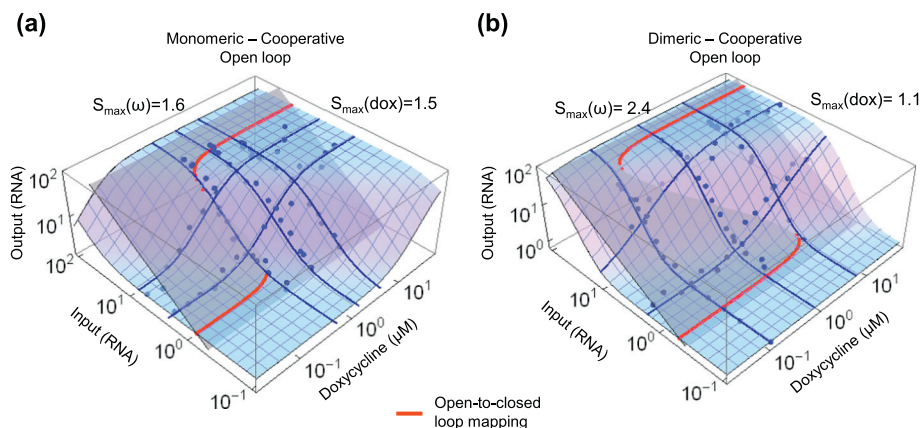

Fig. 3. Intersection of equivalence plane and f_{OLM} classifies two parent feedback loops as bistable. The blue and gray surfaces stand for the fitted f_{OLM} and the measured equivalence plane, respectively, fitted to experimental data (dots). The red curve is their intersection, the open-to-closed loop mapping. The maximal values of the S are calculated for the f_{OLM} with $b = 0.01 \, V_{max}$ by fixing either dox or ω. (a) Open-loop measurements of the $P_{[tetO]7}$-sc-rtTA circuit; S_{max} (ω, dox = 1.37) = 1.6; S_{max} ($\omega = 2.11$, dox) = 1.6. (b) Open-loop measurements of the $P_{[tetO]7}$-rtTA circuit; S_{max}(ω, dox = 0.91) = 2.4; S_{max}($\omega = 1.93$, dox) = 1.1.

are expected to be similar. Consequently, the steady-state expression measured in the feedback loop can be directly compared to the value determined by feedback opening (Fig. 1b), provided that some general conditions are met (see Discussion). In the second step, we compared these two values. We found that the open-to-closed loop mapping matched up with the steady-state expression level measured in the feedback loop (Fig. 2f). The expression increased continuously and steeply when the TF-DNA affinity (i.e., dox concentration) passes a certain value, which is a typical behavior of monostable positive feedback loops.

Identification of bistability by loop opening

Next, we opened the loops with cooperative promoters, controlled by either the monomeric (Fig. 3a) or the dimeric TF (Fig. 3b). The sensitivity of $f_{OLM}(\omega, dox)$ with respect to the input (ω) was higher than one for both open loops, which indicates that the feedback loop is bistable. Indeed, there was a range of dox concentration, at which the intersection

of the f_{OLM} with the equivalence plane resulted in three, (two stable and one unstable) steady state. Thus, both parent feedback loops are classified bistable.

The maximal sensitivity of the f_{OLM}, $S_{max}(\omega)$, has a major impact on the bistable range of a parameter. For the monomeric–cooperative circuit, $S_{max}(\omega)$ is 1.6. This value increased to 2.4 for the dimeric–cooperative circuit (Fig. 3b), and the bistable range of the dox concentration (i.e., TF-DNA affinity) became broader, reflecting the joint effect of dimerization and cooperativity (Fig. 3).

Measurement of the time scale of reactions and identification of the slow transient kinetics

To predict the transition rates for a bistable system, we have to combine the f_{OLM}, which is defined in the steady state, with information on noise and the time scale of reactions (Fig. 1b). To specify the time scale of reactions, we determined the RNA and protein decay rates and the transcription and translation rates (Table S2). With these parameters,
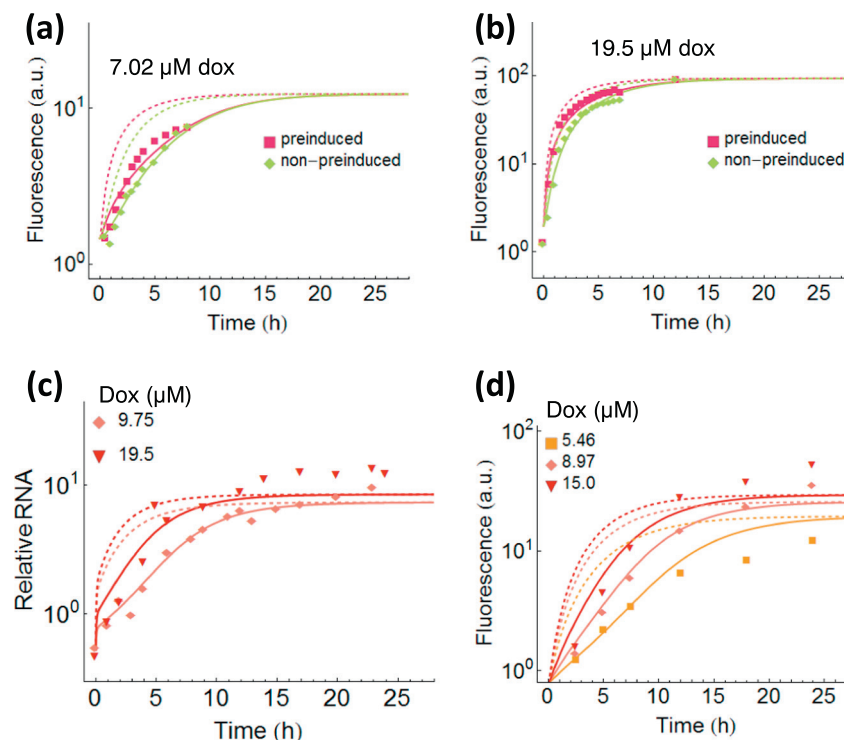

Fig. 4. Long transient phase upon the addition of dox to the cells. The curves represent the solution of the model without (dashed line) and with (full line) the extension to fit the transient kinetics. Dox was added at the indicated concentration at $t = 0$ h. (a and b) Induction kinetics in open-loop-like constructs, in which sc-rtTA activates the expression of P$_{[tetO]2}$-GFP (see transient kinetics strain in Table S1). The expression of sc-rtTA was either pre-induced by estradiol (red) or induced at $t = 0$ h together with the addition of dox (green). Expression of GFP was measured with flow cytometry. To reach intermediate expression levels of sc-rtTA, we applied 0.8 (a) and 7.28 (b) nM estradiol. (c and d) Induction kinetics of the monomeric–noncooperative feedback loop (P$_{[tetO]1}$-sc-rtTA). To report the feedback activity, we measured the mRNA of the sc-rtTA (c) or the GFP expression driven by sc-rtTA (d).

we extended the f_{OLM} into a kinetic model. We tested whether this model predicts correctly the kinetics of expression in open-loop-like constructs. For this purpose, we analyzed the time course of expression of green fluorescent protein (GFP) under the control of the monomeric form of rtTA. Interestingly, the induction of expression was slower than expected from the time scales of protein and RNA turnover (Fig. 4a and b; see Modeling transient kinetics in the Supplementary Information). By varying the order of induction of the rtTA expression and dox addition, it became clear that the slower-than-expected increase of GFP expression persisted even if rtTA was pre-expressed (Fig. 4a and b). This indicates that the long transient phase arises due to the slow transport of the externally added ligand, dox, into the cell or due to its slow association with the protein inside the cell. The model was extended and fitted to the slow transient kinetics in the open-loop-like construct. Subsequently, we tested the prediction of the new model on the monostable feedback loop, which can be done deterministically. The prediction was in good agreement with the observed time series upon the addition of dox (Fig. 4c and d).

Measurement of noise

We made a preliminary prediction of noise intensity based on the time scale of the constitutive processes (mRNA and protein turnover). A simple model involving only synthesis and decay, also known as birth–death process, results in a Poisson distribution, characterized by a Fano factor (variance/mean) = 1 [23]. Interestingly, the housekeeping gene *PRE2*, which was used as a control for the single-molecule fluorescence in situ hybridization (smFISH), had a Fano factor close to 1 (Fig. 5a and b). On the other hand, the distribution of the rtTA RNA had a much larger variance, with a Fano factor of around 5, which cannot be explained by such a simple noise model (Fig. 5a and b). This stronger noise is not fully surprising because noise in gene expression can be significantly augmented by operator fluctuations and by other cellular processes [24,25]. Therefore, the model was extended to include operator fluctuations and noise in RNA degradation (Fig. 5c). The parameters were fitted to the smFISH measurements (Supplementary Information, Determination of parameter values for RNA distribution by linear noise approximation), and the new extended and fitted model was in good agreement with the measured RNA distribution (Fig. 5a and b).

Comparison of deterministic and stochastic descriptions of the f_{OLM}

The open-loop function is a deterministic concept and can be considered to be a steady-state solution of ordinary differential equations. To predict the transition rates, the deterministic model has to be converted to a stochastic one (Fig. 1b). This conversion is accurate, provided that the stochastic model of the open-loop function yields a mean value that is identical or similar to the deterministic value. The two values are identical, for example, for the mRNA birth–death process (Fig. 5a and b, see *PRE2*). However, this correspondence between the deterministic and stochastic models may be lost when the system is strongly nonlinear and the noise is large [26,27]. Such an effect was observed for a TF that displays stochastic nucleocytoplasmic shuttling [28].

We examined the effect of noise on the dimeric–cooperative open loop as it displays the response with the largest S in this study, and therefore, it is highly nonlinear. To explore how much noise shifts the value of the output mRNA, we performed stochastic simulation with the extended and fitted noise model. It yielded mean output RNA similar to the value of the deterministic function, f_{OLM} (Fig. 5d). This demonstrates that the effect of noise on this nonlinear f_{OLM} is negligible and the function can be used for accurate predictions. Thus, the loop opening bypasses the effect of noise. We also confirmed that gene expression in the open loop reaches a steady state after 24 h, independent of the initial condition, that is, it does not display hysteresis (Fig. S4). Furthermore, the distribution of gene expression in the corresponding open-loop-like constructs was unimodal (Fig. S3c).

Interestingly, there was also a good match between the (deterministic) open-to-closed loop mapping and the stochastic model of the monostable feedback loop (Fig. 2f, orange circles), which reveals that even the closed-loop response can have very similar stochastic and deterministic descriptions, provided it is monostable.

The predicted transition rates agree with the measurements

Upon extending the f_{OLM} using the reaction time scales and fitted noise, we reclosed the loop to predict the transition rates, both from the low to the high state and also in the opposite direction (high to low) for the two bistable circuits (Fig. 6). We also calculated the transition rates with the model not fitted to noise and transient kinetics for comparison. The simple noise model, characterized by smaller noise intensity, yielded slower transitions in the bistable range than the fitted, extended noise model (Fig. 6a–g). On the other hand, the transient kinetics reduced the transition rates only outside but not inside of the bistable range (Fig. 6b), exactly opposite to the effect of noise.

To test the predictions experimentally, we prepared pre-cultures with either low or high TF expression states, which define the initial condition, to measure how quickly they switch to the other
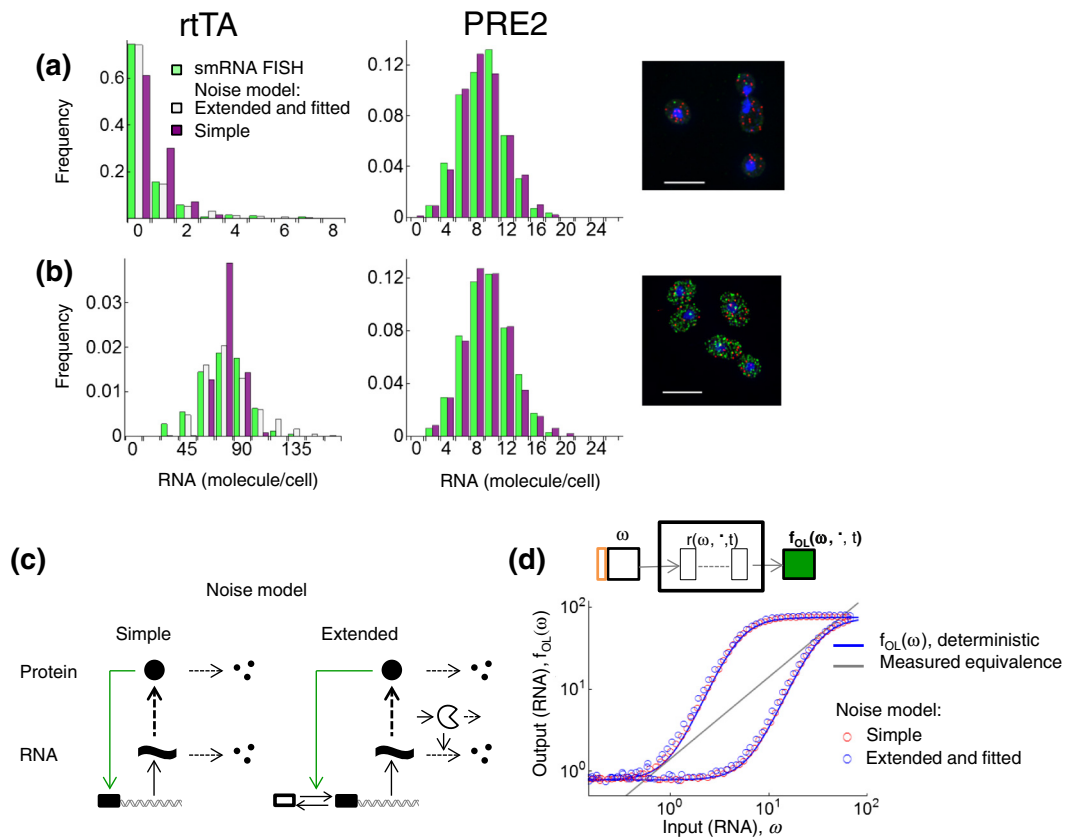
Fig. 5. Extension of the model to fit the measured noise. (a and b) FISH images and distributions of rtTA and PRE2 RNA molecules in cells containing the $P_{[tetO]7}$-rtTA feedback loop either uninduced (a) or induced with 19.5 μM dox for 24 h in cultures with the high initial condition (b). We calculated the mean (molecules/cell), coefficient of variation (CV), and the Fano-factor (FF) for the measured distribution (subscript M) and the distribution simulated ($n = 1000$) with the simple (subscript S) or the extended and fitted noise model (subscript E; see Mathematical modeling, simple and extended noise model). (a) The un-induced cells. For rtTA: mean = 0.49; CV_M = 2.31; FF_M = 2.41 (green, n = 280); CV_S = 1.46; CV_E = 2.22. For *PRE2*: mean = 9.2; CV_M = 0.32; FF_M = 0.94; CV_S = 0.33. (b) The induced cells. For rtTA: mean = 82.6; CV_M = 0.24; FF_M = 4.80 (green, n = 171); CV_S = 0.11; CV_E = 0.26. For *PRE2*: mean = 10.0; CV_M = 0.31; FF_M = 0.98; CV_S = 0.32. The images were obtained by z-projection of decomposed image stack of smFISH with the following coloring: blue, DAPI; green, rtTA; red, PRE2; scale bar: 5 μm. (c) To obtain a model that fits the experimental RNA distribution, the simple model is extended by operator fluctuation (forward and backward arrows) and enzymatic RNA degradation (Pac-Man). The thick dashed arrows indicate the step that is broken to open the feedback loop. (d) Comparison of the output RNA calculated by deterministic and stochastic models. To convert $f_{OLM}(\omega)$ into a model, reactions (r), were specified, which introduce time-dependent variables and parameters (denoted: •). The steady-state solution of the deterministic model recreates the original $f_{OLM}(\omega)$. The mean RNA values were calculated by the simulation of the corresponding stochastic model (see Mathematical modeling, Conversion of the $f_{OLM}(\omega)$ to a reaction model). $f_{OLM}(\omega)$ corresponds to the thick curves at dox = 0.12 and 7 μM in Fig. 3b.

state. In the bistable range, the observed transition rates were in good agreement with the predictions using the fitted noise (Fig. 6b and g). Outside of the bistable range, the model with the fitted transient kinetics predicted well the observations (Fig. 6b). These results and the model predictions reveal that noise is the main determinant of transitions inside the bistable range, while transient kinetics is the main determinant of the transitions outside of the bistable range. It is important to reiterate that the transition rates were predicted without choosing or fitting parameter values to the observed transition rates.

For the dimeric–cooperative circuit, transitions from the low to the high state were only observed close to the bistability boundary at the higher dox concentration (Fig. 6g). Opposite transitions were observed close to the lower bistability boundary. Thus, there is a broad range of dox concentrations at which essentially no transitions are expected to occur between the two states. This range is positioned in the middle of the bistable range, determined by the open-to-closed loop mapping. Indeed, we have not observed any transition in this range of dox concentration even after 10 days (Fig. 6h).
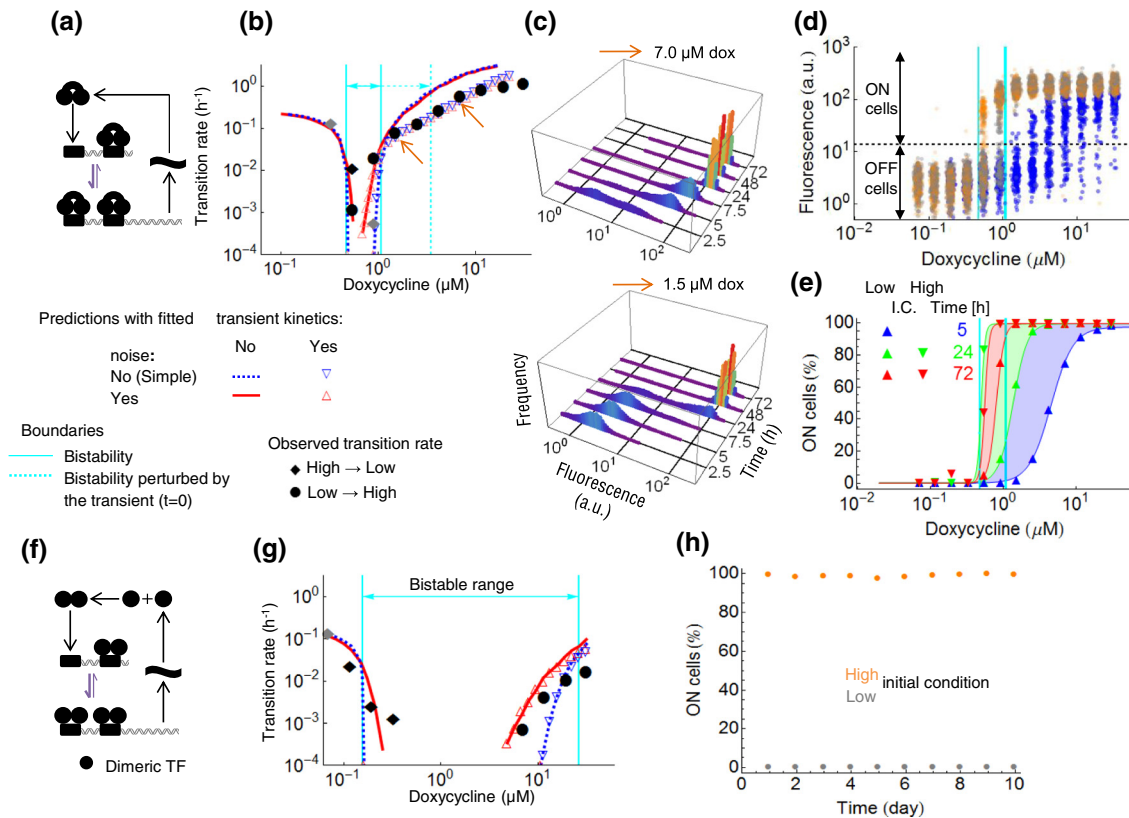
Fig. 6. Predicted and measured transition rates for the bistable, the monomeric–cooperative ($P_{[tetO]_7}$-sc-rtTA), (a–e) and the dimeric–cooperative ($P_{[tetO]_7}$-rtTA) (f–h) feedback loops. (a) Scheme of the feedback loop. (b) The orange arrows indicate the dox concentrations for which the time evolution of the fluorescence histograms is shown (in c). The gray symbols denote transition rates at the detection limit (see Materials and Methods, Fitting of transition rates). (c) Fluorescence histograms of cells with the low initial condition. (d) Measurement of hysteresis experiments. Cells with low (gray dots) or high (orange dots) initial condition (I.C.) were grown for 72 h; 5 h measurements are shown only for the low I. C. (blue). (e) Measurement of hysteresis expressed in terms of ON cell percentages. Data are shown for cultures 5 h, 24 h, and 72 h after setting the initial condition. Identical to those shown in (d) are the 5 h and 72 h. The 24 h data are in Ref. [20]. (f) Scheme of the feedback loop. (g) Comparison of the measured and predicted transition rate for the dimeric–cooperative feedback loop. (h) Long-term hysteresis experiment with cells exposed to 0.92 μM dox.

For the monomeric–cooperative circuit, transitions were detected in both directions in the bistable range (Fig. 6b). Thus, equilibrium is expected to ensue in an experimentally realistic time scale. This can be visualized by plotting the experimental data in terms of hysteresis profiles, which is typically used to assess bistability, directly in feedback loops. For both initial conditions, we plotted the percentage of ON cells, that is, the proportion of cells in the high state (Fig. 6d and e). The range of dox concentrations at which the ON cell percentage in each culture remains close to the respective initial condition defines the hysteresis range. These two distinct expression states (OFF and ON cells) represent two "synthetic" cell fates. Interestingly, the hysteresis range changed with time for the monomeric–cooperative feedback loop (Fig. 6e). At early time points (5 h), the hysteresis range was broader than the bistability range (Fig. 6e). At a later time point

(72 h), the hysteresis nearly collapsed. This also implies that in noisy systems, hysteresis experiments may fail to distinguish bistable feedback loops from monostable ones after long periods of time.

Appearance of bimodality far away from the bistable range

When noise induces transitions between two stable states, both states become populated, resulting in a bimodal distribution. That is why bimodality is considered as a hallmark of bistability in noisy systems. However, it was surprising to observe that the transitions are accompanied with a bimodal distribution of GFP expression well beyond the bistable range for the monomeric–cooperative circuit (Fig. 6b and c). The range of this bimodality was around three times broader than the bistable range. We expected that the transient kinetics may be responsible for the

extension of the bimodality range because it prolongs the phase during which the TF-DNA affinity is approaching the final value upon the addition of dox to the cells (Fig. 6b, cyan dashed line), and it is this affinity that determines the bistability boundary. To visualize this, we superimposed single-cell trajectories of stochastic simulations onto a steady-state manifold perturbed by the transient kinetics. This manifold reflects the temporal changes in the bistability (Fig. 7, green surface). Initially, only few cells cross the unstable part of the manifold because it is far above the low expression state. As time progresses, the transient effect peters and the manifold recedes; the majority of cells transit as soon as the lower fold in the manifold crosses the dox concentration to which the cells are exposed. This explains how transient kinetics can slow down the transition rates and why bimodality, a sign of bistability, appears far away from the bistable range.
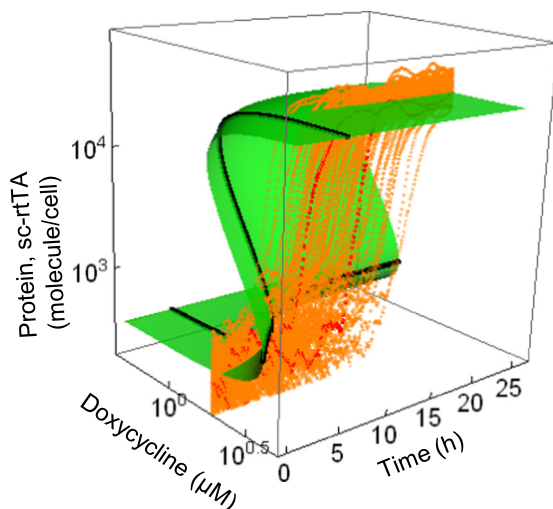

Fig. 7. Visualization of the effect of transient kinetics on the transitions. The parameter values for the monomeric–cooperative feedback loop were used for the simulation. The steady-state manifold (green surface) is perturbed by the transient kinetics to represent the temporal evolution of the TF-DNA affinity due to the slow effect of the externally added dox. Individual trajectories of stochastic simulations (with the model extended to fit noise and transient kinetics) are shown in orange and red. The horizontal black curve represents the evolution of the perturbed fold bifurcation point. The vertical black curve indicates the manifold at the time when the fold point passes the dox concentration that was used for the stochastic simulation (dox = 1.8 μM).

Discussion

Relation between bistability, bimodality, and hysteresis

Bimodality has been viewed as a sign of bistability, and hysteresis as the proof of bistability [29]. Our results reveal that neither hysteresis experiments nor bimodality can delimit the bistable range in noisy gene circuits. The hysteresis range shrinks with time (Fig. 6e) due to the noise-induced transitions and can even collapse in feedback loops that have a narrow bistable range. While hysteresis range may coincide with the bistable range at a particular time point, the length of this period is likely to vary from system to system. Bimodality, a potential sign of bistability, appeared far away from the bistable range due to the slow transient kinetics (Fig. 6b and c). Indeed, an increasing number of models have been identified, where bimodality appears without bistability or even in the absence of feedback regulation [30–33].

Since feedback opening bypasses noise, the open-to-closed loop mapping can determine whether a system is monostable or bistable and can delimit the bistable range.

Prediction of transition rates by feedback opening

Traditional modeling requires parameters for all reactions that comprise the feedback loop. However, models retain unidentified components, mechanisms, and parameters even after detailed measurements. In particular, binding constants are often missing or are inconsistent. For example, reported values for the dissociation equilibrium constants of the tetR-*tet* operator scatter over 3 orders of magnitude [11], which is relevant for rtTA, being a fusion protein of tetR. Furthermore, parameter values measured *in vitro* may significantly deviate from their values *in vivo* [12,34]. Therefore, several parameters are left free and then directly fitted to the transition rates, which makes true prediction impossible.

To predict the transition rates, we employed an inverse approach. By opening the feedback loop, we obtained an open-loop function, which lumps the steady-state response of all reactions in the feedback loop but does not resolve the time scale of any of them. To extend this function into a model, we performed kinetic and noise measurements. This extension has to be performed in a way that the model recreates the original steady state open-loop function (Fig. 5d, diagram). Not all reactions in the loop have to be identified. After measuring the core constitutive processes, including mRNA and protein turnover, we extended the model with a few additional parameters to fit the noise in gene expression and the transient kinetics (Fig. 1b). This was sufficient to

successfully predict the transition rates. We expect that, in general, it will be important to characterize the slow reactions (e.g., protein decay rate), since fast reactions (e.g., phosphorlyation and dephosphorylation) are expected to be in equilibrium relative to the slow reactions.

The success of this approach may lie also in the fact that the initial steps of modeling were performed deterministically, which is typically more robust than the direct stochastic modeling of the whole feedback system [35,36].

Noise and bistability jointly determine transition rates

Inside the bistable range, the sensitivity of the f_{OLM} and noise are the key determinants of the transition rates. In the monomeric–cooperative loop, the $S_{max}(\omega)$ is 1.6. This value was 2.4 for the dimeric–cooperative loop, due to the dimerization. The system with higher sensitivity can be visualized by potential wells separated by higher barriers. This explains why the dimeric–cooperative loop is more stable than the monomeric–cooperative one: transi-

tions were too slow to be detected even after 10 days of incubation, that is, after more than 100 cell generations (Fig. 6h).

The open-to-closed loop mapping determines the steady-state expression levels and the bistable range of a parameter. Is this deterministic description relevant for bistable systems, knowing that it cannot be directly verified in noisy feedback loops? Our results indicate that the determination of the bistability boundaries permits targeted system identification (Fig. 8). Noise was the key determinant of the transitions inside the bistable range but not outside of it (Fig. 8, left). In this monostable range, we had to characterize transient kinetics to explain the transitions. The slow transient kinetics can be viewed as a temporal change in the potential barrier (Fig. 8, right).

The role of transient kinetics in cell fate transitions

When a parameter is in the monostable range in the vicinity of the bistable range, the slow transient kinetics is likely to be the rate-limiting step in the transitions. In such cases, the activity of the
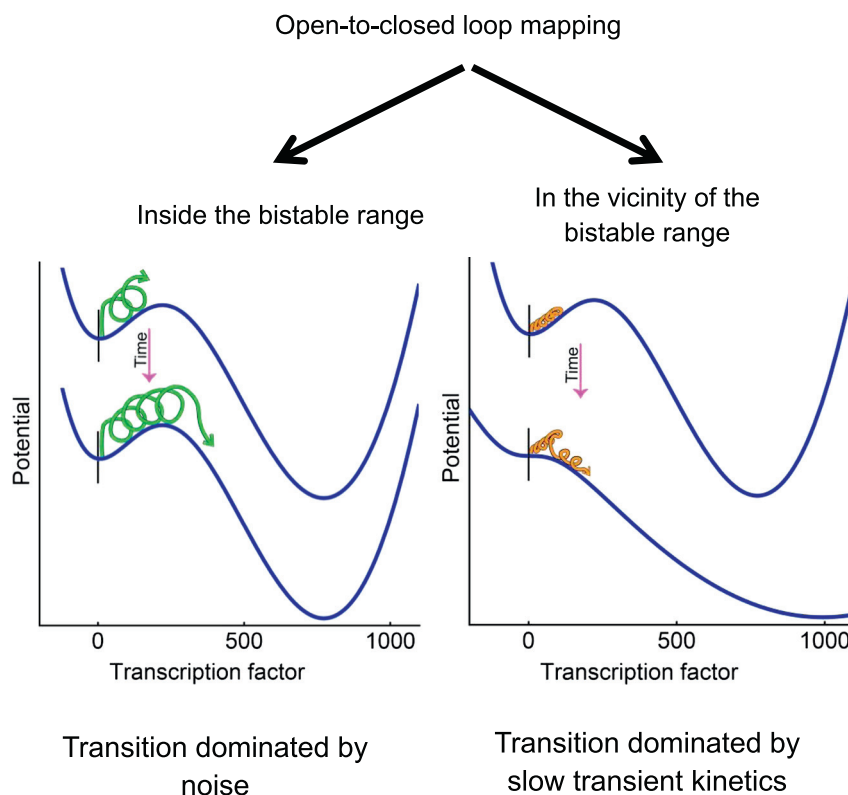

Fig. 8. The role of bistability, noise, and transient kinetics in the cell fate transitions. If a network displays steady-state bistability, as determined by feedback opening, the depth of the potential wells and noise are the main determinants of the transition rate (left). If the parameters of the network are outside but in the vicinity of the bistable range, the transitions are determined by the long transient phase, which can arise due to slow transport, metabolism, or other deterministically described transient cellular process (right).

feedback loop is controlled by an extracellular factor that evokes slow changes in transport, metabolism, or signal transduction. The two distinct cell fates can be maintained only transiently. However, such a transient phenomenon may be of considerable utility, since an increasing number of studies revealed that alternative fates exist transiently in many cells and organisms [5,37–40]. It is possible that differentiation should be considered as series of transient events, and the steady state is reached only in the terminal stage [7]. Upon the completion of differentiation, only a true bistable state can warrant long-term stability. In this case, transitions will be induced by noise and exemplified by noise in gene expression. Such transitions can destabilize cell fates, which can hamper cellular reprogramming [6], but can also help adaptation by diversifying the phenotypes of immune cells to combat pathogens.

Validity of prediction by feedback opening

In this study, we opened simple positive feedback loops. Can we expect that the opening is a valid approach for more complex networks? Two aspects of the loop opening are particularly relevant to more complex networks: (1) the theorem that deduces the existence of bistability from open-loop properties and (2) the stochasticity in the open loop.

With respect to the first aspect, a general theorem states that if the open-loop function is sigmoidal (i.e., the open-loop function has an S higher than one) and satisfies some general conditions, the parent feedback loop is bistable, independent of the time scale of the reactions [13]. Positive feedback loops with cooperative binding and dimerization, which were used in our work, satisfy the general conditions. However, if a network contains also a negative feedback loop, bistability is not guaranteed. In such dual positive–negative feedback loops, the concentrations of the components may oscillate over time rather than converge to one of the stable states. In the experimental practice, however, such restrictions may be less severe as the feedback system can be directly measured whether it displays oscillations. If it does not oscillate but displays signs of bistability, bimodality, and hysteresis, it is likely that the open-loop function will correctly predict the existence of bistability, even if a more complex network contains a negative feedback loop.

The aforementioned theorem is defined in a deterministic framework. We are not aware of the theoretical studies that formulate the open-loop approach in a stochastic framework, which is relevant to noisy gene networks. Therefore, we performed the following tests to show that the deterministic and stochastic descriptions of the open loop are similar. First, we showed that there is no hysteresis after 24 h in the open loop. Second, the distribution of gene expression is unimodal. Third, we compared the f_{OLM},

which is defined deterministically, to the mean value of the output calculated using the expanded model upon the identification of the time scale of the main reactions. The two values were similar, that is, there is no marked stochastic deviant effect [27]. Further studies will be needed to explore how the open-loop function is affected by noise in more complex networks.

Feedback opening and the subsequent model extension are expected to be useful to predict transition rates and identify the main determinants of cell fate transitions: bistability in the deterministic sense, noise, and transient kinetics. This distinction may also help in engineering cell fate transitions.

Materials and Methods

Design of synthetic circuits and yeast strains

Three major strain types were used in this study: the feedback, Input/Output, and Equivalence Assessment cells (Table S1). The feedback cells contained a feedback circuit, a fluorescent reporter construct ($P_{[tetO]2}$- yEGFP), and a construct to adjust the high condition (P_{GAL}- (sc-)rtTA), which is identical to the open-loop input construct.

The Input/Output cells contained the open-loop output, open-loop input constructs, and a constitutively expressed GEV. The Equivalence Assessment cells contained the ghost output (P_{GAL}–(sc-)rtTAΔ(45/45):: yellow fluorescent protein), the open-loop input construct, and a constitutively expressed GEV. The expression of the open-loop input and ghost-output constructs was controlled by GEV. GEV is a transcription activator consisting of a Gal4p DNA-binding domain, an estradiol receptor, and a VP16 activation domain. RNA expression was tuned over a broad range by adding estradiol at a concentration between 0 and 200 nM [41].

Design of the output construct

The two requirements, lack of interference and preservation of expression properties, make opposing demands on the optimal scale of the mutation to construct the output. For example, if the output gene contains a minor (e.g., point) mutation in the DNA-binding domain of the TF, the properties of the encoding mRNAs are likely to be preserved, and the loop is successfully broken because the TF will not bind to the DNA. However, a TF with a minor mutation may still cross-dimerize with the wild-type TF translated from the input RNA, interfering with the signaling in the open loop. A large-scale mutation, whereby the entire coding region is replaced by a heterologous sequence, eliminates the interference, but the dynamic range of the expression may be reduced. To find the maximal length of the replacement with a minimal effect on mRNA expression, we built a series of genetic replacement constructs by varying the length of the sequence retained from the original gene (Fig. S1a and b).

Construction of yeast strains

All yeast strains are derivatives of *S. cerevisiae* W303, except for the strains to test the expression range of *GAL2* gene as a function of the length of the replaced open reading frame (ORF). All genetic constructs were integrated into the chromosome with a single copy, with the exception of the GEV construct, which has around five copies, and the $P_{[tetO]2}$-GFP construct, which has three copies.

The feedback, open-loop input, the open-loop output, and ghost output constructs share a common core promoter and transcriptional terminator of *CYC1*. The input and ghost output were controlled by the P_{GAL}, whereas the feedback and output constructs were controlled by $P_{[tetO]1}$ or $P_{[tetO]7}$ for noncooperative and cooperative binding, respectively. Into each feedback construct, an optimized stem-loop was inserted to avoid growth alterations [20]. The same stem-loop was also inserted in the corresponding open-loop input, open-loop output, and ghost output constructs.

To construct the open-loop output and ghost output constructs, we flanked the yellow fluorescent protein sequence with 45-bp sequences from both ends of the rtTA ORF. The flanking sequences of sc-rtTA and rtTA ORFs are identical because sc-rtTA was constructed by inserting humanized tetR sequence into the rtTA sequence [20].

To minimize the position effect, we integrated the genes with promoters containing tet operators to the *ura3* locus and those with P_{GAL} to the *ade2* locus. Using diploid cells for the optimized constructs made it possible to have two constructs with the same promoter at the same locus, which is essential for constructing the Equivalence Assessment strains. In addition, the transformations followed the order of (1) GEV, (2) open-loop input, and then (3) open-loop output, ghost output, or feedback construct, in order to have identical sequence and copy number of GEV and open-loop input constructs between the different strains.

Growth conditions

Cultures were grown at 30 °C, and the OD_{600} was kept below 1.0; were refreshed by diluting the cultures twice a day. A sample was collected for measurement, and the cell density was between 0.6 and 1.0. For the steady-state RNA measurements, cultures were grown for 24 h. To set the initial condition in the feedback loops, we added 0.5% galactose to the medium to drive expression under the control of the P_{GAL} promoter through the endogenous Gal4p, as previously described [20].

To determine RNA decay rate constants, shutoff assays were performed. The cells were cultured overnight with 0.5% galactose and transferred to a refreshment medium containing 0.04% galactose for further growth for 4 h. To shut off transcription, the cells were pelleted and cultured further in medium without galactose. As described, 5 ml culture was collected with dry ice-cooled methanol [41]. Decay rates were obtained by linear regression.

Flow cytometry [20] and beta-galactosidase assay [14] were performed as described previously.

RNA quantification

RNA was quantified with qPCR and smFISH as previously described [20]. The overall efficiency for the input primer pair, which was identical for both the rtTA/sc-rtTA primer pairs, was 1.931; the efficiency for the output primer pair (F: 5′-CGGGGGATCCATGCCTA-GATTA-3′; R: 5′-ACTGACAGAAAATTTGTGCCCAT-3′) was 1.934. The forward primer sequence is identical for the input and the output.

Absolute quantification of cellular RNA molecules was performed by smFISH. The results from smFISH were utilized for assessing the noise in gene expression in the feedback strains and for converting the RNA quantified in qPCR to the absolute mRNA number in the cell. We obtained the constant ratio α (Supplementary Information, Scaling of output signal for fitted equivalence) by quantifying the RNA at high expression state with the dimeric–cooperative and monomeric–cooperative feedback strains with both qPCR and smFISH. In the indicated experimental conditions, all cells were *PRE2* positive with 10.51 ± 0.75 (mean ± sd) RNA molecule per cell. The background level of rtTA RNA (false positive) count was ~0.03 spots per cell, in cells without the rtTA construct (Table S1, Ych294). The spot intensity distribution was unimodal, indicating that a single molecule was detected at each spot (Fig. S5) [42].

Fitting of transition rates

To fit transition rates with the low initial condition, samples were collected at 2.5, 5, 7.5, 24, 48, and 72 h. With the high initial condition, samples were collected at 24, 48, and 72 h; earlier time points were omitted because of the slow dilution of the GFP signal during cell division.

The ON and OFF cell population was separated by a threshold value. The threshold was set equal to the geometric mean of the maximally induced (at 19.5 μM dox) fluorescence intensity and the uninduced fluorescence intensity measured at 72 h.

At most dox concentrations, detectable transitions of sufficient rates occur only in one direction. In these cases, we obtained the best fits for the transition rates with data expressing OFF cell proportion (r) and with inverse-square (Y^{-2}) weighting. The low-to-high state transition was fitted with the low initial condition, $r(t) = e^{-k_{up}t}$, and the high-to-low state transition was fitted with the high initial condition, $r(t) = 1 - e^{-k_{down}t}$.

When the bistable range is narrow, transitions occur in both directions. Consequently, the percentage of OFF cells stays between 4% and 96% at 72 h. In these cases, we performed fitting with equations describing bidirectional transitions without weighting.

For the low initial condition:

$$r(t) = \frac{k_{down} + k_{up}\, e^{-(k_{up}+k_{down})t}}{k_{up} + k_{down}}$$

For the high initial condition:

$$r(t) = \frac{k_{down} - k_{down}\, e^{-(k_{up}+k_{down})t}}{k_{up} + k_{down}}$$

The values with the lower standard error were taken from the fitting.

Due to the fluctuations in conditions, we did not consider the data that were close to the detection limit of a change, less than 4% difference between *r(2.5 h) and r(72 h)*. This imposes the upper and lower detection limit of transition rates. For the low initial condition experiments, the limits are $k_{up} = 1.3\ h^{-1}$, when *r(2.5 h)* = 0.04; and $k_{up} = 5.6 \times 10^{-4}\ h^{-1}$, when *r(72 h)* = 0.96. A similar detection limit can be established for the reverse transition: $k_{down} = 0.13\ h^{-1}$, when *r(24 h)* = 0.96; and $k_{down} = 5.6 \times 10^{-4}\ h^{-1}$, when *r(72 h)* = 0.04.

Acknowledgments

Appendix A. Supplementary Data

Supplementary data to this article can be found online at http://dx.doi.org/10.1016/j.jmb.2016.07.024.

References

[1] M. Arnoldini, I.A. Vizcarra, R. Pena-Miller, N. Stocker, M. Diard, V. Vogel, et al., Bistable expression of virulence genes in salmonella leads to the formation of an antibiotic-tolerant subpopulation, PLoS Biol. 12 (2014), e1001928 http://dx.doi.org/10.1371/journal.pbio.1001928.

[2] G. Balazsi, A. van Oudenaarden, J.J. Collins, Cellular decision making and biological noise: from microbes to mammals, Cell. 144 (2011) 910–925.

[3] D. Jukam, B. Xie, J. Rister, D. Terrell, M. Charlton-Perkins, D. Pistillo, et al., Opposite feedbacks in the Hippo pathway for growth control and neural fate, Science. 342 (2013) 1,238,016, http://dx.doi.org/10.1126/science.1238016.

[4] M. Bednarz, J.A. Halliday, C. Herman, I. Golding, Revisiting bistability in the lysis/lysogeny circuit of bacteriophage lambda, PLoS One. 9 (2014), e100876 http://dx.doi.org/10.1371/journal.pone.0100876.

[5] N. Mirouze, Y. Desai, A. Raj, D. Dubnau, Spo0A~P imposes a temporal gate for the bimodal expression of competence in *Bacillus subtilis*, PLoS Genet. 8 (2012), e1002586 http://dx.doi.org/10.1371/journal.pgen.1002586.

[6] S. Pacini, Deterministic and stochastic approaches in the clinical application of mesenchymal stromal cells (MSCs), Front. Cell Dev. Biol. 2 (2014) 50, http://dx.doi.org/10.3389/fcell.2014.00050.

[7] J. Ladewig, P. Koch, O. Brustle, Leveling Waddington: the emergence of direct programming and the loss of cell fate hierarchies, Nat. Rev. Mol. Cell Biol. 14 (2013) 225–236.

[8] A.M. Walczak, J.N. Onuchic, P.G. Wolynes, Absolute rate theories of epigenetic stability, Proc. Natl. Acad. Sci. U. S. A. 102 (2005) 18,926–18,931.

[9] J.X. Zhou, M.D. Aliyu, E. Aurell, S. Huang, Quasi-potential landscape in complex multi-stable systems, J. R. Soc. Interface. 9 (2012) 3539–3553.

[10] P. Érdi, J. Tóth, Mathematical Models of Chemical Reactions : Theory and Applications of Deterministic and Stochastic Models, Princeton University Press, Princeton, N.J, 1989.

[11] C. Berens, D. Porschke, Recognition of operator DNA by Tet repressor, J. Phys. Chem. B 117 (2013) 1880–1885.

[12] R. Garcia-Contreras, P. Vos, H.V. Westerhoff, F.C. Boogerd, Why *in vivo* may not equal *in vitro*—new effectors revealed by measurement of enzymatic activities under the same *in vivo*-like assay conditions, Febs J. 279 (2012) 4145–4159.

[13] D. Angeli, J.E. Ferrell Jr., E.D. Sontag, Detection of multistability, bifurcations, and hysteresis in a large class of biological positive-feedback systems, Proc. Natl. Acad. Sci. U. S. A. 101 (2004) 1822–1827.

[14] C. Hsu, S. Scherrer, A. Buetti-Dinh, P. Ratna, J. Pizzolato, V. Jaquet, et al., Stochastic signalling rewires the interaction map of a multiple feedback network during yeast evolution, Nat. Commun. 3 (2012) 682, http://dx.doi.org/10.1038/ncomms1687.

[15] Y.T. Maeda, M. Sano, Regulatory dynamics of synthetic gene networks with positive feedback, J. Mol. Biol. 359 (2006) 1107–1124.

[16] M.C. Inniss, P.A. Silver, Building synthetic memory, Curr. Biol. 23 (2013) R812–R816.

[17] K.C. Ma, S.D. Perli, T.K. Lu, Foundations and emerging paradigms for computing in living cells, J. Mol. Biol. 428 (2016) 893–915.

[18] M. Wu, R.Q. Su, X. Li, T. Ellis, Y.C. Lai, X. Wang, Engineering of regulated stochastic cell fate determination, Proc. Natl. Acad. Sci. U. S. A. 110 (2013) 10,610–10,615.

[19] A. Kamionka, M. Majewski, K. Roth, R. Bertram, C. Kraft, W. Hillen, Induction of single chain tetracycline repressor requires the binding of two inducers, Nucleic Acids Res. 34 (2006) 3834–3841.

[20] C. Hsu, V. Jaquet, M. Gencoglu, A. Becskei, Protein dimerization generates bistability in positive feedback loops, Cell Rep. 16 (2016) 1204–1210.

[21] I. Majer, A. Hajihosseini, A. Becskei, Identification of optimal parameter combinations for the emergence of bistability, Phys. Biol. 12 (2015) 066,011, http://dx.doi.org/10.1088/1478-3975/12/6/066011.

[22] N. Rai, R. Anand, K. Ramkumar, V. Sreenivasan, S. Dabholkar, K.V. Venkatesh, et al., Prediction by promoter logic in bacterial quorum sensing, PLoS Comput. Biol. 8 (2012), e1002361 http://dx.doi.org/10.1371/journal.pcbi.1002361.

[23] M. Thattai, A. van Oudenaarden, Intrinsic noise in gene regulatory networks, Proc. Natl. Acad. Sci. U. S. A. 98 (2001) 8614–8619.

[24] A. Raj, C.S. Peskin, D. Tranchina, D.Y. Vargas, S. Tyagi, Stochastic mRNA synthesis in mammalian cells, PLoS Biol. 4 (2006), e309 http://dx.doi.org/10.1371/journal.pbio.0040309.

[25] S. Tsuru, J. Ichinose, A. Kashiwagi, B.W. Ying, K. Kaneko, T. Yomo, Noisy cell growth rate leads to fluctuating protein concentration in bacteria, Phys. Biol. 6 (2009) 036015, http://dx.doi.org/10.1088/1478-3975/6/3/036015.

[26] O.G. Berg, J. Paulsson, M. Ehrenberg, Fluctuations and quality of control in biological cells: zero-order ultrasensitivity reinvestigated, Biophys. J. 79 (2000) 1228–1236.

[27] M.S. Samoilov, A.P. Arkin, Deviant effects in molecular reaction pathways, Nat. Biotechnol. 24 (2006) 1235–1240.

[28] L. Cai, C.K. Dalal, M.B. Elowitz, Frequency-modulated nuclear localization bursts coordinate gene regulation, Nature. 455 (2008) 485–490.

[29] A.J. Ninfa, A.E. Mayo, Hysteresis vs. graded responses: the connections make all the difference, Sci. STKE 2004 (2004), pe20 http://dx.doi.org/10.1126/stke.2322004pe20.

[30] R. Hermsen, D.W. Erickson, T. Hwa, Speed, sensitivity, and bistability in auto-activating signaling circuits, PLoS Comput. Biol. 7 (2011), e1002265 http://dx.doi.org/10.1371/journal.pcbi.1002265.

[31] A. Lipshtat, A. Loinger, N.Q. Balaban, O. Biham, Genetic toggle switch without cooperative binding, Phys. Rev. Lett. 96 (2006) 188,101, http://dx.doi.org/10.1103/PhysRevLett.96.188101.

[32] A. Ochab-Marcinek, M. Tabaka, Bimodal gene expression in noncooperative regulatory systems, Proc. Natl. Acad. Sci. U. S. A. 107 (2010) 22,096–22,101.

[33] T.L. To, N. Maheshri, Noise can induce bimodality in positive transcriptional feedback loops without bistability, Science. 327 (2010) 1142–1145.

[34] C. Chen, R. Bundschuh, Quantitative models for accelerated protein dissociation from nucleosomal DNA, Nucleic Acids Res. 42 (2014) 9753–9760.

[35] D.J. Wilkinson, Stochastic modelling for quantitative description of heterogeneous biological systems, Nat. Rev. Genet. 10 (2009) 122–133.

[36] T. Gedeon, P. Bokes, Delayed protein synthesis reduces the correlation between mRNA and protein fluctuations, Biophys. J. 103 (2012) 377–385.

[37] G. Yao, C. Tan, M. West, J.R. Nevins, L. You, Origin of bistability underlying mammalian cell cycle entry, Mol. Syst. Biol. 7 (2011) 485, http://dx.doi.org/10.1038/msb.2011.19.

[38] J.W. Veening, O.A. Igoshin, R.T. Eijlander, R. Nijland, L.W. Hamoen, O.P. Kuipers, Transient heterogeneity in extracellular protease production by *Bacillus subtilis*, Mol. Syst. Biol. 4 (2008) 184.

[39] L.S. Weinberger, R.D. Dar, M.L. Simpson, Transient-mediated fate determination in a transcriptional circuit of HIV, Nat. Genet. 40 (2008) 466–470.

[40] G.M. Suel, J. Garcia-Ojalvo, L.M. Liberman, M.B. Elowitz, An excitable gene regulatory circuit induces transient cellular differentiation, Nature. 440 (2006) 545–550.

[41] M.M. Bonde, S. Voegeli, A. Baudrimont, B. Seraphin, A. Becskei, Quantification of pre-mRNA escape rate and synergy in splicing, Nucleic Acids Res. 42 (2014) 12,847–12,860.

[42] A. Raj, P. van den Bogaard, S.A. Rifkin, A. van Oudenaarden, S. Tyagi, Imaging individual mRNA molecules using multiple singly labeled probes, Nat. Methods 5 (2008) 877–879.
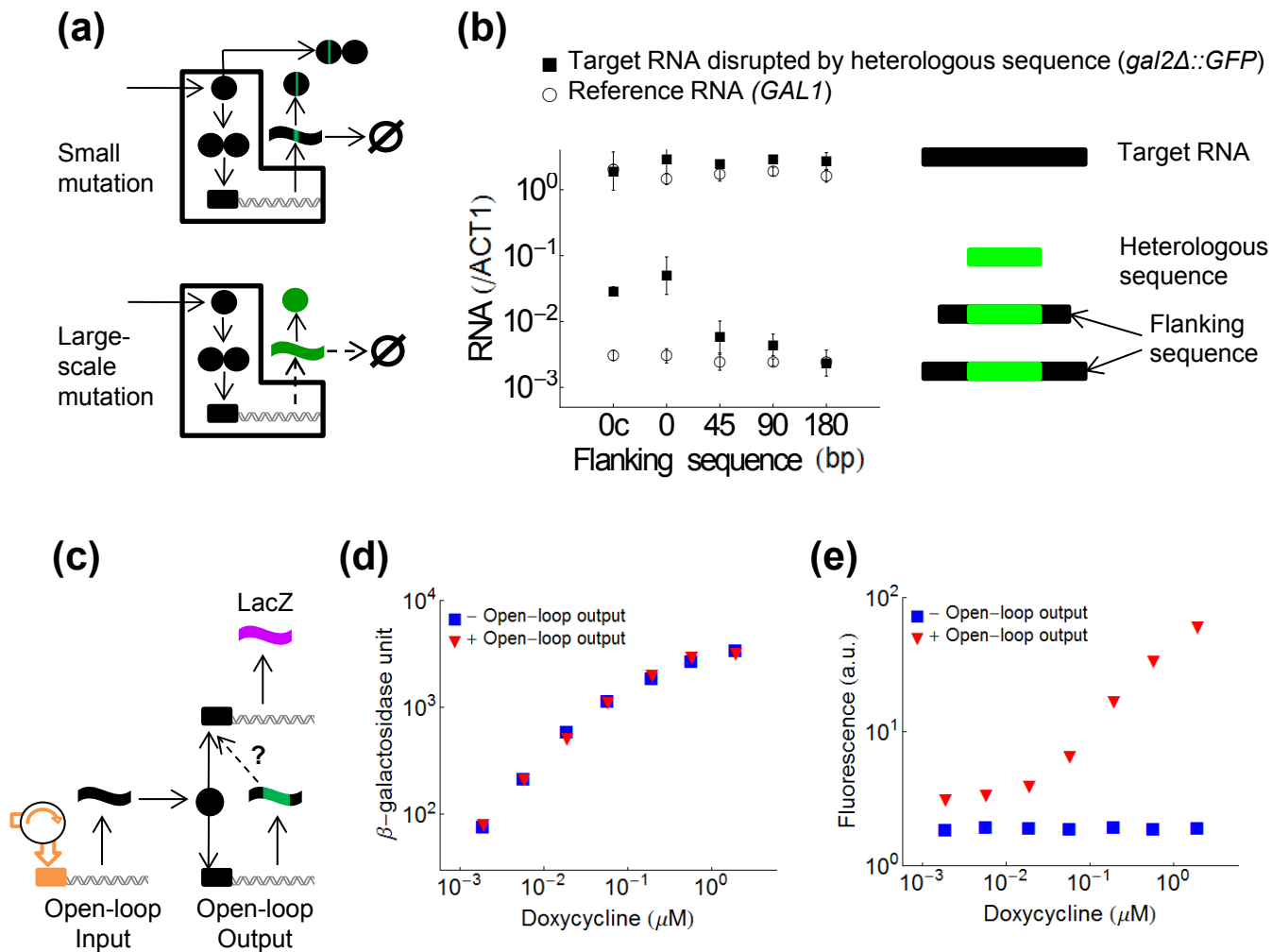
Fig. S1. Design strategies and interference assessment of the open-loop output construct. (a) Design strategies of the output RNA. If the mutation in the RNA is small (upper panel), the translated protein contains a small mutation, which may fail to prevent it from interfering with the wt protein. If the mutation is large (lower panel), the RNA synthesis and decay rates may change (dashed arrows). (b) The expression range of the target gene (*GAL2*) and the reference *GAL1* genes was assessed in the presence of 0 and 0.5% galactose, represented by the lower and upper symbols for each gene. For the *GAL2* gene constructs (0c to 180), segments of different lengths were replaced in the target gene by a heterologous sequence (GFP) so that flanking sequences of indicated lengths remained (strains indicated by "Assessment of flanking region" Table S1). The 0c refers to a full ORF replacement that is transferred to a different chromosomal locus. Error bars stand for standard deviation (*n* = 3). (c-e) Assessment of interference by the open-loop output construct. The open-loop output RNA must not interfere with the other reactions in the loop. Therefore, we tested if the output protein heterodimerizes with the input protein (rtTA) by assessing how the output changes the response of an rtTA target promoter (P[tetO]4-*GAL1*c). The promoter response was read out using lacZ as a reporter gene. The expression of the output was also under control of the P[tetO]4-*GAL1*c promoter. To test the strongest possible interference, the output was made without a stem-loop so that its translation was not attenuated ("Interference assessment" strains, Table S1) (c). LacZ expression was measured by a β-galactosidase assay in strain either with (+) or without (-) the presence of the open-loop output construct. A constant rtTA expression was induced with 5.2 nM estradiol. The ratio of β-galactosidase activity of cells containing to those lacking the open-loop output construct is 0.97±0.16 (mean ± *sd*, *n*=18 over the dox range measured in three independent experiments), which indicates the absence of interference of the output (d). The expression level of the open-loop output construct in (d) was monitored with flow cytometry in order to confirm the presence of the output protein, utilizing the heterologous YFP sequence in the output (e).
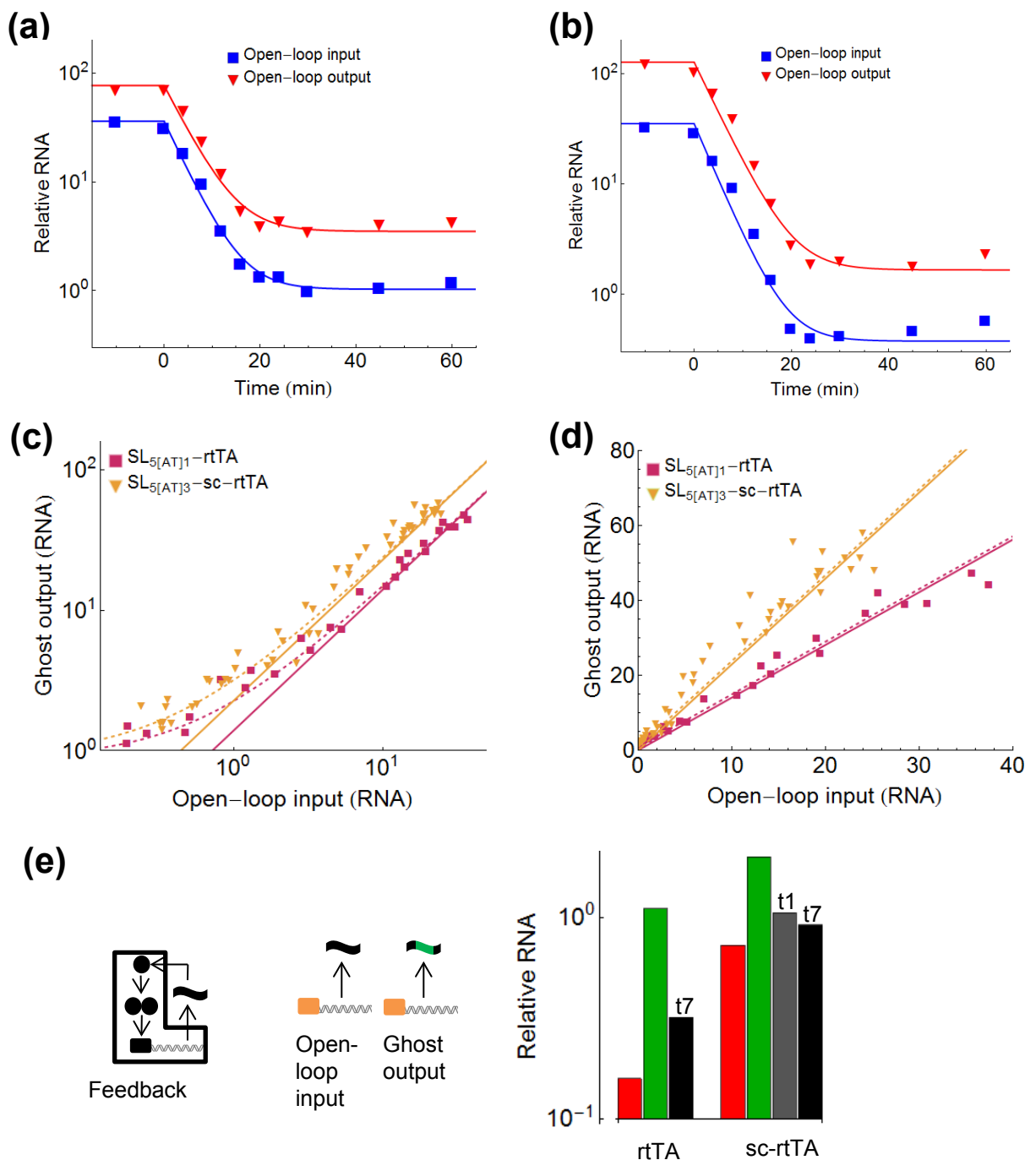
Fig. S2. Assessment of the equivalence between the input and output mRNAs.
(a, b) Decay rates of the input and output mRNAs in Equivalence Assessment cells (see Ych214.2 (a) and Ych258 (b) in Table S1). Their expression was induced and maintained with 0.5% galactose. To stop RNA production, the cells were washed to remove galactose at time=0 (see Materials and Methods, Growth conditions). Decay rate constants (estimate ± its standard error) of input and output for $SL_{5[AT]1}$-rtTA were 0.22±0.01 and 0.20±0.02 (min^{-1}) respectively (a) and 0.24±0.02 and 0.21±0.02 (min^{-1}) for $SL_{5[AT]3}$-sc-rtTA (b). As an internal control, the *GAL1* mRNA decay rates in these experiments were 0.18±0.01 (a) and 0.21±0.01 (min^{-1}) (b). (c, d) The RNA equivalence assessment with the Equivalence Assessment cells (Table S1). The slopes of the fitted lines (*s*) were determined with linear regression (see values in Table S2). For sc-rtTA, the data are also presented in Fig. 2d. The dashed curves represent the fits of the linear function ($b + s\ input$) where b is the basal expression of the ghost output. The full lines represent the above linear function without the basal expression. The data were presented in logarithmic axes (c) and linear axes (d). (e) Comparison of basal expression in the strains for equivalence assessment (red, green) and in the strains for feedback loops (gray, black) (Feedback cells, Table S1). Cells were grown in media without inducers. To compare the (sc-)rtTA RNA (red) with the corresponding ghost-output RNA (green), the rtTA and sc-rtTA RNAs were calibrated with corresponding scaling factor (*s*). Black and gray: (sc-)rtTA in the feedback strains with either $P_{[tetO7]}$ (t7) or $P_{[tetO1]}$ (t1) promoters.
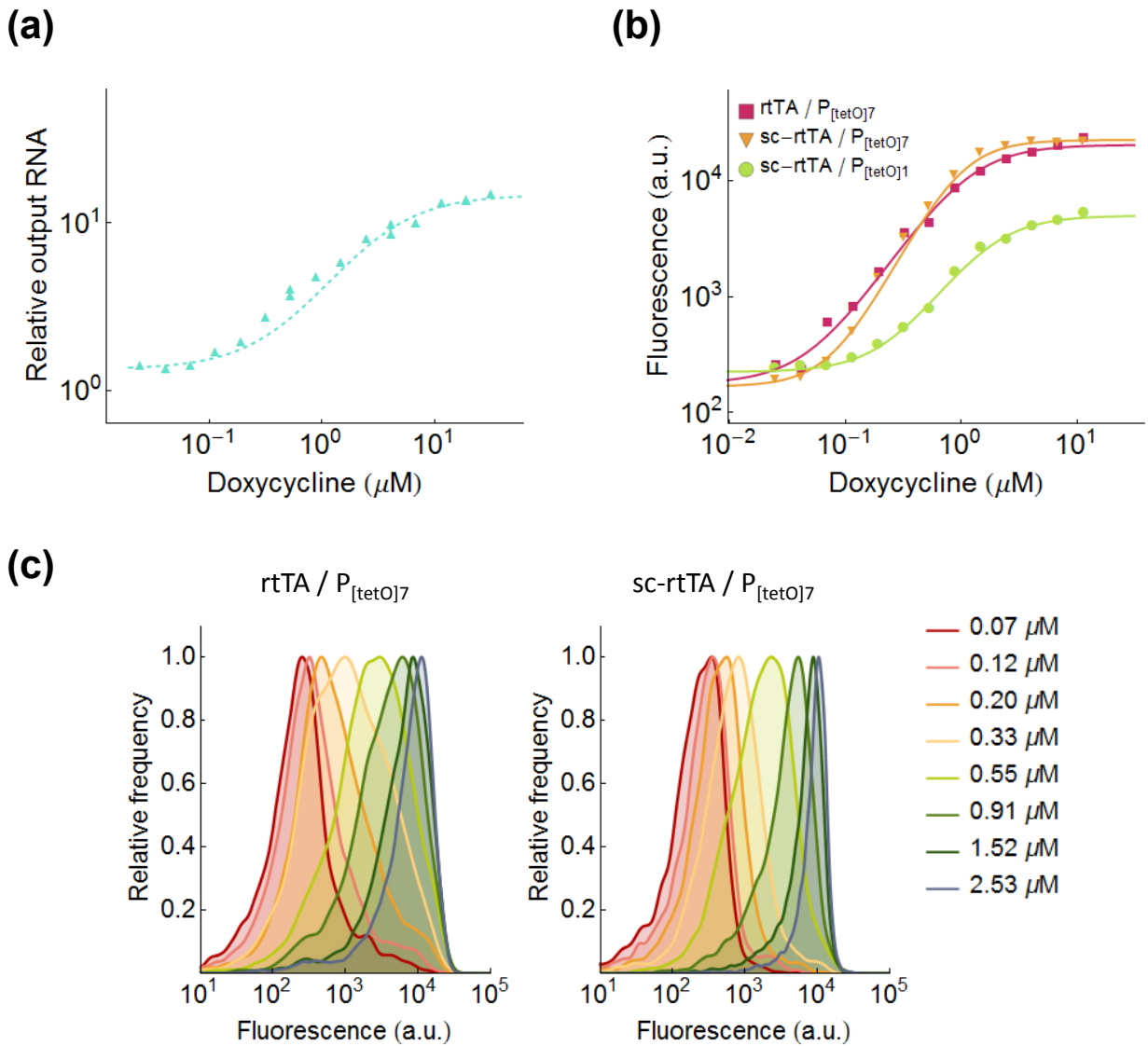
Fig. S3. Determination of the Hill coefficient for the response of gene expression to doxycycline.
(a) mRNA expression in the input / output cell, with $P_{[tetO]1}$ promoter driven by a constant amount of sc-rtTA (RNA (ω) = 3.79, estradiol = 0.57 nM) (see Ych257 in Table S1). The steady-state amount of output RNA was measured as the concentration of doxycycline was varied. Dashed line, the fitted $f_{OLM}(\omega, dox)$ open-loop function. The Hill coefficient for $f_{OLM}(dox)$ was $n_2 = 1.24$. (b) Determination of Hill coefficients for the doxycycline response, n_2, with flow cytometry. For this purpose, cells similar to the I/O strains were constructed with the exception that the SL-output was replaced by GFP (strains indicated with "Hill coefficient for doxycycline response" in Table S1); in this way, there is no inhibition of translation and GFP fluorescence can be measured. A constant input expression was induced with 5.2 nM estradiol. Lines, nonlinear fitting with a simple Hill function with basal expression. The fitted Hill coefficients for rtTA/$P_{[tetO]7}$, sc-rtTA/$P_{[tetO]7}$, sc-rtTA/$P_{[tetO]1}$ in response to dox are 1.50 ± 0.18 ($n=6$), 2.02 ± 0.12 ($n=3$) and 1.38 ± 0.14 ($n=6$), (mean $\pm$ sd) respectively. These fitted values were taken to restrict the range of the Hill coefficients for dox response (n_2) in the fitting of the corresponding open-loop function, $f_{OLM}(\omega, dox)$ (see SI text, Fitting of open-loop functions, $f_{OLM}(\omega, dox)$). (c) GFP fluorescence distribution in strains used for the doxycycline response curves (as in (b)). The relative frequency is scaled so that the maximum frequency is set to 1.
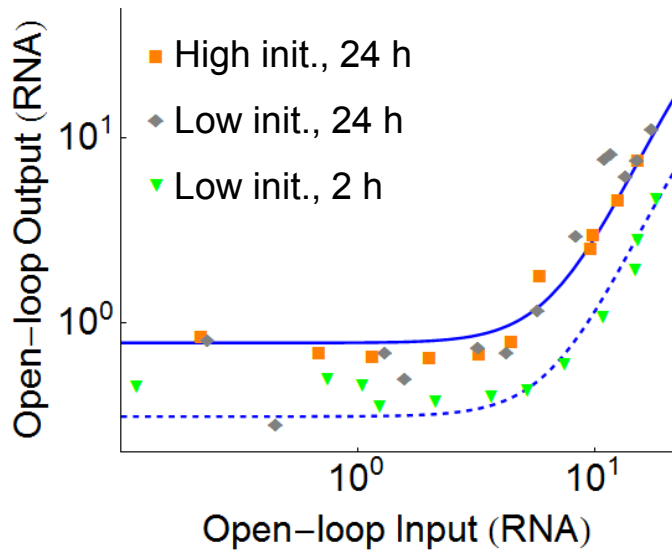
Fig. S4. Feedback opening reached steady-state in 24 hours.
The input-output response for the cooperative-dimeric circuit was measured at 2 or 24 h after uninduced (Low init.) cells were grown with 0.1 μM doxycycline. For high initial condition (High init.), the cells were induced with 0.5% galactose and 1.95 μM doxycycline before washed and transferred to 0.1 μM doxycycline. qPCR was performed with primer pairs for the input (5'-GGGAAAGCTGGCAAGATTTTTTA-3'; 5'-GTGTACCTAAATGTACTTTTGCTCCAT-3', efficiency 1.868) and output (5'-ATCTGCCCTTTCGAAAGATCCCAA-3'; 5'-GCATCGGTAAACATCTGTTTGTATAGTTCAT-3', efficiency 1.870). Solid line indicates $f_{OLM}(\omega$, dox= 1.95 μM); dashed line, 0.4 x $f_{OLM}(\omega$, dox= 1.95 μM)
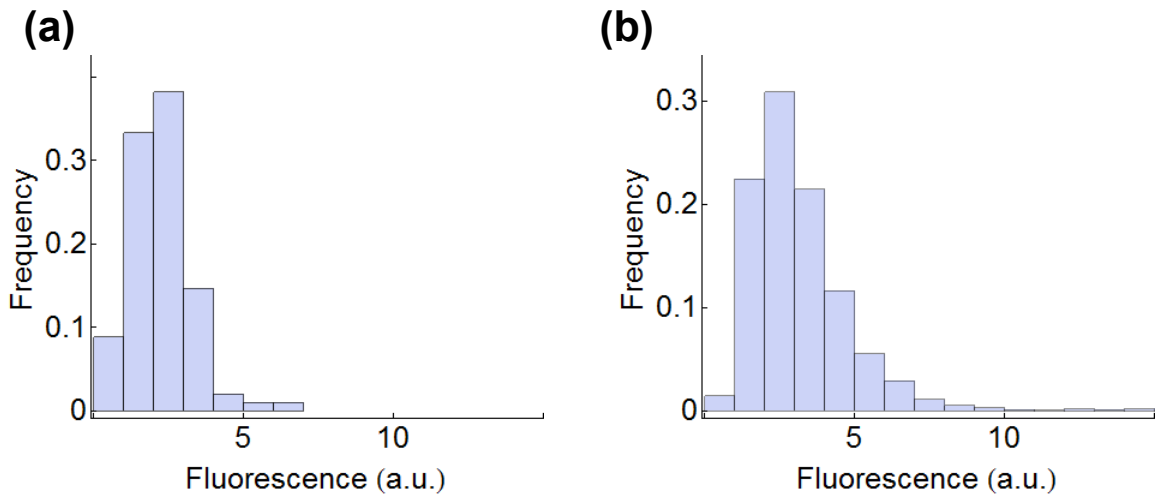
Fig. S5. Distribution of raw fluorescence intensity of the detected spots in the smFISH experiment prior to background subtraction.

Data were obtained from smFISH experiments for Fig. 5a, b with cells containing the cooperative-dimeric feedback loop (see Yvj87.2 in Table S1). 0.98% (n=102) and 1.89% (n=6834) of the spots were detected with very high fluorescence intensity (>11) for the uninduced (a) and induced (b) cells, respectively. The distribution was unimodal in both cases, indicating each spot detected a single mRNA molecule because in the opposite case, multimodal distribution would have appeared. The spots with very high fluorescence intensity may reflect to clumps of mRNA molecules; yet given the low occurrence in the experiments, presence of clumps was negligible.

Supplementary Tables

Table S1. Yeast strains.

Diploid Strain	Haploid parents (A / alpha)	ade2:: **ADE2**_	ura3:: **URA3**_	his3:: **HIS3**_	Function
Ych207.3	Yvj40.3			P_*MRP7* ∣ GEV (pPR1)	I/O
	Yvj71.8	P_*GAL1*UAS-*CYC1*c ∣ SL_5[AT]1∣ rtTA (pVJ46)	P_[tetO]7- *CYC1*c ∣ SL_5[AT]1 ∣ rtTAΔ(45/45)::YFP (pCH067)		
Ych290.2	Yvj40.3			P_*MRP7* ∣ GEV (pPR1)	I/O
	Ych285.2	P_*GAL1*UAS-*CYC1*c ∣ SL_5[AT]3 ∣ sc-rtTA (pCH102)	P_[tetO]7- *CYC1*c ∣ SL_5[AT]3 ∣ rtTAΔ(45/45)::YFP (pCH104)		
Ych257	Yvj40.3			P_*MRP7* ∣ GEV (pPR1)	I/O
	Ych252.8	P_*GAL1*UAS-*CYC1*c ∣ SL_5[AT]3 ∣ sc-rtTA (pCH102)	P_[tetO]1- *CYC1*c ∣ SL_5[AT]3 ∣ rtTAΔ(45/45)::YFP (pCH103)		
Ych214.2	Ych211.2	P_*GAL1*UAS-*CYC1*c ∣ SL_5[AT]1 ∣ rtTAΔ(45/45)::YFP (pVJ47)		P_*MRP7* ∣ GEV (pPR1)	Equivalence Assessment
	Yvj69.3	P_*GAL1*UAS-*CYC1*c ∣ SL_5[AT]1 ∣ rtTA (pVJ46)	(pRS306)		
Ych258	Ych248.5	P_*GAL1*UAS-*CYC1*c ∣ SL_5[AT]3 ∣ rtTAΔ(45/45)::YFP (pCH100)		P_*MRP7* ∣ GEV (pPR1)	Equivalence Assessment
	Ych251.1	P_*GAL1*UAS-*CYC1*c ∣ SL_5[AT]3 ∣ sc-rtTA (pCH102)	(pRS306)		
Yvj87.2*	Yvj79.2		P_[tetO]7- *CYC1*c ∣ SL_5[AT]1 ∣ rtTA (pCH068)	P_*MRP7* ∣ GEV (pPR1)	Feedback
	Yvj70.1	P_*GAL1*UAS-*CYC1*c ∣ SL_5[AT]1 ∣rtTA (pVJ46)	P_[tetO]2- *CYC1*c ∣ *yEGFP* (pABG10)		
Ych260.2*	Yvj80.1		P_[tetO]7- *CYC1*c ∣ SL_5[AT]3 ∣ sc-rtTA (pCH91)	P_*MRP7* ∣ GEV (pPR1)	Feedback
	Ych250.2	P_*GAL1*UAS-*CYC1*c ∣ SL_5[AT]3 ∣ sc-rtTA(pCH102)	P_[tetO]2- *CYC1*c ∣ *yEGFP* (pABG10)		
Yvj109.5*	Yvj107.5		P_[tetO]1- *CYC1*c ∣ SL_5[AT]3 ∣ sc-rtTA (pCH083)	P_*MRP7* ∣ GEV (pPR1)	Feedback
	Ych250.2	P_*GAL1*UAS-*CYC1*c ∣ SL_5[AT]3 ∣ sc-rtTA (pCH102)	P_[tetO]2- *CYC1*c ∣ *yEGFP* (pABG10)		

Diploid Strain	Haploid parents	Integration locus (plasmid)			Function
	A / alpha	*ade2:: **ADE2**_*	*ura3:: **URA3**_*	*his3:: **HIS3**_*	
Ych259.2	Yvj40.3			P_*MRP7* ∣GEV (pPR1)	Transient kinetics
	Ych250.2	P_*GAL1*UAS-*CYC1*c ∣ SL_5[AT]3 ∣sc- rtTA (pCH102)	P_[tetO]2- *CYC1*c ∣ *yEGFP* (pABG10)		
Ych288	Ych283.1		P_[tetO]4-*GAL1*c ∣ *LacZ* (pAnt179)	P_*MRP7* ∣GEV (pPR1)	Interference assessment
	Ych171.2	P_*GAL1*UAS-*CYC1*c ∣ rtTA (pCH099)			
Ych289.1	Ych283.1		P_[tetO]4-*GAL1*c ∣ *LacZ* (pAnt179)	P_*MRP7* ∣GEV (pPR1)	Interference assessment
	Ych284.1	P_*GAL1*UAS-*CYC1*c ∣ rtTA (pCH099)	P_[tetO]1- *CYC1*c ∣ rtTAΔ(45/45)::YFP (pCH098)		
Ych279.6	Ych278.6		P_[tetO]7- *CYC1*c ∣ *yEGFP* (pAB G11)	P_*MRP7* ∣GEV (pPR1)	Hill coefficient for dox response
	Yvj67.4	P_*GAL1*UAS-*CYC1*c ∣ SL_5[AT]1 ∣ rtTA (pVJ46)			
Ych269	Yvj92.7		P_[tetO]1- *CYC1*c ∣ *yEGFP* (pCH001)	P_*MRP7* ∣GEV (pPR1)	Hill coefficient for dox response
	Ych241.7	P_*GAL1*UAS-*CYC1*c ∣ SL_5[AT]3 ∣ sc-rtTA (pCH102)			
Ych296.3	Yvj93.3		P_[tetO]7- *CYC1*c ∣ *yEGFP* (pAB G11)	P_*MRP7* ∣GEV (pPR1)	Hill coefficient for dox response
	Ych241.7	P_*GAL1*UAS-*CYC1*c ∣ SL_5[AT]3 ∣ sc-rtTA (pCH102)			
Ych294[*]	Yvj40.3			P_*MRP7* ∣GEV (pPR1)	smFISH negative control
	Ych89.2	(pRS402)	P_[tetO]2- *CYC1*c ∣ *yEGFP* (pABG10)		

Haploid Strain	Mating Type Parent strain	Genotype (plasmid)	Function
HHS75.2	MAT A SY991	*FIG1*:: P_*GAL2* ⏐ GFP ⏐ T_*CYC1_HIS3* (pSS29)	Assessment of flanking region
HHS72.4	MAT A SY991	*GAL2*:: P_*GAL2* ⏐ gal2Δ(0/0)::GFP ⏐ T_*GAL2* ⏐ *HIS3* (pSS51)	Assessment of flanking region
HHS73.2	MAT A SY991	*GAL2*:: P_*GAL2* ⏐ gal2Δ(45/45)::GFP ⏐ T_*GAL2* ⏐ *HIS3* (pSS52)	Assessment of flanking region
HHS71.1	MAT A SY991	*GAL2*:: P_*GAL2* ⏐ gal2Δ(90/90)::GFP ⏐ T_*GAL2* ⏐ *HIS3* (pSS50)	Assessment of flanking region
HHS74.2	MAT A SY991	*GAL2*:: P_*GAL2* ⏐ gal2Δ(180/180)::GFP ⏐ T_*GAL2* ⏐ *HIS3* (pSS53)	Assessment of flanking region

[*] Constructed as in [20].

Table S2. Parameters used in the modeling.

	Description	Value	Unit
δ_p	Protein decay rate constant [**]	0.0095[***]	min^{-1}
μ	Translation rate constant [**]	0.54, SL$_{5[AT]1}$ 4.83, SL$_{5[AT]3}$	min^{-1}
δ_m	RNA decay rate constant	0.2291[***]	min^{-1}
s	Scaling factor for the measured equivalence plane: Open-loop input / Ghost-output	1.40, SL$_{5[AT]1}$-rtTA 2.29, SL$_{5[AT]3}$-sc-rtTA	-
α	RNA concentration re-scaling constant (smFISH / qPCR relative RNA)	2.11, SL$_{5[AT]1}$-rtTA 2.31, SL$_{5[AT]3}$-sc-rtTA	-
λ_{OFF}	Promoter inactivation rate constant [*]	13.3, rtTA$\rightarrow$ P$_{[tetO]7}$ 11.5, sc-rtTA $\rightarrow$ P$_{[tetO]7}$ 6.4, sc-rtTA $\rightarrow$ P$_{[tetO]1}$	min^{-1}
	Production rate for the RNA degradation enzyme [*]	0.20	min^{-1}

[*] Used in the model to fit RNA noise; see Supplementary Information for details.

[**] Determined in [20].

[***] Mean of decay rate of rtTA and sc-rtTA.

Supplementary information

Mathematical modelling

Contribution of Bistability and Noise to Cell Fate Transitions Determined by Feedback Opening

Chieh Hsu, Vincent Jaquet, Farzaneh Maleki, & Attila Becskei

Contents

Open-to-closed loop mapping

The open-to-closed loop mapping serves to identify the steady-state expression levels in the feedback loop based on the open-loop function without the need to identify the time scale of individual reactions.

The intersection of the open-loop function $f_{OL}(\omega)$ and equivalence plane defines steady-state levels in the feedback loops

The open-loop function is fitted to data obtained by measuring steady-state expression levels of the input (ω) and output (η) mRNAs in the open-loop constructs at specific doxycycline *(dox)* concentrations:

$$\eta = f_{OL}(\omega, dox) \tag{1}$$

The steady-state expression level of the feedback loop is obtained by re-closing the loop, i.e. by equating the input (ω) and output (η), assuming an ideal equivalence between the input and output:

$$\eta = \omega \tag{2}$$

Combining (1) and (2) results in $f_{OL}(\omega, dox) = \omega$. We replace ω with x to distinguish the steady-state expression in the feedback loop system (x) and termed the resulting function of one variable (dox) open-to-closed loop mapping:

$$x = f_{OTCL}(dox). \tag{3}$$

x is the steady-state expression levels in a bistable system provided some conditions are met, as detailed by Angeli et al [1]. Most importantly, the system has to be monotone. Monotonicity is lost if the system contains for example a negative feedback loop.

Scaling of output signal for fitted equivalence, $f_{EQ}(\omega)$

In real systems, the input and output mRNAs may be scaled differently. The input RNA (ω) is identical to the original RNA inside the feedback loop. On the other hand, the output RNA is different and may have different synthesis rates. Using linear regression, we can obtain the scaling factor s (see Table S2) between the open-loop input and ghost output mRNA (see e.g. Fig. S2c, d):

$$\eta = f_{EQ}(\omega) = s\,\omega \tag{4}$$

For ideal equivalence, $s = 1$.

To reclose the loop, $\eta = f_{OLM}(\omega, dox) = f_{EQ}(\omega, dox) = s\,\omega$.

Alternatively, we convert first f_{OLM}, fitted to experimental data, to an ideal open-loop function f_{OL}:

$$f_{OL}(\omega) = f_{OLM}(\omega)/s, \tag{5}$$

and then we proceed as described to obtain (3).

See also in the following section "Basal expression in open and closed loops" for further discussion.

Fitting of open-loop functions, $f_{OLM}(\omega, dox)$

Nonlinear regression was used to fit the parameters in the open-loop functions $f_{OLM}(\omega, dox)$. To construct the function, Hill functions were used for cooperative promoter response and a dimerization term, κ was used for dimerization:

$$\kappa = \frac{\delta_{mo}{}^2 (k_d + \delta_{di})}{4\delta_{di}{}^2 k_a},$$

where δ_{mo}, δ_{di}, k_a and k_d are the rate constants of monomer decay, dimer decay, association and dissociation in the rtTA dimerization process, respectively [2].

When no good fit was obtained in this way, which was the case for the monomeric-noncooperative feedback loop ($P_{[tetO]1}$ sc-rtTA), then alternative functions were sought.

To fit the open-loop function, $f_{OLM}(\omega, dox)$ at least two data series were used: (1) by varying the input at three different fixed dox concentration and (2) by varying dox at one or more fixed input values.

To match the variations in doxycycline activities used for the open-loop and closed loop measurements, a 24 h hysteresis experiment with high initial condition was performed. To reduce the parameter search in the fitting of the output RNA versus dox and input RNA data, we restricted the range of Hill coefficient for doxycycline response, n_2, with gene expression data obtained with flow cytometry (Fig. S3b). The range corresponded to mean±*sd* obtained from biological replicates.

The variable ω represents the input (rtTA or sc-rtTA) RNA as measured with qPCR. The *dox* in the functions represents the doxycycline concentration (μg/ml); 1 μg/ml doxycycline = 1.95 μM.

Basal expression in open and closed loops

The output construct was designed in a way to reduce basal expression (Fig. S1b, Materials and Methods). The basal expression of the output decreases with increasing length of the flanking sequences (Fig. S1b). However, there is a limit to which the basal expression can be reduced. Indeed, our measurements show that the basal expression in the feedback loop is lower than in the output constructs. Therefore, we subtracted the basal expression in the ghost output b from the fitted to the equivalence line $f_{EQf}(\omega) = s\omega + b$ to obtain $f_{EQ}(\omega) = f_{EQf}(\omega) - b$ (Fig. S2c, d, dashed and full lines).

In order to assess the validity of this extrapolation, the basal expression in the feedback loops was adjusted to values comparable to or higher than the b in the open-loop; the prediction of the transition rates were equally good in the fitted and the extrapolated part (manuscript in preparation).

When the open-loop function was re-closed to determine the steady-state expression for the feedback loop, the basal expression was measured in the feedback constructs and we set the value b/V_{max} to match the feedback expression dynamic range, the ratio of maximally induced (at 19.5 μM doxycycline) expression level to the uninduced expression level.

Fitted open-loop functions, $f_{OLM}(\omega, dox)$

Dimeric- cooperative system (rtTA → P$_{[tetO]7}$)

$$f_{OLM}(\omega, dox) = V_{max} \frac{r_{dim}(\omega)^{n_1}}{\dfrac{k_1}{dox^{n_2}} + r_{dim}(\omega)^{n_1}} + b \qquad (6)$$

where

$$r_{dim}(\omega) = \omega + \frac{\kappa - \sqrt{4\omega\kappa + \kappa^2}}{2}$$

The following values were fitted:

$V_{max} = 74.48$; $k_1 = 0.036$; $\kappa = 719.7$; $n_1 = 1.462$; $n_2 = 1.32$; $b = 0.78$.

V_{max} was fitted in the context of $f_{OLM}(dox)$ and the rest of the parameters were fitted in the context of the $f_{OLM}(\omega)$ function.

Monomeric - cooperative system (sc-rtTA → P$_{[tetO]7}$)

$$f_{OLM}(\omega, dox) = V_{max} \frac{\omega^{n_1}}{\dfrac{k_1}{dox^{n_2}} + \omega^{n_1}} + b \qquad (7)$$

where the following parameters were fitted in the context of the $f_{OLM}(\omega, dox)$ function.

$V_{max} = 54.64$; $k_1 = 8.71$; $n_1 = 1.942$; $n_2 = 1.9$; $b = 0.78$.

Monomeric - noncooperative system (sc-rtTA → P$_{[tetO]1}$)

$$f_{OLM}\left(\omega, dox\right) = V_{max} \frac{\omega^{n_1}}{\dfrac{k_1}{dox^{n_2}} + \omega^{n_1}} \frac{\omega^{n_3}}{k_2 + \omega^{n_3}} + b \tag{8}$$

where the following parameters were fitted in the context of the $f_{OLM}(\omega, dox)$ function.

$V_{max} = 39.80;\ k_1 = 3.15;\ k_2 = 5.69;\ n_1 = 0.451;\ n_2 = 1.24;\ n_3 = 0.795;\ b = 0.33.$

Extension of the open-loop function into a kinetic model

Inclusion of mRNA and protein turnover (synthesis and decay): simple model

For the prediction of time dependent behavior, the open-loop function has to be extended into a model, which incorporates information on the time-scale of the reactions. In other words, the reactions within the "black box" between the input and output have to be specified so that the nonlinearity of the overall $f_{OL}(\omega, dox)$, open-loop function, remains valid. The reactions can be specified to an arbitrary degree of detail but in practice, some reactions always remain lumped. In this way, the open loop can be simulated stochastically to predict the mean expression (see e.g. Fig. 5d) or upon re-closing the loop, the transition rates can be predicted by stochastic simulation.

We will first consider only the RNA production and degradation reactions, lumping all the other reaction steps (1D system) to illustrate the principles of the extension. Later, we include the protein reactions (2D system).

Specifying the time-scale of the reaction in the 1-dimensional (1D) system (opening at the RNA level)
The open-loop function at steady state is defined by the following mapping:

$$f_{OL}:\ \omega \ \rightarrow \ \eta \tag{9}$$

where the input ω and output η stand for the RNA molecules. Therefore, we consider first the time-scale of RNA reactions, which is specified by the decay constant, δ_m. Adding back time dependency, relation (9) is re-written as a differential equation describing the open-loop system:

$$\frac{d\eta}{dt} = \delta_m \left(f_{OL}\left(\omega, dox\right) - \eta \right) \tag{10}$$

Thus, the production rate of the mRNA is given by $\delta_m f_{OL}(\omega)$. The nonlinear responses due to protein dimerization, binding of the activator to the promoter, etc. are lumped into the function, $f_{OL}(\omega)$.

The corresponding (re-)closed loop system is:

$$\frac{dRNA}{dt} = \delta_m f_{OL}\left(RNA, dox\right) - \delta_m RNA \tag{11}$$

Introduction of the variable for the protein (2D system)
Next, we illustrate how to include the protein, P. If only linear reactions are specified, the originally fitted open-loop function, $f_{OL}(\omega, dox)$ can be retained as a transfer function without the need to decompose it.

Thus, the reactions for RNA and protein turnover are specified in the following way for the open-loop system:

$$\frac{d\eta}{dt} = \delta_m f_2\left(P\right) - \delta_m \eta \tag{12}$$

$$\frac{dP}{dt} = \mu\omega - \delta_P P \tag{13}$$

Both the input ω and the output η correspond to RNA. In contrast to the 1D system, the nonlinear transfer function $f_2(P)$ maps protein P into RNA. Therefore, we wanted to re-define $f_2(P)$ that maps RNA into RNA in order to use the originally defined mapping (9).

The transfer functions in the two systems (1D and 2D) have to generate the same output. Therefore,

$$f_2(P) = f_{OL}(\omega(P)) \tag{14}$$

where, $\omega(P) = \dfrac{\delta_P P}{\mu}$ (from steady-state solution of (13)).

Interestingly, the direction of this mapping protein to ω (ie. RNA) is opposite to the direction of the flow of biological information (RNA to protein). Thus, last reaction species preceding the input has to be converted into ω.

In this way, the 2-variable closed system can be reconstituted with the original mapping (9) :

$$\frac{dRNA}{dt} = \delta_m f_{OL}(\omega(P)) - \delta_m RNA , \tag{15}$$

$$\frac{dP}{dt} = \mu RNA - \delta_P P$$

Re-scaling for the absolute RNA concentration
Since the input and output RNAs were measured in relative units, their concentration units have to be rescaled to molecule number / cell (RNA) from relative mRNA values. Because mRNAs including the $f_{OLM}(\omega)$ is determined by RT-qPCR, a proportionality constant (α) multiplies the RNAs measured by qPCR. RNA = α RNA$_{qPCR}$ (see Table S2).

In the following equations, the open-loop function corresponds to the direct fits to the measurements using qPCR but all the variables (RNA and protein) and parameters have absolute molecule / cell dimension.

$$\frac{dRNA}{dt} = \alpha\frac{\delta_m}{s} f_{OLM}(\omega(P)) - \delta_m RNA \tag{16}$$

$$\frac{dP}{dt} = \mu RNA - \delta_P P \tag{17}$$

, where

$$\omega(P) = \frac{\delta_P P}{\alpha\mu} \tag{18}$$

These equations were used for modelling of the feedback loop (simple deterministic model), e.g. for the induction kinetics of the monomeric – noncooperative loop.

Extension of model to fit the measured noise

Simple noise model
The simple noise model corresponds to the process described by equations (16), (17) and (18). The Gillespie stochastic simulation algorithm (SSA) was used to simulate the above processes.

Extended noise model: telegraphic promoter model and enzymatic mRNA degradation

To take the telegraphic promoter model into account, the above time scale specification for an open-loop function is applied to the promoter activation step (and not to the RNA production directly). In turn, the active promoter produces the RNA, leading to a production function that reaches a maximum speed. The saturation function for the telegraphic promoter is then equal to the $f_{OLM}(\omega)$ function normalized by V_{max}:

$$\frac{f_{OLM}(\omega)}{V_{max}} = \frac{\lambda_{ON}}{\lambda_{OFF} + \lambda_{ON}} \tag{19}$$

On the left hand side, both the numerator and denominator are measured quantities and the *s* drops out.

Accordingly, the following steps and reaction rate constants were defined for promoter and RNA kinetics in the stochastic simulation algorithm (SSA):

Reaction   Reaction rate

$I \rightarrow A$ $\lambda_{ON} = \lambda_{OFF} \dfrac{f_{OLM}(\omega)}{V_{max} - f_{OLM}(\omega)}$ (20)

where $\omega = \dfrac{\delta_P P}{\alpha \mu}$

$A \rightarrow I$ λ_{OFF}

$A \rightarrow A + RNA$ $\alpha \dfrac{V_{max} \delta_m}{s}$

$RNA \rightarrow 0$ $\delta_m \dfrac{E}{\langle E \rangle}$

λ_{OFF} and $<E>$ are calculated with the help of linear noise approximation (LNA) (see in the later section, Determination of parameter values for RNA distribution by linear noise approximation), λ_{ON} can be then obtained from the above equation (19).

Extension of model to fit transient kinetics

Two types of GFP induction experiments were performed in Fig. 4a, b: with and without pre-induced rtTA. In both cases, the induction kinetics was slower than expected from the decay rates. The speed of induction of a gene without feedback depends only on the decay rates and not on the first order production (synthesis) rates, such as transcription and translation rates (see next section "The speed of induction is affected only by the decay and not by the synthesis rates").

Therefore, any additional reactions accounting for the delay must occur between doxycycline uptake and association of doxycycline with the protein rtTA. In order to introduce such a function for the transient kinetics, a time-dependent term was included that affects the production rate in a nonlinear manner (e.g. transcription rate controlled by the promoter) because varying the production rate constant does not affect the speed of induction (see section "Incorporation of transient kinetics").

The speed of induction is affected only by the decay and not by the synthesis (transcription and translation) rates

The induction of GFP (see also Fig. 4a,b, pre-induced condition) is described by the following system of differential equations:

$$\frac{dRNA}{dt} = V_m - \delta_m RNA$$

$$\frac{dP}{dt} = \mu\, RNA - \delta_p P$$

The subscripts m and p represent mRNA and protein, respectively. To describe the condition for induction, the initial values for both the mRNA and protein are set to 0, and the system yields the following solution:

$$RNA(t) = V_m \frac{1}{\delta_m}\left[1 - e^{-t\delta_m}\right]$$

$$P(t) = V_m\left(\frac{\mu}{\delta_m \delta_p (\delta_p - \delta_m)}\right)\left[\delta_p\left(1 - e^{-\delta_m t}\right) - \delta_m\left(1 - e^{-\delta_p t}\right)\right]$$

It can be seen that the system's time scale is determined by the decay rates δ_m and δ_p and the transcription and translation rates shift the concentration only linearly.

Incorporation of the transient kinetics

To describe the transient kinetics, a perturbation function ($i(t)$) was constructed which describes the lower intracellular concentration / association of doxycycline upon induction, before reaching the steady-state. Thus, the TF-DNA affinity term was modified:

$$\frac{k_1}{dox^{n_2}}\left(1 + i(t)\right)^{n_i} \tag{21}$$

The perturbation decreases with time at a rate of $\delta_i = 0.006$ min^{-1}.

$$\frac{di}{dt} = -\delta_i i \tag{22}$$

The following values were fitted to RNA data obtained from the monomeric-noncooperative feedback loop (P$_{[tetO]1}$-sc-rtTA) induction (Fig. 4c): $n_i = 0.75$ and the initial concentration $i(0) = i_0 = 18.2$.

To check the transient kinetics with the fluorescence reporter (Fig. 4a,b,d), we approximated the response function of P$_{[tetO]2}$-GFP with that of monomeric-noncooperative system (sc-rtTA → P$_{[tetO]1}$): $V_{max}/b = 100$; $b = 0.5$; $\mu = 18.6$. The fluorescence intensity of the GFP protein was fitted for each measurement.

Additional methods for modeling

Stochastic simulations

Stochastic simulations were performed with the Gillespie SSA [3]. The actual simulations for the detection of transition between the two states were preceded by a pre-run. The pre-runs serve to obtain the probability distribution for a given initial condition. In order to reproduce the experimental conditions the following doxycycline concentrations were applied in the pre-run: 0 and 19.5 µM for the low and high initial conditions, respectively. Afterward, the actual doxycycline concentrations were applied and the simulation proceeded until the concentration of the activator reached the threshold value. The threshold value is the geometric mean of the concentrations of the activator at the low and the high states of the bistable system calculated at the geometric mean of the two doxycycline concentrations at which the fold bifurcations occur.

Specifically for the low initial condition, only the basal expression was allowed to proceed in the pre-run for twice of the protein half-life so that the initial values for the RNA, protein corresponded to the deterministic steady-state values of the actual basal expression. For the extended and fitted model, the inactive promoter state $I = 1$ and the steady-state value of the RNA degrading enzyme were taken for the pre-run. The perturbation function for the transient kinetics was applied only in the low initial condition.

Calculation of logarithmic sensitivities

Formula used to calculate logarithmic sensitivities:

$$S(\omega) = \frac{\partial \ln f_{OLM}(\omega, dox)}{\partial \ln \omega}$$

$$S(dox) = \frac{\partial \ln f_{OLM}(\omega, dox)}{\partial \ln dox}$$

Equations for the potentials

The potentials in Figure 1a and 8 were obtained by integrating $F(x)$ with the respect to x.

$$\frac{dx}{dt} = F(x) = V_{max}\frac{x^2}{x^2 + K_d^2} - \delta_x x + b$$

Where V_{max} = 1000, b = 10 and δ_x = 1. In Figure 1a, K_d = 471 and 354 in the left and right panel, respectively. In Figure 8, K_d = 429 for the left panel and the upper curve in the right panel and 408 for lower curve in the right panel.

Determination of parameter values for RNA distribution by linear noise approximation (LNA)

LNA was used to obtain analytical expressions for the *CV* (coefficient of variation = standard deviation / mean) of the RNA distribution, based on the extended and fitted noise model. All parameters in this model were determined experimentally by direct fitting, except for λ_{OFF} and *<E>*. In order to obtain their values, two sets of equations for *CV* were obtained for the measurements of the feedback constructs at maximally induced (at 19.5 μM doxycycline) and the uninduced expression levels. Measuring these two *CV* values permits the calculation of the above two unknown parameters.

The following notation was used for LNA [4]:

$$\dot{x} = F = S.V \tag{23}$$

$$B = S.diag(V).S^T \tag{24}$$

$$\dot{Cov} = J.Cov + (J.Cov)^T + B \tag{25}$$

F: vector field, *S*: stoichiometry matrix, *V*: reaction rates vector

B: diffusion matrix, *Cov*: covariance matrix, *J*: Jacobian of *F*

The above reactions system includes 5 variables:

$$V=\begin{bmatrix} \delta_P \langle E \rangle \\ \delta_P E \\ \lambda_{ON,b}(1-I) \\ \lambda_{OFF}I \\ \lambda_{ON}(1-A) \\ \lambda_{OFF}A \\ \alpha \dfrac{V_{max}\delta_m}{s}(I+A) \\ \delta_m \dfrac{E}{\langle E \rangle}RNA \\ \mu RNA \\ \delta_P P \end{bmatrix} \qquad S=\begin{bmatrix} 1 & -1 & 0 & 0 & 0 & 0 & 0 & 0 & 0 & 0 \\ 0 & 0 & 1 & -1 & 0 & 0 & 0 & 0 & 0 & 0 \\ 0 & 0 & 0 & 0 & 1 & -1 & 0 & 0 & 0 & 0 \\ 0 & 0 & 0 & 0 & 0 & 0 & 1 & -1 & 0 & 0 \\ 0 & 0 & 0 & 0 & 0 & 0 & 0 & 0 & 1 & -1 \end{bmatrix} \qquad (26)$$

To set the same burst size, the same λ_{OFF} value was taken for the basal and activator dependent promoter kinetics. $\lambda_{ON,b}$ and λ_{ON} are the activation rates of promoters related to basal and feedback respectively which were expressed from

$$\frac{\lambda_{ON,b}}{\lambda_{ON,b}+\lambda_{OFF}}=\frac{b}{V_{max}} \qquad (27)$$

$$\frac{\lambda_{ON}}{\lambda_{ON}+\lambda_{OFF}}=\frac{f_{OLM}(\omega)}{V_{max}} \qquad (28)$$

where $\omega=\dfrac{\delta_P P}{\alpha\mu}$

$f_{OLM}(\omega)$ is the fitted function with parameters specified in Table S2. V_{max} and b were measured in the feedback constructs. For 0 dox, Equation (27) applies; and for 19.5 µM dox, Equations (27) and (28) apply. In this way, $\lambda_{ON,b}$ and λ_{ON} become constant multiples of λ_{OFF}. Putting Equation (25) at the steady-state, variance of RNA will be obtained as a function of λ_{OFF} and $<E>$. Then by solving $Cov(RNA)/RNA^2 = CV^2_{experiment}$ at 0 and 19.5 µM dox, λ_{OFF} and $<E>$ are obtained.

References

[1] Angeli D, Ferrell JE, Jr., Sontag ED. Detection of multistability, bifurcations, and hysteresis in a large class of biological positive-feedback systems. Proc Natl Acad Sci U S A. 2004;101:1822-7.

[2] Buchler NE, Louis M. Molecular titration and ultrasensitivity in regulatory networks. J Mol Biol. 2008;384:1106-19.

[3] Gillespie DT. General Method for Numerically Simulating Stochastic Time Evolution of Coupled Chemical-Reactions. Journal of Computational Physics. 1976;22:403-34.

[4] Elf J, Ehrenberg M. Fast evaluation of fluctuations in biochemical networks with the linear noise approximation. Genome Res. 2003;13:2475-84.

IV. Modulation of the bistable region of positive feedback loops

Modulation of the bistable region of positive feedback loops

Vincent Jaquet[a], Chieh Hsu[a,b] & Attila Becskei[a]

[a]Biozentrum, University of Basel, Klingelbergstrasse 50/70, 4056 Basel, Switzerland

[b]School of Biosciences, University of Kent, Canterbury, Kent CT2 7NJ, UK

To whom correspondence should be addressed. E-mail: attila.becskei@unibas.ch

Transition rate / bistability / positive feedback loop / synthetic gene network

Noisy bistable systems, where the expression fluctuates between two distinct states of activity, are ubiquitous in cell biology and plays an important role in bacterial surviving and cell-fate determination. We investigated here the bistable region of positive feedback loops where a transcription factor activates its own transcription. The existence and the extension of this bistable region depend on the presence of molecular ultrasensitive reactions. The noise of the system was low and therefore the transition rates between the two states were dropping abruptly in the vicinity of the bistable boundaries. By mapping this dropping, we were able to compare the bistable region of feedback loops with different ultrasensitive reactions and identified the parameters which varied the extension of the bistable region. We showed that the basal expression is a major parameter as it shrinks the bistable range and up to a certain value made even the bistable range totally disappear.

Introduction

Positive feedback loops are recurring patterns in genetic regulatory network as their ability to generate bistability - the maintenance of two stable expression states under identical conditions - is broadly used in many biological processes like cell-fate determination, microbial adaptation by bet-hedging strategy or cancer onset [22-25]. The simple presence of a feedback loop is however not sufficient to generate bistability, it needs that at least one reaction within the loop has a non-linear switch-like response, termed ultrasensitive response [6-8]. A reaction response is ultrasensitive when its logarithm sensitive is higher than 1 [11]. In absence of it, the feedback loop is strictly monostable and therefore the expression converges to a single steady-state level. Reaction steps like titration by inhibitor molecules, multisite phosphorylation and dimerization can have an ultrasensitive response [9, 31, 32].

These ultrasensitive reactions do not control only the absence or presence of bistability but also the broadness of the bistable range. Indeed when the feedback loop has more than one or when the ultrasensitive reaction has a steeper response, the range of the bistability is extended [33]. The boundaries of the bistable range can be mapped easily in absence of noise due to hysteresis behavior of bistable system. By increasing the value of a parameter representing some property of a system, the expression of the feedback components will suddenly jump to the high expression state at a particular parameter value. When this parameter value is then decreased, the jump back to the low expression state occurs at a much lower parameter value. The parameter values where the expression jumps define the bistable range [34]. However, most of the reactions occurring within the cells are noisy due to small number of reactant, which can lead to significant statistical fluctuations in molecule number and reaction rate [35]. Higher this noise is, more frequent and larger is the part of bistable range where transitions between the two expression states occur.

In this work, we show that when the system has low noise, transitions in the bistable range occur essentially in the vicinity of its boundaries and therefore the transition rates can be used to approximate the bistable region. We illustrated this point in positive feedback loops where a synthetic transcription factor (TF) activates its own expression in *S. cereviseae*. Then by comparing the bistable regions of loops having alternative configuration of ultrasensitive reactions, we illustrated how extension of the bistable region can be modulated.
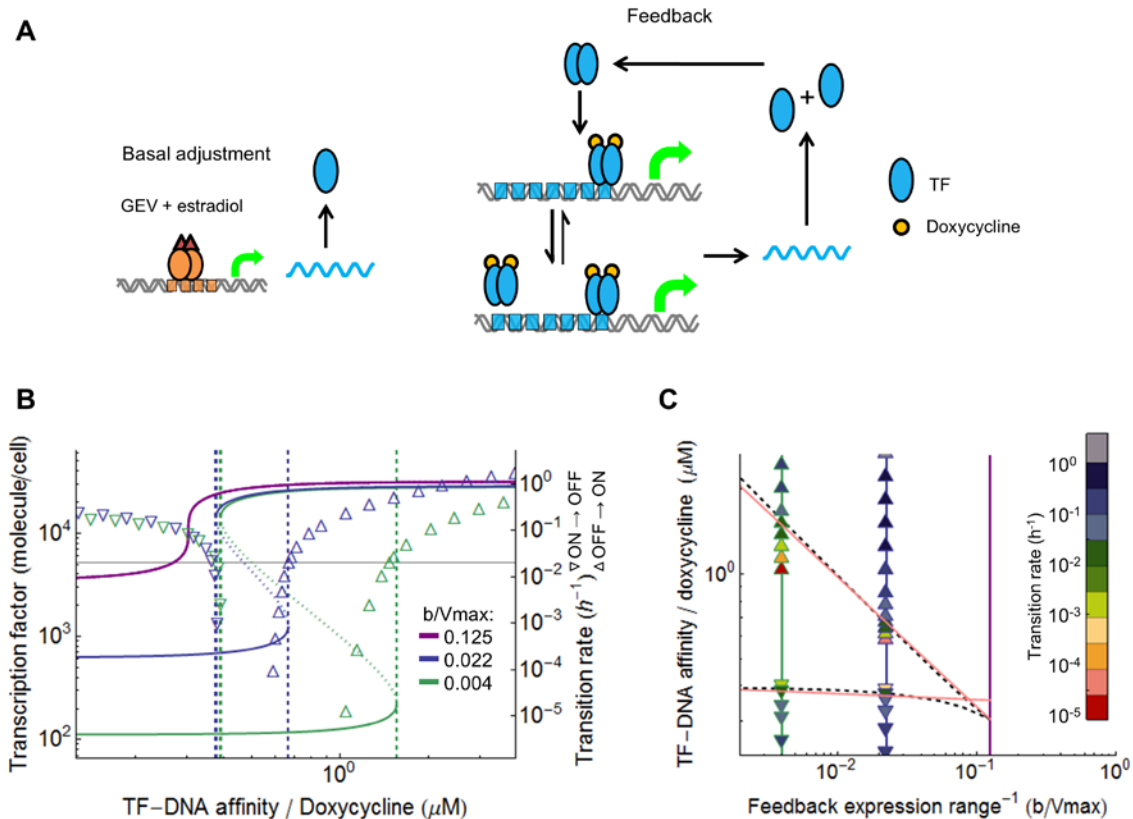
Figure 1. Design and models of a transcriptional positive feedback loop with basal expression adjusted. (A) Feedback loop design. The genetic circuit was composed of two main constructs. A positive feedback construct, where TF activates its own expression and a basal adjustment construct which able external control of TF concentration. (B) The positive feedback was bistable for a range of TF-DNA affinities (doxycycline concentration) and for interval of feedback expression range. The bistable range of doxycycline is between by the dashed vertical lines. The number of steady-state expression levels of TF varied as function of TF-DNA affinities from a single stable one (full line) in the monostable range to three, one unstable (dashed line) and two stable (full lines) in the bistable range. Three different feedback expression ranges (b/Vmax) were evaluated by varying the basal expression. Stochastic simulations were used to predict the transition rates from high to low expression state (triangle pointing down) and from the low to the high state (triangle pointing up). (C) Stability diagram displays the bistable region (delimited by the black dashed lines) as a function of the TF-DNA affinity and feedback expression range for the same feedback loop as in (B). The feedback expression ranges evaluated in (B) were indicated by vertical lines of the same color. The mathematical model is provided in the materials and methods, mathematical modelling.

Results

Design of feedback loops

Our analysis focuses on a synthetic positive feedback loop that consists of a TF, which binds its own promoter in yeast (Figure 1A). The TF, reverse tet-transcriptional activator (rtTA) from tet-ON system binds *tet* operator when it forms a homodimer and is bound by doxycycline ligand [36, 37]. To this extend, doxycycline concentration is used to adjust the affinity of the TF to the *tet* operator. The feedback expression states vary as a function of doxycycline. At low concentration only the low expression state exists, at middle concentration corresponding to the bistable range both states are possible and finally at high concentration only the high state exists. As mentioned in the introduction, positive feedback loop displays bistability, only in the presence of ultrasensitive reactions, therefore two reactions were tuned: the homodimerization of the TF and its cooperative binding to the promoter. The homodimerization was modulated by comparing the native rtTA with a monomeric version of it, where two DNA binding domains were fused in such way that it does not need to dimerize prior to bind *tet* operator [38]. The cooperative binding of the promoter was varied by having either one or seven *tet* operators, which results in absence or presence of cooperative binding, respectively [39].

The dynamic range of the feedback expression, which represents the expression ratio of high to low state, later called feedback expression range determines also the bistable range. Indeed, when the low state expression is increased by a higher basal expression, it reduces the feedback expression range as well as the steepness of ultrasensitive response and by consequence the bistable range [11]. In our synthetic genetic circuit, the feedback expression range was modulated with the basal adjustment construct which increased gradually the basal concentration of TF in presence of estradiol (see Materials and Methods, Design of synthetic circuits and yeast strains).

The transition rates in the vicinity of the bistable boundaries

In a system where noise is absent, the transitions from a state to another occur at the bistable boundaries. When the system has low noise, transitions can also occur within the bistable range, however their frequencies decrease strongly when going toward the center of the bistable range [33]. In order to illustrate this phenomenon better, we built a simple feedback loop model including the dynamic of mRNA and protein and where all the reactions are mass actions except the production of mRNA which is a Hill function with a basal term (see Materials and Methods, Mathematical modeling). The Hill coefficient was set to 2, which means that at least one

74

ultrasensitive reaction was present within the loop. Indeed higher the sensitivity or the number of ultrasensitive reactions, higher the Hill coefficient is and in opposite in absence of ultrasensitive reaction, the Hill coefficient is 1.

The bistable region of the system was restricted to specific range of doxycycline concentration and up to a certain feedback expression range (Figure 1B,C). The increase of the basal expression was reducing the bistable range in doxycycline concentration dimension. The transition rates were obtained by simulating transitions between the two states with Gillespie stochastic simulation algorithm [21]. The simulations were preceded by a pre-run to set the cells at either the low or high expression state corresponding to the low and high initial condition. For the transitions from the high and low expression states named ON → OFF transitions, the rates dropped almost vertically in the vicinity of the bistable boundaries for the both feedback expression ranges evaluated. For the OFF → ON transitions, the rates dropped less abruptly when going into the bistable range, however a slight bending of the rate variation was observed as the rates increase less steeply outside the bistable range. Interestingly, the OFF → ON and ON → OFF transition rates at the bistable boundaries were always around 0.02 h^{-1}, which corresponds to an average transition of two days.

In order to characterize better the bistable region we used stability diagrams which show the types of stability, monostable or bistable, as we move around the parameter space (Figure 1C) [40]. This diagram illustrated even better that the transitions rates vary steeply in the vicinity of the bistable boundaries. By performing a linear regression of the transition rates at 0.02 h^{-1}, the position of the bistable boundaries can be estimated.

Validation of the estimation of the bistable boundaries by transition rates

In order to determine if the transition rates are also dropping significantly at the bistable boundaries for an in-vivo system, we measured the transition rates for systems where the bistable boundaries are known. Two feedback circuits which have their bistable boundaries determined by the open-loop approach were used to this end [33]. In brief, the open-loop approach consists to break a component in the loop into an input and output. This creates a reaction chain starting by the input passing through all the components of the broken loop and ending at the output. The open-loop function indicates the output as function of the input. The first feedback has two ultrasensitive reactions: cooperative binding and dimerization of the TF ($P_{[tetO]7}$-rtTA) whereas
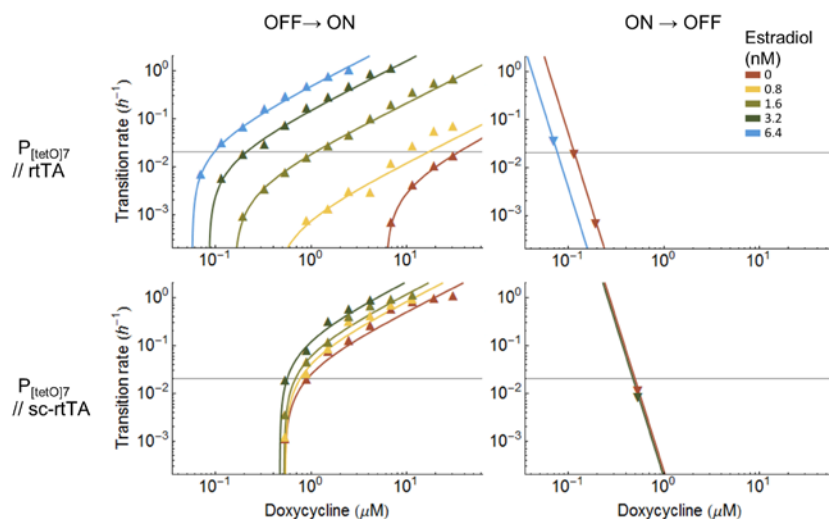
Figure 2. Measured transition rates in feedback circuits between the two expression states. The transition rates from OFF to ON (left panels) and from ON to OFF expression states (right panels) for the dimeric - cooperative (Upper panels) and monomeric – cooperative (lower panels) feedback loops are plotted as function of doxycycline concentration. The feedback expression range was adjusted by the estradiol concentration which controls the basal expression (see materials and methods, design of synthetic circuits and yeast strains). At each feedback expression range, the OFF → ON and ON → OFF transition rates are fitted as function of doxycycline concentration by a linear regression and by a power regression, respectively. The threshold used in figure 3 (horizontal black line) is set at 0.02 h⁻¹.

the second one has only cooperative binding ($P_{[tetO]7}$-sc-rtTA). The transitions rates were measured at several feedback expression range for a range of doxycycline concentrations (See materials and methods, Estimation of the bistable region by measuring transition rate variation) (Figure 2). For a given feedback expression range, the OFF → ON transition rate variation as function of doxycycline concentration was approximated by a linear function and the ON → OFF transition rates, where the variation was much steeper, were fitted by a power regression. This permitted to interpolate the doxycycline concentration at which the transition rate value was 0.02 for a given feedback expression range. Interestingly, the parameter values at which the transition rates were expected to be 0.02 h⁻¹ were all near the bistable boundaries (Figure 3A). The bistable boundaries were therefore approximated by linear regression of those parameter values (see materials and methods, Estimation of the bistable region by measuring transition rate variation).

As expected the bistable region for the dimeric feedback loop was larger than the monomeric loop in the feedback expression range and in the doxycycline concentration dimensions.

Variation of the bistable region in feedback loop with various ultrasensitive reactions

To approximate the bistable boundaries of four other feedback loops, we used the 0.02 h^{-1} transition rate threshold. Their transitions rates were also following linear and power function for OFF → ON and ON → OFF transitions, respectively (Figure S1). A feedback loop circuit having only dimerization as ultrasensitive reaction where having as expected, a smaller bistable range than the feedback loop which have in addition cooperative binding (Figure 3B) [41].

The bistable region of a dual positive-negative feedback loop was evaluated. This negative feedback loop was created by introducing in the feedback loop with two ultrasensitive reactions *tet* operators downstream of the TATA box which is known to inhibit transcription [42]. The bistable region was as expected smaller than the original feedback loop without negative interaction. Interestingly, the bistable range of the dual positive-negative feedback loop is smaller in the feedback expression range than the feedback loops with only a single ultrasensitive reaction but it is broader of them in the doxycycline concentration dimension. This illustrated that the parameters which influence the bistable range in the two dimensions are not the same.

Two other feedback loops with tTA TF were also investigated. rtTA was derived from tTA and their main functional difference lies when they form a complex with the doxycycline; tTA unbinds *tet* operator whereas rtTA binds it [43]. The estimated bistable regions indicates that tTA behaves similarly than rtTA in the extent that it binds cooperatively to the promoter as the cooperative loop had a larger region and that there is also another ultrasensitive reaction as the non-cooperative loop had still a decent bistable region. These observations were confirmed by the open-loop approach as the logarithm sensitivity of the open-loop function of both feedback loops were higher than 1 and in addition the function for the cooperative loop was steeper than the non-cooperative one (Figure S2).
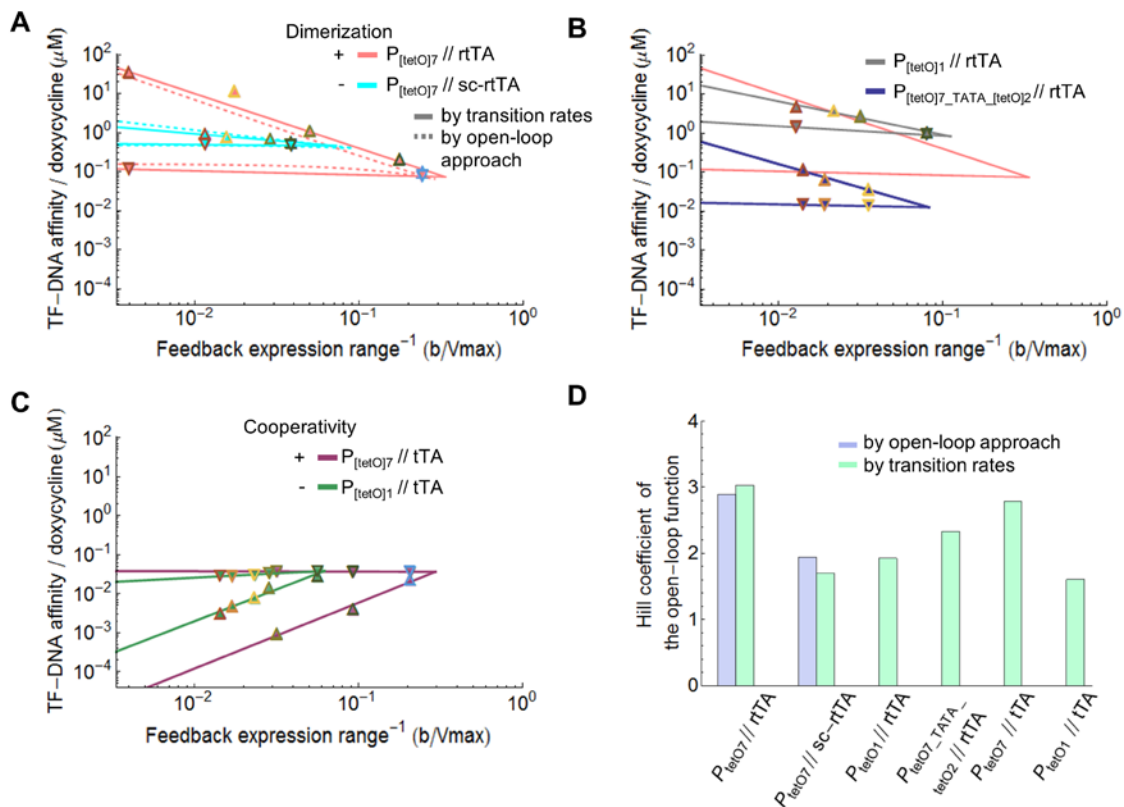
Figure 3. Prediction of the bistable region with transition rates. Transition rates at 0.02 h⁻¹ (triangles) were used to estimate the boundaries of the bistable region (full lines) by linear regression of their logarithm values. The OFF → ON (triangles pointing up) and ON → OFF (triangles pointing down) transition rates were interpolated from the measurements in figure 2 and S1 at each feedback expression range (contour color refers to the estradiol concentration used). The left-most series of data in each plot represent experiments with the lowest basal expression, (estradiol = 0 nM). (A) The bistable boundaries mapped by the open-loop approach [33] (dashed lines) and estimated with transition rates (full lines) for the dimeric – cooperative (pink) and monomeric – cooperative (cyan) (sc-)rtTA feedback loops. (B) The estimated bistable regions of the dimeric – non-cooperative (gray lines) and the dual positive-negative (blue lines) feedback loops. The bistable region of the dimeric – cooperative feedback loop from (A) is showed as a help for comparison. (C) The estimated bistable regions of feedback loops with tTA TF with (purple lines) and without (green lines) cooperative promoter. (D) Hill coefficients of the open-loop functions of the feedback loops fitted from the open-loop approach (blue) or calculated from transition rates via the cusp points in (A, B, C) (green).

The Hill coefficient of the open-loop function determines solely the extension of the bistablility in the feedback expression range dimension

As mentioned earlier the basal expression can reduce the steepness of ultrasensitive response and therefore reduce also bistable range. This can be visualized in the stability diagrams of any of the feedback loops investigated. When the feedback expression range is decreased the range of doxycycline concentration at which bistability occurs receded also and up to a critical basal at the tip of the bistable region where bistability is not anymore possible whatever is the doxycycline concentration. This tipping point is named cusp point in bifurcation theory [40]. The mathematical relations between the basal expression and the bistable range can be explained by deriving the maximum logarithm sensitivity of the open-loop function for a feedback loop where this function can be assumed to be a Hill function with a basal term ($f(x) = V_{max} \dfrac{x^n}{x^n + K_d^{\ n}} + b$).

$$S_{max} = n\left(1 + 2\frac{b}{V_{max}}\left(1 - \sqrt{1 + \frac{V_{max}}{b}}\right)\right)$$

Where n stands for the Hill coefficient, b and V_{max} for the basal and maximal production rate, respectively and K_d for the TF-DNA dissociation constant. Here K_d and therefore doxycycline concentration as included into this constant does not influence the maximum sensitivity of open-loop function. In opposite, the basal/V_{max} ratio and the Hill coefficient does influence. This equation also shows that when the basal expression is increased the maximum sensitivity is decreased. As mentioned earlier, when the maximum logarithm sensitivity is equal to 1 the system is not anymore bistable and this corresponds to cusp point [11]:

$$\left(\frac{b}{V_{max}}\right)_{cusp} = \frac{(n-1)^2}{4n}$$

This indicates that the extension of the bistable region in the feedback expression range dimension is only determined by the Hill coefficient of the open-loop function. It is important to note that here the Hill coefficient accounts for all ultrasensitive reactions and not only for cooperative binding as the open-loop function was approximated by a simple Hill function with a basal term. On the right of the cusp point, the system is strictly monostable. This was confirmed by the unimodal distribution of cell fluorescence which reported the concentration of the TF in

P[tetO]1-tTA feedback loop when exposed to high basal (Figure S3). Inversely, the Hill coefficient of the open-loop can be estimated by knowing the cusp point and using the above equation (Figure 3D). For the dual positive-negative feedback loop, this can also be done and the equations were provided in the materials and methods, Mathematical modeling.
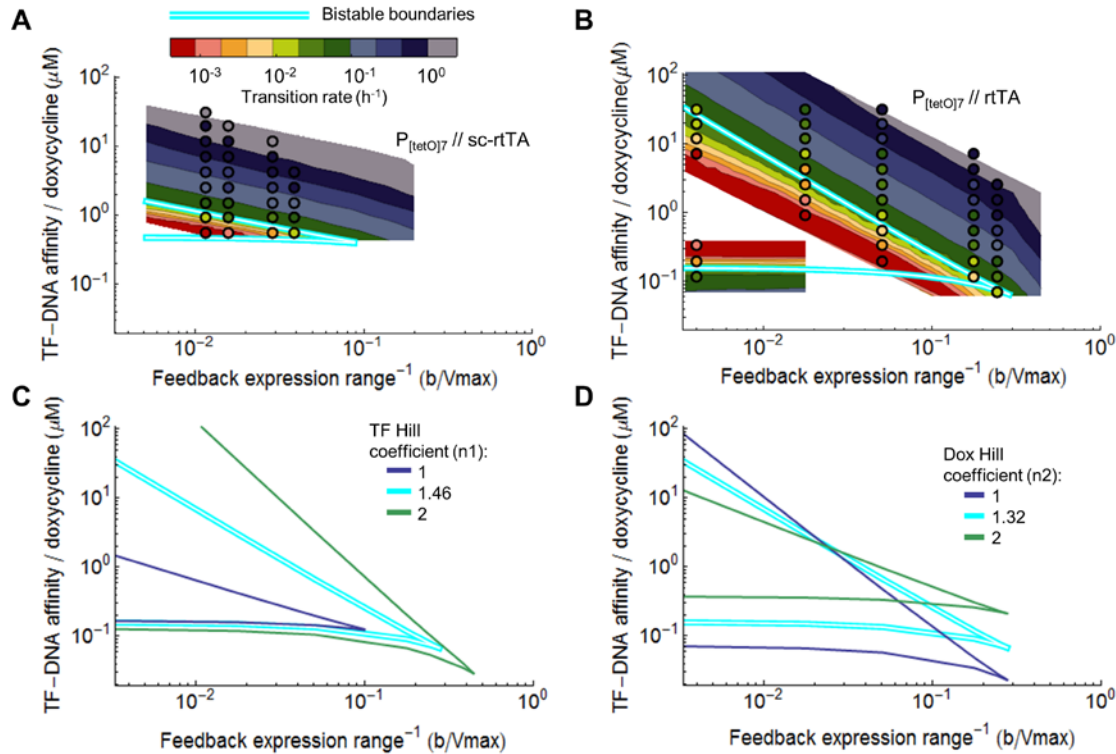

Figure 4. The extension of the bistable region depends on the TF and doxycycline Hill coefficient of the open-loop function of the feedback loop. (A,B) Predicted (contour diagram) and observed (circles) transition rates (indicated by a color scale) for monomeric (A) and dimeric (B) loops. The open-loop approach is used to map the bistable boundaries (same as data in figure 3A). The predicted transition rates were obtained by stochastic simulations (Materials and methods, Mathematical modeling). Differences between predicted and observed transition rates can be seen by the distance in the color-scale. The inset in the bottom left corner in (A) stands for the transitions from the ON → OFF expression state. (C-D) Prediction of the extension of the bistable region of P[tetO]7-rtTA loop (as in A) by modulating the TF (C) and doxycycline (D) Hill coefficient. Dimerization of rtTA TF in this loop explained the presence of the bistable region when the TF Hill coefficient was 1.

The Hill coefficient of doxycycline shrinks the bistable region

The doxycycline concentration range at which bistability occurs is however more complex as it depends on several parameters. To understand it, we analyzed for same feedback loops as in figure 2 and 3A as their parameter values were known. The model used to represent the system was more complex than the simple one used in figure 1B as it was extended to fit transient kinetics and noise from in-vivo measurements in order to predict accurately the transition rates observed [33]. The goodness of the model and the parameter values can be evaluated by comparing the transition rates predicted by stochastic modelling and the ones measured (Figure 4A, B). The higher the Hill coefficient of the TF was, the larger the bistable range in the both dimensions, feedback expression range and doxycycline was (Figure 4C). This shrinking can however not explain the very narrow range of doxycycline concentration where bistability occurs for the monomeric feedback loop. The Hill coefficient of doxycycline explained this reduction as a higher coefficient reduced the width of the bistable range (Figure 4D). The doxycycline Hill coefficient fitted from the open-loop function was 1.9 and 1.32 for the monomeric and dimeric loop, respectively[33]. The bistable range in the feedback expression range dimension did not vary with the doxycycline Hill coefficient; this is due to the fact that it depends solely on the TF Hill coefficient as explained earlier.

Discussion

Determination of the presence and extension of bistability can be done by different experiments. Hysteresis experiments where the distribution of an initially fully uninduced and induced population is compared after a certain time can indicate the presence of a bistable range [28]. When the bistable region is narrow, however the detection of the bistability can be missed [33]. The other disadvantage of the hysteresis experiment is that the bistable range cannot be delimited as the hysteresis shrinks over time. The open-loop approach in opposite can delimit precisely the bistable range, however as new strains need to be created it is more time consuming. The prediction of the bistable region by the transition rates as presented here is an intermediate alternative as it can estimate the bistable region without the need to create new strains.

We demonstrated here that tTA bound cooperatively the promoter and that its dimerization alone can support bistability which is in contradiction with previous findings [30] (Figures 3C and 2SA). There was a difference between the construction of the feedback loops as we introduced a stem-loop upstream of tTA sequence in order to reduce translation rate about 100 fold and avoid

growth defect which they also reported [41]. Without this inhibition, it was impossible to observe normal hysteresis in rtTA feedback loops. Furthermore, the open-loop approach was performed differently and by two different methods. In their figure 1B, the inducer is used as a proxy for the input variable for determining the open-loop function and as it was demonstrated later on, the inducer and the input have different open-loop functions [29, 33]. In their figure S1, the open-loop function was correct as the input was varied. Unfortunately, only the upper part of the input range was measured when the open-loop function starts to saturate as the minimal galactose amount used to drive P_{GAL1} was 0.01% which corresponds already to half of the maximum activity [4, 44].

A bistable gene expression may be in certain conditions not ideal. Therefore the network should be able to switch between a monostable and bistable regimes. It can do it simply by increasing its basal expression over the cusp point and ensures to be in a strict monostable regime. We showed here that the modulation of the bistable region can be done by different components of the system. The number of TF binding sites in the promoter as well as dimerization of the TF enhances the bistable range in the feedback expression range making it more robust to increase of the basal expression, whereas negative feedback can reduce it. The bistable range can also be modified at the strength of the TF-DNA binding by various mechanisms including the binding affinity of the ligand and how cooperative the binding of the ligand is. The combination of those different mechanisms may have been used through life to optimize gene network response.

Materials and Methods

Design of synthetic circuits and yeast strains

The feedback circuit were built with four different constructs inserted into the chromosome of *S. cerevisiae* W303, as previously described [41]. There were a construct containing the feedback loop, a fluorescent reporter construct ($P_{[tetO]2}$-yEGFP), a construct expressing constitutively GEV TF [45] and finally a P_{GAL}-rtTA/sc-rtTA/tTA expression cassette. The feedback loop construct was composed of the sequence of a TF either rtTA, sc-rtTA or tTA and a promoter driven by these TF as it contained either 1 or 7 *tet* operators. In order to avoid growth alterations an optimized stem-loop was inserted [41]. The florescent reporter construct indicated the expression level of the TF by flow cytometry measurements [41]. The P_{GAL}-rtTA/sc-rtTA/tTA expression cassette had two functions, it generated the high initial condition needed to measure the ON → OFF transition rates and it permitted to modulate the feedback expression range by increasing the

basal expression. Indeed GEV TF binding affinity to P_{GAL} promoter can be modulated in a graded manner by the estradiol concentration [46]. The feedback expression range was measured as the ratio of the TF RNA between the low and the high expression state. The RNA was quantified by qPCR as previous described [41]. RNA of (sc-)rtTA was sampled after the appropriate initial condition and 24h-incubation without and with 19.5 μM of doxycycline for the low and high expression state, respectively. For tTA feedback loops, it is the opposite i.e. for the low state 0.1 μM of doxycycline is used and 0 μM for the high state. The expression value at the high state of $P_{[tetO]7}$-rtTA feedback loop at 0nM estradiol is used for the high state of the dual positive-negative feedback loop. The strains for the open-loop approach in figure S2 were built as previously described [33]. The yeast strains are described in Table S1.

Estimation of the bistable region by measuring transition rate variation

The transition rates are fitted from the measurement of the proportion of cell at the low expression state overtime from a population initially where all cells were at the high expression state for the high initial condition or at the low expression state for the low initial condition [33]. Only minor modifications were done in the growth condition for the feedback loops containing tTA TF. At high initial condition, the cells were induced with 0.03% galactose overnight, while 0.2 μM doxycycline kept the cells inactivate at the low initial condition. The initial condition cultures were then inoculated without washing in wells containing a range of doxycycline and estradiol. Only the cells for the 7.5 h measurement for the low initial condition were washed twice by centrifugation, discarding the supernatant and resuspended in medium without doxycycline prior to be inoculated.

The bistable boundaries were approximated in the doxycycline and feedback expression range space with the transition rates when their value was 0.02 h^{-1}. Transition rates were measured at different feedback expression range and for several doxycycline concentrations. In order to determine the doxycycline concentration at which the rate was 0.02 h^{-1} for a given feedback expression range, regression of the rate values as function of doxycycline is performed (see Figure 2 and S1). For the OFF → ON and ON → OFF transition rates, linear regression with inverse-square (Y^{-2}) weighting and power regression were used, respectively. For the tTA feedback loops, transition rates measured at a doxycycline concentration below 0.0028 μM were not considered for the regression as their values were similar to the ones in absence of

doxycycline. As there were only a single ON → OFF transition rate for $P_{[tetO]7}$-rtTA at 6.4 nM and $P_{[tetO]7}$-sc-rtTA and the slope of the regression of $P_{[tetO]7}$-rtTA at 0nM was used.

The two bistable boundaries are then estimated by linear regression of the rates at 0.02 h^{-1} by taking the logarithm values of their doxycycline concentration and feedback expression range (see Figure 3). The boundary at lower doxycycline concentration was approximated by ON → OFF transition rates and the boundary at higher concentration was determined by OFF → ON transition rates for rtTA feedback loops. This was the opposite for tTA loops.

Mathematical modeling

The predicted transcription rates in figure 4 A, B were obtained by stochastic simulations by using equation and parameter values as previous described [33]. This was also the case for the model and parameter values used to map the bistable region by the open-loop approach in figures 3A, and 4C,D. For the figure 1b, two differential equations describe the feedback loop inspired from $P_{[tetO]7}$-sc-rtTA loop:

$$\frac{dM}{dt} = V_{max} \frac{P^n}{\frac{K_d^{\,n}}{dox^n} + P^n} + b - \delta_m M$$

$$\frac{dP}{dt} = \mu M - \delta_P P$$

Where M, P and dox stand for mRNA, protein and doxycycline, respectively. V_{max} and b define the maximal and minimal transcription rate, respectively. n is the Hill coefficient, which indicate how cooperative is the binding of the TF to DNA. K_d is the dissociation constant which define the binding affinity of the TF to DNA. δ_m and δ_p are the degradation rate of the mRNA and protein respectively. μ is the translation rate. The following parameter values were used: V_{max} = 12.6; b = 0.0504 (green), 0.2817 (blue) or 1.575 (purple); n = 2; K_d = 2833; δ_m = 0.2291; δ_p = 0.0095; μ = 4.836.

The open-loop function of the dual positive and negative feedback loop is described as follow:

$$f(x) = V_{max} \frac{x^n}{x^n + K_d^{\,n}} \frac{K_d^{\,n}}{x^n + K_d^{\,n}} + b$$

The maximum sensitive of the open-loop function and the cusp point are the following:

$$S_{max} = \frac{\sqrt{2}n}{\left(3+\sqrt{9+\dfrac{2V_{max}}{b}}\right)\sqrt{3+\sqrt{9+\dfrac{2V_{max}}{b}}+\dfrac{V_{max}}{b}\dfrac{b}{V_{max}}}}$$

$$\left(\frac{b}{V_{max}}\right)_{cusp} = \frac{4+\left(1+3n^2\right)\left(-3+\sqrt{1+3n^2}\right)}{54n^2}$$

Acknowledgments

Author contributions

A.B. designed the project. C.H. performed the initial experiments with tTA feedback constructs. V.J. did the experiments and data analysis. A.B. and V.J. wrote the paper.

References

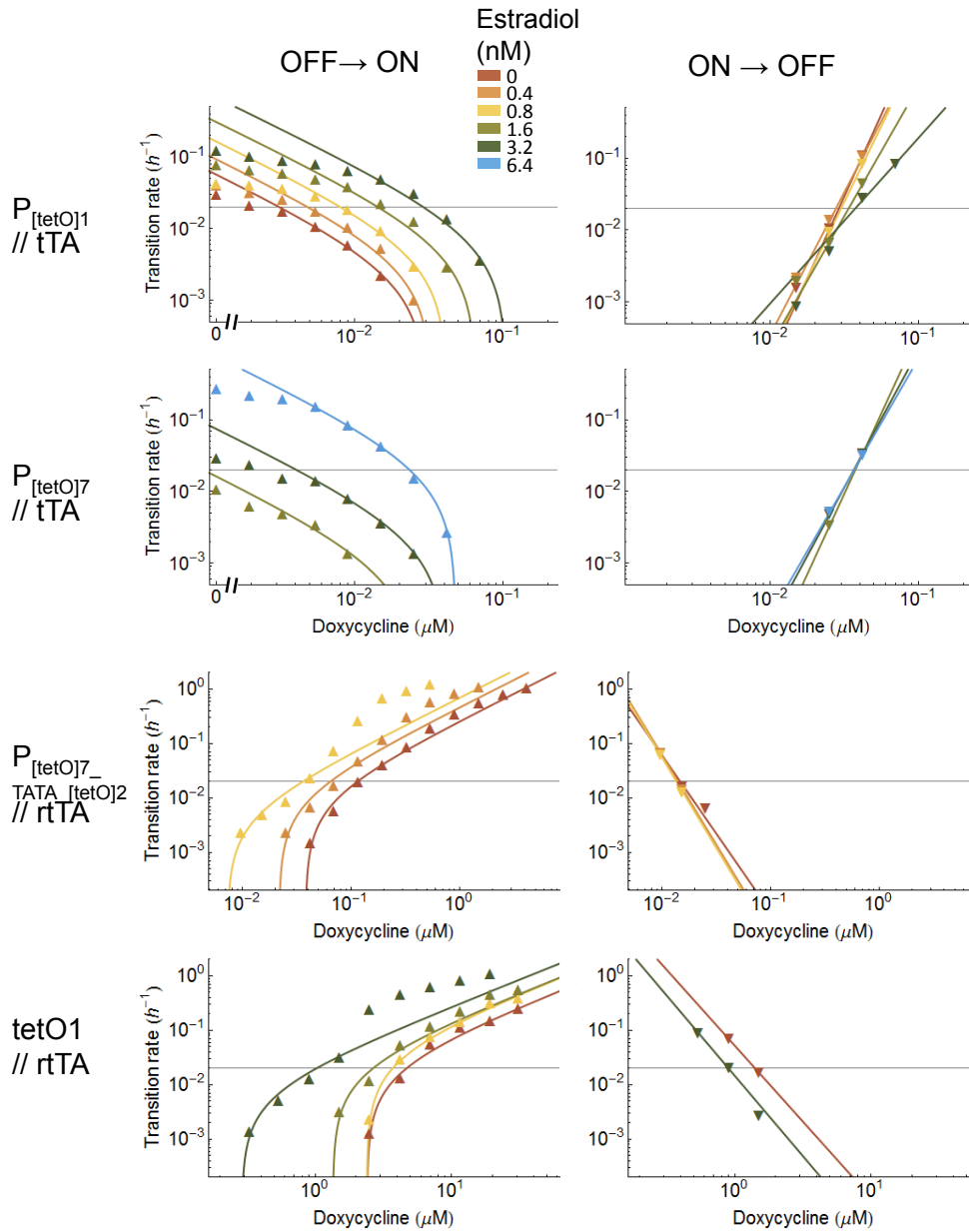The references are together with the references of the thesis.

Figure S1. Measured transition rates between the two expression states in feedback circuits. The transition rates from OFF to ON (left panels) and from ON to OFF expression states (right panels) for 4 different feedback loops are plotted as function of doxycycline concentration. The feedback expression range was adjusted by the estradiol concentration which controls the basal expression (see materials and methods, design of synthetic circuits and yeast strains). At each feedback expression range, the OFF → ON and ON → OFF transition rates are fitted as function of doxycycline concentration by a linear regression and by a power regression, respectively. The threshold used in figure 3 (black horizontal line) is set at 0.02 h^{-1}.
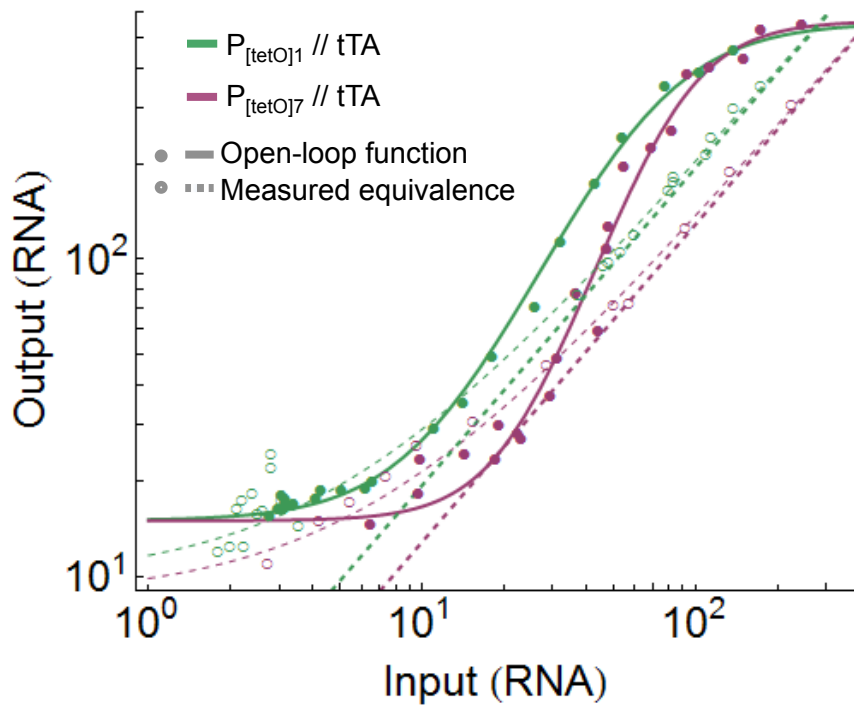
Figure S2. Open-loop measurements for tTA feedback loops. The input and output RNA is measured as the activity of the GAL promoter was varied by estradiol at 0.012 and 0.003 μM doxycycline for $P_{[tetO]1}$ and $P_{[tetO]7}$, respectively. The data for the open-loop function were fitted to Hill function with basal term (see main text) and the measured equivalence to linear function, *s input + b*, where b is the basal expression of the ghost output. The fitted values for open-loop function of $P_{[tetO]1}$ are: V_{max}=541.30, b=14.19, K_d=66.57, n=2.00 and of $P_{[tetO]7}$ are: V_{max}=548.57, b=14.54, K_d=82.67, n=2.75. The fitted values for measured equivalence of $P_{[tetO]1}$ are: s=1.94, b=9.73 and of $P_{[tetO]7}$ are: s=1.29, b=8.59. The thick dashed lines for the measured equivalence are the linear function without b.
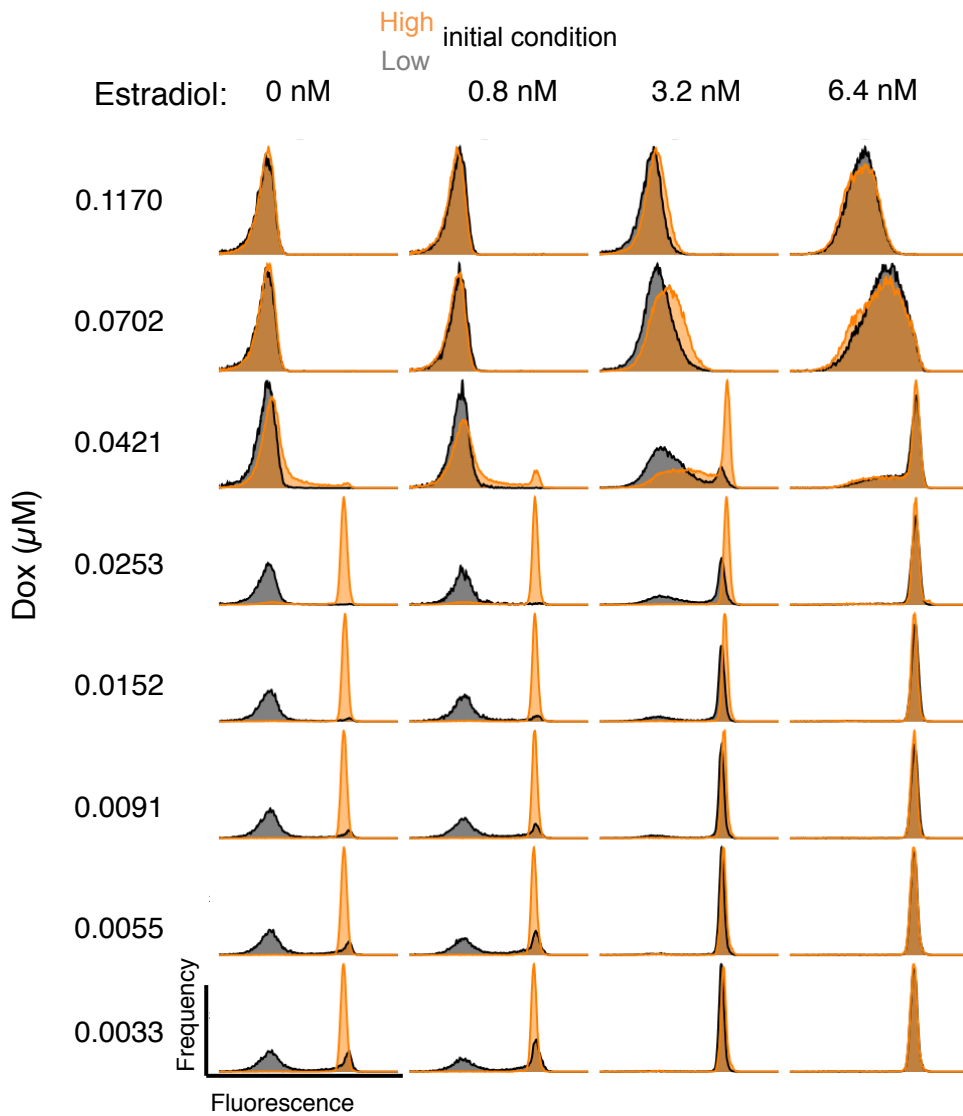
Figure S3. Hysteresis plots illustrating shrinking of the bistable range as function of the basal for $P_{[tetO]1}$-tTA feedback loop. Cell population set initially to the low or high state of activity during the low or high initial condition, respectively. Measurements are performed after initial condition and 24h-incubation in the indicated doxycycline concentration. The rtTA activity in the feedback loops in the cells was reported with GFP. The distribution of the fluorescence signal is shown. This figure is related to figure 3C as it shows part of its results. The two initial conditions have different distributions for a large range of doxycycline concentration when basal is low at 0nM and 0.8 nM estradiol. This indicates that the doxycycline bistable range is large there which is also what we get in figure 3C for the first and third series of triangles from the left. At 3.2 nM estradiol, the difference of distribution is only significant at 0.0421 µM doxycycline indicating a very narrow bistable range. This is also what we observed in figure 3C. Finally, at 6.4 nM when the dynamic range is higher than the cusp point, 0.221 versus 0.057, we don't observe anymore hysteresis and the distributions are unimodal indicating that the system is in the monostable range.

Supplementary Tables

Table S1. Yeast strains.

Diploid Strain	Haploid parents	Integration locus (plasmid)			Function
	A / alpha	*ade2:: ADE2_*	*ura3:: URA3_*	*his3:: HIS3_*	
Yvj87.2[*]	Yvj79.2		P_[tetO]7- *CYC1*c ǀ SL_5[AT]1 ǀ rtTA (pCH068)	P_*MRP7* ǀ GEV (pPR1)	Feedback
	Yvj70.1	P_*GAL1*UAS-*CYC1*c ǀ SL_5[AT]1 ǀrtTA (pVJ46)	P_[tetO]2- *CYC1*c ǀ *yEGFP* (pABG10)		
Yvj99[*]	Yvj89.1		P_[tetO]1- *CYC1*c ǀ SL_5[AT]2 ǀ rtTA (pVJ42)	P_*MRP7* ǀ GEV (pPR1)	Feedback
	Yvj91.6	P_*GAL1*UAS-*CYC1*c ǀ SL_5[AT]2 ǀrtTA (pCH094)	P_[tetO]2-*CYC1*c ǀ *yEGFP* (pABG10)		
Yvj151.3[*]	Yvj150.3	P_[tetO]7-TATA-[tetO]2 *CYC1*c ǀ rtTA (pMG01)		P_*MRP7* ǀ GEV (pPR1)	Feedback
	Ych178.2	P_*GAL1*UAS-*CYC1*c ǀ rtTA (pCH099)	P_[tetO]1- *CYC1*c ǀ *yEGFP* (pCH001)		
Ych260.2[*]	Yvj80.1		P_[tetO]7- *CYC1*c ǀ SL_5[AT]3 ǀ sc-rtTA (pCH91)	P_*MRP7* ǀ GEV (pPR1)	Feedback
	Ych250.2	P_*GAL1*UAS-*CYC1*c ǀ SL_5[AT]3 ǀ sc-rtTA(pCH102)	P_[tetO]2- *CYC1*c ǀ *yEGFP* (pABG10)		
Yvj139.1	Yvj134. 1		P_[tetO]1- *CYC1*c ǀ SL5[AT]1- ǀ tTA (pCH077)	P_*MRP7* ǀ GEV (pPR1)	Feedback
	Ych150.7	P_*GAL1*UAS-*CYC1*c ǀ SL_5[AT]1 ǀtTA (pCH085)	P_[tetO]2- *CYC1*c ǀ *yEGFP* (pABG10)		
Yvj138.48	Yvj133.4		P_[tetO]7- *CYC1*c ǀ SL_6[AT]0 ǀ tTA (pCH061)	P_*MRP7* ǀ GEV (pPR1)	Feedback
	Yvj135.8	P_GAL1UAS-CYC1c ǀ SL_6[AT]0 ǀtTA (pCH062)	P_[tetO]2- *CYC1*c ǀ *yEGFP* (pABG10)		
Yvj143	Yvj40.3			P_*MRP7* ǀ GEV (pPR1)	I/O
	Ych151.5	P_*GAL1*UAS-*CYC1*c ǀ SL_5[AT]1 ǀtTA (pCH085)	P_[tetO]1- CYC1c ǀ SL_5[AT]1 ǀ tTAΔ(45/45)::YFP (pCH066)		
Yvj142	Yvj40.3			P_*MRP7* ǀ GEV (pPR1)	I/O
	Ych107.1	P_GAL1UAS-CYC1c ǀ SL_6[AT]0 ǀtTA (pCH062)	P_[tetO]7- CYC1c ǀ SL_6[AT]0 ǀ rtTAΔ(45/45)::YFP (pCH058)		

[*] Constructed as in [33].

V.   Discussion

In this work, we achieved to map precisely the expression steady states and therefore the bistable range of transcriptional positive feedback loops and in addition to predict the transition rates between the two expression states. All the technics and frameworks developed in this work may be apply in the future to characterize better transcriptional positive feedback loops involving in many essential biological processes such as cell differentiation, microbial adaptation and cancer onset [22-25].

In detail, we showed that dimerization is an ultrasensitive reaction which can support bistability. Even though it was expected it had not been demonstrated in-vivo [41]. This finding has a significant impact as most of the proteins forms homomeric complex [47, 48].

We improved the open-loop approach for transcriptional feedback loop by opening at the mRNA level as so far the loop-opening was performed by fusing the TF with fluorescent protein [29, 30, 33]. The distortion of the open-loop function by using the fusion protein is expected to be larger as the production and decay rates of the input fusion protein, output reporter protein and the output mRNA, which are all part of the open-loop reaction chain, are different from the rates of the original transcription factor. In addition, the binding affinity as well as the ability to initiate the transcription of the input fusion protein may have been altered too [49]. By opening at the mRNA, the input mRNA and its protein are the original ones and the output protein is not in the open-loop reaction chain. The only distortion remaining is from the output mRNA and this one can be minimized by adding flanking sequences identical to the original mRNA in the loop.

We showed that the transition rates can be used in a system where the noise is low to determine if the system is bistable and if it is, to estimate the bistable region (see chapter 4). The advantage to use the transition rates in comparison to the open-loop approach resides in the fact that no new strains need to be created.

We showed in-vivo that an increase of the basal production reducing the feedback expression range can switch positive feedback loop from a bistable to a strictly monostable regime. In addition, we illustrated that the extension of the bistable region depend on the sensitivity of the open-loop function to the transcription factor concentration and its ligand concentration. The

ligand was doxycycline which modulates the binding of transcription factor to its DNA binding site.

We developed a framework to predict the transition rates in bistable systems [33]. Indeed, by building a stochastic model, where the parameter values were determined by the open-loop approach and the measurements of the noise and transient kinetics of the system, we were able to predict the transition rates observed. This framework allows also determining which processes influence the transition rates between the noise and the slow transient kinetics.

Finally we developed a series of stem-loop to modulate the translation rate over a broad 100-fold range. This is likely to be useful in synthetic biology as overexpressed regulators slow down cell growth and can also induce bistability if included in a positive feedback loop [50].

Outlook

To measure the open-loop function we quantified the mRNA by qPCR and therefore obtained the mean without any information on the distribution of the mRNA. If the system has a large noise and its nonlinearity is strong, the measured open-loop function can be less steep as it is in reality [51]. In our system, the deviation was minimal as we tested it by stochastic simulations (see Figure 5D in [33]) and the noise was low in the feedback loop. It will be interesting to extend the open-loop approach to deal in the case the noise is large. This could be done by measuring with smFISH the distribution of the mRNA in the open-loop function and then by performing signal processing to get the original open-loop function.

A second possible extension will be to improve the design of the output in the open-loop. Indeed, even though the decay rates were similar, the basal production as well as the synthesis rate were different from the ones of the original transcription factor. Therefore extrapolation was needed at low input value as the basal of the output was higher than the basal of the input and the open-to-closed loop mapping needed to be scaled by the measured equivalence as its slope was not 1. Increasing slightly the flanking region may improve the matching, however control for interference need to be performed. We can think also that the difference of length between the input and output, which was shorter may play a role, however for the two tTA feedback loops the length of the outputs and inputs were the same but the slope was 1.94 and 1.29. Funnily, it seems that there was an inverse trend between the strength of the stem-loop inhibition and the slope: $SL_{6[AT]0}$-tTA: 1.29, $SL_{5[AT]1}$-tTA: 1.94, $SL_{5[AT]1}$-rtTA: 1.40, $SL_{5[AT]2}$-rtTA: 1.88(data not shown),

$SL_{5[AT]3}$-sc-rtTA: 2.29. The output sequence for tTA, rtTA and sc-rtTA were identical, only the stem-loop changed. This trend can be difficulty explained because the stem-loop was identical between the input and the output.

A third possible improvement would be to use or develop a mechanism controlling the translation that can be tuned by a ligand [52-54]. Indeed, the stem-loops developed in this project cover a broad range of inhibition and they are reliable as the ratio of inhibition between different stem-loop were similar for GFP and rtTA, however the intensity of a stem-loop cannot be modified. This means that different stem-loops need to be cloned and tested. In opposite, the engineered RNA controllers which inhibition activity can be controlled by a ligand need only one cloning and the inhibition can be modulated afterward. The disadvantage of the use of the ligand controlled inhibition is that the ligand concentration may vary between two experiments and during the experiment if the ligand is air sensitive for instance. This is not the case for the stem-loops developed in this work.

Finally, it will be interesting to apply the framework developed here to predict transitions in a real system like the cell-fate determination as the complexity is higher and open-loop approach as well as transition rate prediction may help to better characterize the regulatory network behind it [55-57].

References

1.   Krebs, J.E., et al., *Lewin's genes XI* 2014: Jones & Bartlett Publishers.
2.   Alberts, B., et al., *Molecular Biology of the Cell (3rd edn).* Trends in biochemical sciences, 1995. **20**(5): p. 210-210.
3.   Dahlman-Wright, K., et al., *International Union of Pharmacology. LXIV. Estrogen receptors.* Pharmacological reviews, 2006. **58**(4): p. 773-81.
4.   Venturelli, O.S., H. El-Samad, and R.M. Murray, *Synergistic dual positive feedback loops established by molecular sequestration generate robust bimodal response.* Proceedings of the National Academy of Sciences of the United States of America, 2012. **109**(48): p. E3324-33.
5.   Cinquin, O. and J. Demongeot, *Roles of positive and negative feedback in biological systems.* Comptes rendus biologies, 2002. **325**(11): p. 1085-95.
6.   Ferrell, J.E., Jr., *Self-perpetuating states in signal transduction: positive feedback, double-negative feedback and bistability.* Current opinion in cell biology, 2002. **14**(2): p. 140-8.
7.   Angeli, D., J.E. Ferrell, Jr., and E.D. Sontag, *Detection of multistability, bifurcations, and hysteresis in a large class of biological positive-feedback systems.* Proceedings of the National Academy of Sciences of the United States of America, 2004. **101**(7): p. 1822-7.
8.   Cherry, J.L. and F.R. Adler, *How to make a biological switch.* Journal of theoretical biology, 2000. **203**(2): p. 117-33.
9.   Ferrell, J.E., Jr. and S.H. Ha, *Ultrasensitivity part I: Michaelian responses and zero-order ultrasensitivity.* Trends in biochemical sciences, 2014. **39**(10): p. 496-503.
10.   Koshland, D.E., Jr., A. Goldbeter, and J.B. Stock, *Amplification and adaptation in regulatory and sensory systems.* Science, 1982. **217**(4556): p. 220-5.
11.   Majer, I., A. Hajihosseini, and A. Becskei, *Identification of optimal parameter combinations for the emergence of bistability.* Physical biology, 2015. **12**(6): p. 066011.
12.   Szallasi, Z., J. Stelling, and V. Periwal, *System modeling in cellular biology.* From Concepts to, 2006.
13.   Fedoroff, N. and W. Fontana, *Genetic networks. Small numbers of big molecules.* Science, 2002. **297**(5584): p. 1129-31.
14.   McAdams, H.H. and A. Arkin, *It's a noisy business! Genetic regulation at the nanomolar scale.* Trends in genetics : TIG, 1999. **15**(2): p. 65-9.
15.   Arkin, A., J. Ross, and H.H. McAdams, *Stochastic kinetic analysis of developmental pathway bifurcation in phage lambda-infected Escherichia coli cells.* Genetics, 1998. **149**(4): p. 1633-48.
16.   McAdams, H.H. and A. Arkin, *Stochastic mechanisms in gene expression.* Proceedings of the National Academy of Sciences of the United States of America, 1997. **94**(3): p. 814-9.
17.   Pedraza, J.M. and A. van Oudenaarden, *Noise propagation in gene networks.* Science, 2005. **307**(5717): p. 1965-9.
18.   Elowitz, M.B., et al., *Stochastic gene expression in a single cell.* Science, 2002. **297**(5584): p. 1183-6.
19.   Raser, J.M. and E.K. O'Shea, *Control of stochasticity in eukaryotic gene expression.* Science, 2004. **304**(5678): p. 1811-4.
20.   Becskei, A., B. Seraphin, and L. Serrano, *Positive feedback in eukaryotic gene networks: cell differentiation by graded to binary response conversion.* The EMBO journal, 2001. **20**(10): p. 2528-35.
21.   Gillespie, D.T., *Exact Stochastic Simulation of Coupled Chemical-Reactions.* Journal of Physical Chemistry, 1977. **81**(25): p. 2340-2361.
22.   Veening, J.W., W.K. Smits, and O.P. Kuipers, *Bistability, epigenetics, and bet-hedging in bacteria.* Annual review of microbiology, 2008. **62**: p. 193-210.

23. Xiong, W. and J.E. Ferrell, Jr., *A positive-feedback-based bistable 'memory module' that governs a cell fate decision.* Nature, 2003. **426**(6965): p. 460-5.

24. Cruz-Ramirez, A., et al., *A bistable circuit involving SCARECROW-RETINOBLASTOMA integrates cues to inform asymmetric stem cell division.* Cell, 2012. **150**(5): p. 1002-15.

25. Kim, D., et al., *A hidden oncogenic positive feedback loop caused by crosstalk between Wnt and ERK pathways.* Oncogene, 2007. **26**(31): p. 4571-9.

26. Gardner, T.S., C.R. Cantor, and J.J. Collins, *Construction of a genetic toggle switch in Escherichia coli.* Nature, 2000. **403**(6767): p. 339-42.

27. Acar, M., A. Becskei, and A. van Oudenaarden, *Enhancement of cellular memory by reducing stochastic transitions.* Nature, 2005. **435**(7039): p. 228-32.

28. Ozbudak, E.M., et al., *Multistability in the lactose utilization network of Escherichia coli.* Nature, 2004. **427**(6976): p. 737-40.

29. Rai, N., et al., *Prediction by promoter logic in bacterial quorum sensing.* PLoS computational biology, 2012. **8**(1): p. e1002361.

30. To, T.L. and N. Maheshri, *Noise can induce bimodality in positive transcriptional feedback loops without bistability.* Science, 2010. **327**(5969): p. 1142-5.

31. Buchler, N.E. and M. Louis, *Molecular titration and ultrasensitity in regulatory networks.* Journal of molecular biology, 2008. **384**(5): p. 1106-19.

32. Buchler, N.E. and F.R. Cross, *Protein sequestration generates a flexible ultrasensitive response in a genetic network.* Molecular systems biology, 2009. **5**: p. 272.

33. Hsu, C., et al., *Contribution of bistability and noise to cell fate transitions determined by feedback opening.* Journal of molecular biology, 2016.

34. Pomerening, J.R., E.D. Sontag, and J.E. Ferrell, Jr., *Building a cell cycle oscillator: hysteresis and bistability in the activation of Cdc2.* Nature cell biology, 2003. **5**(4): p. 346-51.

35. Thattai, M. and A. van Oudenaarden, *Intrinsic noise in gene regulatory networks.* Proceedings of the National Academy of Sciences of the United States of America, 2001. **98**(15): p. 8614-9.

36. Kamionka, A., et al., *Induction of single chain tetracycline repressor requires the binding of two inducers.* Nucleic acids research, 2006. **34**(14): p. 3834-41.

37. Gossen, M., et al., *Transcriptional activation by tetracyclines in mammalian cells.* Science, 1995. **268**(5218): p. 1766-9.

38. Zhou, X., et al., *Improved single-chain transactivators of the Tet-On gene expression system.* BMC biotechnology, 2007. **7**: p. 6.

39. Becskei, A., B.B. Kaufmann, and A. van Oudenaarden, *Contributions of low molecule number and chromosomal positioning to stochastic gene expression.* Nature genetics, 2005. **37**(9): p. 937-44.

40. Strogatz, S.H., *Nonlinear dynamics and chaos: with applications to physics, biology, chemistry, and engineering*2014: Westview press.

41. Hsu, C., et al., *Protein Dimerization Generates Bistability in Positive Feedback Loops.* Cell reports, 2016. **16**(5): p. 1204-10.

42. Buetti-Dinh, A., et al., *Control and signal processing by transcriptional interference.* Molecular systems biology, 2009. **5**: p. 300.

43. Gossen, M. and H. Bujard, *Tight control of gene expression in mammalian cells by tetracycline-responsive promoters.* Proceedings of the National Academy of Sciences of the United States of America, 1992. **89**(12): p. 5547-51.

44. Hsu, C., et al., *Stochastic signalling rewires the interaction map of a multiple feedback network during yeast evolution.* Nature communications, 2012. **3**: p. 682.

45. Louvion, J.F., B. Havaux-Copf, and D. Picard, *Fusion of GAL4-VP16 to a steroid-binding domain provides a tool for gratuitous induction of galactose-responsive genes in yeast.* Gene, 1993. **131**(1): p. 129-34.

46.   Kelemen, J.Z., et al., *Spatial epigenetic control of mono- and bistable gene expression.* PLoS biology, 2010. **8**(3): p. e1000332.

47.   Marianayagam, N.J., M. Sunde, and J.M. Matthews, *The power of two: protein dimerization in biology.* Trends in biochemical sciences, 2004. **29**(11): p. 618-25.

48.   Lynch, M., *The evolution of multimeric protein assemblages.* Molecular biology and evolution, 2012. **29**(5): p. 1353-66.

49.   Snapp, E., *Design and use of fluorescent fusion proteins in cell biology.* Current protocols in cell biology / editorial board, Juan S. Bonifacino ... [et al.], 2005. **Chapter 21**: p. Unit 21 4.

50.   Tan, C., P. Marguet, and L. You, *Emergent bistability by a growth-modulating positive feedback circuit.* Nature chemical biology, 2009. **5**(11): p. 842-8.

51.   Berg, O.G., J. Paulsson, and M. Ehrenberg, *Fluctuations and quality of control in biological cells: zero-order ultrasensitivity reinvestigated.* Biophysical journal, 2000. **79**(3): p. 1228-36.

52.   McKeague, M., R.S. Wong, and C.D. Smolke, *Opportunities in the design and application of RNA for gene expression control.* Nucleic acids research, 2016. **44**(7): p. 2987-99.

53.   Babiskin, A.H. and C.D. Smolke, *Engineering ligand-responsive RNA controllers in yeast through the assembly of RNase III tuning modules.* Nucleic acids research, 2011. **39**(12): p. 5299-311.

54.   Bayer, T.S. and C.D. Smolke, *Programmable ligand-controlled riboregulators of eukaryotic gene expression.* Nature biotechnology, 2005. **23**(3): p. 337-43.

55.   Olsson, A., et al., *Single-cell analysis of mixed-lineage states leading to a binary cell fate choice.* Nature, 2016.

56.   Yao, G., et al., *Origin of bistability underlying mammalian cell cycle entry.* Molecular systems biology, 2011. **7**: p. 485.

57.   Suel, G.M., et al., *An excitable gene regulatory circuit induces transient cellular differentiation.* Nature, 2006. **440**(7083): p. 545-50.

Detailed individual contributions

In the second chapter which corresponds to "Protein dimerization generates bistability in positive feedback loops", Hsu et al (2016) Cell Report, my contributions in the experiments and data analysis was in the experiments necessary for figures: 2, 3A fluorescence, 3B, 4, S1, the mathematical modeling and the cloning of the plasmids named "pVJ".

In the third chapter which corresponds to "Contribution of bistability and noise to cell fate transitions determined by feedback opening", Hsu et al (2016) J Mol Biol, my contributions in the experiments and data analysis was in the experiments necessary for figures: 2C, 4, 6, S3C, the initial mathematical modeling and fitting of figure 4, the mathematical modeling and fitting of the experimental transition rates in figure 6 and the cloning of the plasmids named "pVJ".

In the fourth chapter which corresponds to unpublished manuscript "Modulation of the bistable region of positive feedback loops", my contributions in the experiments and data analysis was in the experiments necessary for all figures (C.H. performed the initial experiments with tTA feedback constructs), the mathematical modeling, the fitting of all the data and the cloning of the plasmids named "pVJ".

Acknowledgments

First of all, I would like to thank Attila Becskei for giving me the opportunity to do my Ph.D. in his lab and for his constant support during all those years. I also thank Chieh as it was a pleasure to work with you all along this long project. I am thankful to all the lab members for the nice atmosphere and particularly Farzaneh and Mümün for the fruitful collaboration on part of the project. Finally, I would like to thank my family for their unconditional love, encouragement and support.

Curriculum vitae

Vincent Jaquet

Häsingerstrasse 35
4055 Basel
(+41) 79 611 76 28
vjaquet@gmail.com
vincent.jaquet@unibas.ch

Birthdate   29.01.1987
Nationality   Swiss
Citizenship   Saint-Imier (BE)

Education

2012- Today	**Biozentrum, university of Basel, Basel, Switzerland** **PhD thesis in Systems biology**
2009– 2011	**Swiss Federal Institute of Technology (ETHZ), Zurich, Switzerland** **MSc in Systems biology**
2006 – 2009	**Swiss Federal Institute of Technology (EPFL), Lausanne, Switzerland** **BSc in Life Science and Technology**
2003 – 2006	**High school Blaise Cendrars, La Chaux-de-Fonds, Switzerland** **Option biology and chemistry**

Publications

2016	**Contribution of bistability and noise to cell fate transitions determined by feedback opening** **C Hsu*, V Jaquet*, F Maleki & A Becskei	*Co-first author** **Journal of molecular biology**
2016	**Protein Dimerization Generates Bistability in Positive Feedback Loops** **C Hsu*, V Jaquet*, M Gencoglu & A Becskei	*Co-first author** **Cell reports**
2012	**Stochastic signalling rewires the interaction map of a multiple feedback network during yeast evolution** **C Hsu, S Scherrer, A Buetti-Dinh, P Ratna, J Pizzolato, V Jaquet, A Becskei** **Nature communications**